UNIVERSITÀ DEGLI STUDI DI TRIESTE

UNIVERSITÀ DEGLI STUDI DI TRIESTE

XXXVIII CICLO DEL DOTTORATO DI RICERCA IN

Scienze della terra, fluidodinamica e matematica. Interazioni e metodiche

The Frasnian–Famennian boundary (Late Devonian) in Peri-Gondwana and South China. New data from the Carnic Alps (Italy) and Longmenshan (Sichuan, China): conodont biostratigraphy, stable isotope analysis, and correlation

Settore scientifico-disciplinare: **GEOS 02/A**

DOTTORANDO / O
XIAOYU JIN

COORDINATORE
PROF. STEFANO MASET

SUPERVISORE DI TESI
PROF. CARLO CORRADINI

CO-SUPERVISORE DI TESI
PROF. MARCO FRANCESCHI

ANNO ACCADEMICO 2024/2025

Abstract

We integrate conodont biostratigraphy, carbonate microfacies, and stable carbon–oxygen isotopes from two new Frasnian–Famennian (F–F) successions that bracket contrasting depositional settings: the Plan di Zermula D (PZD) section in the Carnic Alps (Peri-Gondwana) and the Qinglongxia (QLX) sections in the Longmenshan (South China). PZD captures a deep-water basinal record within the Pal Grande Formation, including a ~25cm dark pelitic bed and a continuous seven-zone conodont succession from FZ 13b through the *Palmatolepis crepida* Zone. The F–F boundary is fixed immediately above the pelite by the FAD of *Pa. subperlobata* and coincides with a +1.8‰ $\delta^{13}C_{carb}$ rise (peak 3.31‰), a typical Upper Kellwasser positive excursion. Conodont diversity collapses by ~80% at the boundary and recovers stepwise to ~20 taxa in the *Pa. crepida* Zone.

In contrast, the shallow-water QLX A section (Shawozi–Maoba formations) lacks a diagnostic black shale but resolves a clear facies trajectory across the base of the FZ 13b–*Pa. crepida* undifferentiated interval and through its lower part: shallowing to shoal-margin packstone (M4; samples QLXA 116–117) records the "*linguiformis* regression," followed by deepening to M2 at sample G30, tentatively tied to the Upper Kellwasser transgression, and renewed regressive shoaling above. Against a high shallow-water $\delta^{13}C_{carb}$ baseline (~2.96‰), QLX A shows an anomalous negative excursion, reaching a minimum of 1.62‰ at G29. We tentatively link this excursion to an initial volcanogenic CO_2 perturbation preceding the Kellwasser positive peak (Retallack/Racki–Schobben model), although additional geochemical constraints are needed, and high shallow-water baseline $\delta^{13}C$ values may have damped or masked any subsequent positive shift.

Contents

1. Introduction

1.1 Late Devonian and the Frasnian–Famennian Event

The Devonian Period (419.6–358.9 Ma; ICS, v2024/12) marks a transformative phase in Earth history, coupling major evolutionary innovations with systemic environmental change. Rapid terrestrialization of vascular plants, explosive fish diversification, and the first tetrapods coincided with pronounced CO_2 fluctuations and a secular rise in O_2, underscoring tight biosphere Earth system feedbacks (House, 2002; Ma et al., 2016; Becker et al., 2020; Fig. 1).

In particular, the Late Devonian was a period of profound ecological and environmental upheaval, coincident with intensified tectonic activity. On land, lycopsid forests and archaeopteridalean trees deep, efficient root systems intensified weathering and nutrient delivery, linking vegetation change to redox instability and faunal turnover (Scott & Glasspool, 2006; Berry & Marshall, 2015). The first seed plants emerged by the Late Famennian (Prestianni & Gerrienne, 2010). Concurrent orogenesis and large igneous province activity (e.g., Viluy Traps; Kola province) likely amplified climatic and oceanographic stress (Racki, 1998; Courtillot et al., 2010; Averbuch et al., 2005; Wu et al., 2013). Stratigraphic evidence ultimately records a greenhouse–icehouse transition culminating in the latest Devonian glaciation (Lakin et al., 2016). Against this backdrop of long-term environmental perturbation, the Late Devonian culminated in a series of closely spaced biotic crises. Among them, the Frasnian–Famennian (F–F) event was one of the most severe biodiversity losses of the Phanerozoic and a defining ecological turning point of the Devonian.

The F–F evet, also called the Kellwasser event. In the rock record, the event is expressed as two rather globally correlatable, organic-rich units of black limestone or shale: the Lower Kellwasser (LKW) and Upper Kellwasser (UKW) intervals. Named after classic sections in the Kellwasser Valley (Harz Mountains, Germany), both intervals coincide with positive $\delta^{13}C$ excursions that are widely interpreted as evidence for global (or at least basin wide) marine anoxia (Roemer, 1850; Eder & Franke, 1982; Walliser, 1996; House, 2002; Carmichael et al., 2019). The F–F boundary is placed between the top of the *Palmatolepis linguiformis* Zone (now FZ 13c; Klapper et al., 2004; Girard et al., 2005; Klapper & Kirchgasser, 2016; Becker et al., 2020) and the basal Famennian conodont zone traditionally termed the *Palmatolepis triangularis* Zone (Ziegler & Sanderg, 1990), which was formally renamed the *Palmatolepis subperlobata* Zone by

Spalletta et al. (2017). Meanwhile it is marked by a synchronous suite of biotic signals: the extinction of characteristic Frasnian *Palmatolepis* taxa (notably *Palmatolepis bogartensis* Stauffer, 1938) together with *Ancyrodella*, the first appearance of *Palmatolepis subperlobata* Branson & Mehl, 1934, and a flood of *Palmatolepis ultima* Ziegler, 1958. Geochronologically, GTS 2024 places the boundary at 372.15 ± 0.46 Ma, with high-precision U–Pb and astrochronologic constraints refining it to 371.93–371.78 Ma; the two Kellwasser pulses lasted ~200 kyr and ~150 kyr, separated by ~600 kyr, indicating a multiphase tempo paced by orbital forcing (De Vleeschouwer et al., 2017; Percival et al., 2018). In Frasnian conodont zonation (FZ), LKW corresponds to the FZ 12 - FZ 13a transition, whereas UKW lies in the upper FZ 13b and briefly extends into FZ 13c, with its top essentially coincident with the F–F boundary (Klapper & Kirchgasser, 2016; Becker et al., 2020; Hartenfels, 2024).

Biologically, the crisis shows marked ecological selectivity and depth partitioning: low- to mid-latitude shallow-marine benthos were hit first, with coral–stromatoporoid reef factories declining rapidly from LKW and terminating at UKW, to be replaced by microbial reefs in the Famennian (Copper, 2002; Stearn, 2015). Tabulate corals were nearly wiped out, shallow-water rugosans suffered major losses whereas deeper-water forms survived preferentially (Sorauf & Pedder, 1986; Wang et al., 2006; Ma et al., 2016). Stromatoporoids experienced ~68% generic extinction, with only localized recovery late in the Famennian (Stearn, 1987, 2015). Brachiopods exhibit turnover of dominant clades and compositional reorganization (retreat of atrypids and pentamerids; rise of productids and athyridids in the Famennian), with strong regional contrasts in diversity trajectories (Johnson et al., 1973; McGhee, 1996; Copper, 1998; Ma et al., 2016). Trilobites underwent family-to-order-level extinctions near UKW, with basin-to-basin variation in tempo (Feist, 2002). Among pelagic or swimming taxa, ammonoids show high extinction (≈67% at genus level, up to ≈88% at species level), whereas nautiloids were more moderately affected; dacryoconarids (Styliolinidae) nearly disappeared at the UKW and never recovered, going extinct immediately after the crisis (House, 1985; Schindler, 1990; Becker, 1993). Conodonts display multi-pulse replacement within UKW: community abundance drops stepwise from the base, canonical Frasnian elements (e.g., *Ancyrodella*, *Ancyrognathus* and parts of the *Palmatolepis*) sequentially retreat, and the extinction of *Palmatolepis linguiformis* Müller, 1956 marks a key step; upon entering the Famennian, biofacies shift from palmatolepid/palmatolepid–polygnathid to

Icriodus-dominated mixed biofacies present in some samples; just above the boundary, *Palmatolepis subperlobata* Branson & Mehl, 1934 first appears and *Palmatolepis ultima* Ziegler, 1958 spikes before early Famennian radiation anchored by *Palmatolepis triangularis* Sannemann, 1955a (Sandberg et al., 1988; Girard & Feist, 1996; Wang & Ziegler, 2004; Sobstel et al., 2006; Huang & Gong, 2016; Hartenfels, 2024). By contrast, Late Devonian extinctions reshaped fish diversity and early vertebrate communities, with the F–F event severely impacting placoderms–especially arthrodires, which lost 63 of 70 genera (~90%) (Sallan & Coates, 2010; Barash, 2014). Overall, within the first-order extinction interval straddling the Frasnian/Famennian boundary, UKW constitutes the principal pulse (Schindler, 1990); both Kellwasser horizons are commonly linked to brief cooling episodes that interrupted an otherwise greenhouse Late Devonian climate (Joachimski & Buggisch, 2002; Joachimski et al., 2009; Lakin et al., 2016; Becker et al., 2020).

As for triggering mechanisms, the F–F crisis was not singly forced but reflectively multi-driver across Devonian time scales. The early impact hypothesis, which cites the Siljan structure, boundary-layer microspherules, weak Ir anomalies, and the Alamo breccia, is now largely disfavored because the evidence does not match in age, size, provenance, or stratigraphic position. (McLaren, 1970; Svensson, 1971, 1973; Claeys et al., 1992; Wang, 1992; Nicoll & Playford, 1993; Claeys & Casier, 1994; Ma & Bai, 2002; Reimold et al., 2005; Morrow et al., 2009; Schulte et al., 2010; Glass & Simonson, 2012). By contrast, volcanism, mercury, and carbon cycle perturbation provides a more coherent framework: large igneous provinces (Yakutsk-Vilyui LIP, Kola, Pripyat–Dnieper–Donets rift zone) overlap temporally with F–F and can, through the release of greenhouse gases and aerosols, the addition of toxic metals and mercury (including methylmercury pathways), nutrient fertilization, and enhanced weathering, drive water-column stratification, widespread anoxia up to euxinia, and brief cooling pulses; Hg enrichments and Hg/TOC co-peaks are reported from multiple sections and commonly co-vary with positive $\delta^{13}C$ excursions, black shales and U–Mo–V redox proxies (Kusznir et al., 1996; Huybers & Langmuir, 2009; Kravchinsky, 2012; Ricci et al., 2013; Percival et al., 2018; Polyansky et al., 2018; Racki et al., 2018; Clapham & Renne, 2019; Racki, 2020). In parallel, terrestrial plant innovations and deep rooting enhanced weathering and nutrient delivery while lowering pCO_2; regional tectonics and eustatic change reshaped habitat distributions; and Milankovitch forcing likely paced the multipulse nature of LKW/UKW (Algeo et al., 1995; Denison et al., 1997; Averbuch et al., 2005; McArthur et al., 2012; De Vleeschouwer et al., 2013, 2014, 2017). Overall, the causation reflects a compound, multi-scale forcing that

produced a complex extinction trajectory that was largely stepwise and gradual. To resolve this complexity, an effective approach is to focus on one key region and, across contrasting palaeogeographic settings and habitats, reconstruct the spatiotemporal coevolution of biotic and environmental signals and their couplings, thereby constraining the mechanisms that underpin the Frasnian to Famennian extinction.

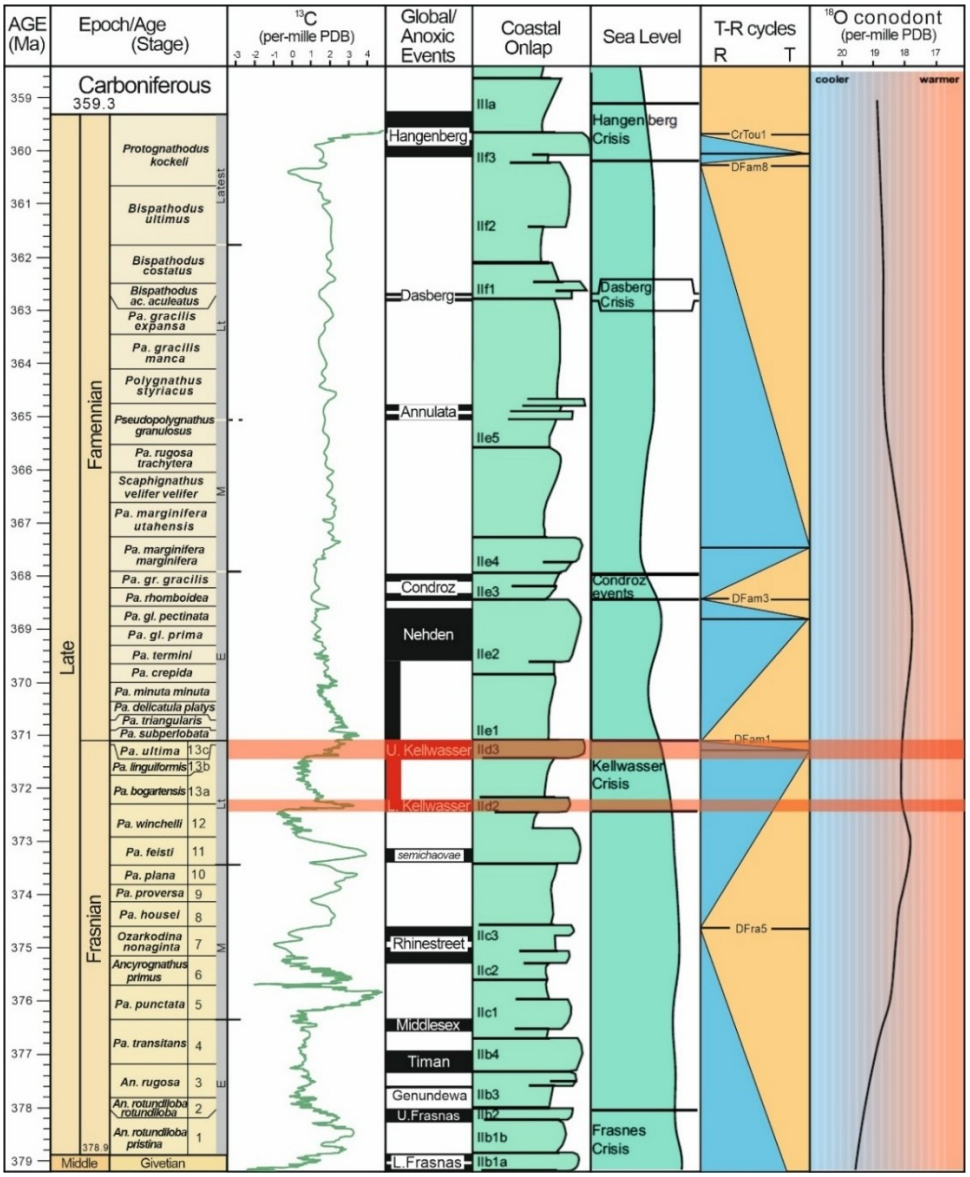

Fig. 1. F-F Frasnian and Famennian (Upper Devonian) chrono- and conodont stratigraphy near the F–F boundary, correlated with global carbon isotope, event, sea-level, and global temperature trend based on conodont oxygen isotopes (modified after Becker et al., 2020); Abbreviations: *An.* - *Ancyrodella*, *Pa.* - *Palmatolepis*, *Po.* - *Polygnathus*.

1.2 Conodonts as stratigraphic and paleoenvironmental tools

Conodonts are microscopic phosphatic elements that represent the feeding apparatus of extinct, eel-like marine vertebrates (Briggs et al., 1983; Purnell et al., 1995; Sweet & Donoghue, 2001; Fig. 2). They appeared in the late Cambrian and flourished until the end of the Triassic, with an evolutionary history of nearly 300 million years (Corradini et al., 2024b). These tiny tooth-like fossils are most commonly preserved in carbonate rocks, but they also occur in shale or chert and can even survive in low-grade metamorphic rocks such as those of the greenschist facies (Rejebian et al., 1987).

Two main taxonomic concepts have traditionally been used for conodont genera. The first is the form genera proposed by Pander (1856), and the second is the natural assemblages first reported by Hinde (1879). Form genera are based on the morphology of single conodont elements, such as coniform, platform, or ramiform types. In contrast, natural assemblages, later termed multielement or apparatus genera, were established when articulated clusters of different element types were found in fine-grained sediments (Sweet & Donoghue, 2001; Corradini et al., 2024). These conodont clusters preserved the original arrangement of the feeding apparatus and revealed the natural anatomical organization of the conodont animal (Aldridge et al., 1987; Purnell, 1995). Studies of multielement apparatuses have shown that conodont elements can be classified into several functional types, including P1, P2, S0, S1, S2, S3/4, and M (Purnell & Donoghue, 1997). Among these, P1 elements, usually of the platform type, evolved most rapidly, have the most distinctive morphology, and are the best preserved. Therefore, they are the most widely used in biostratigraphic studies. Because of their rapid evolutionary turnover, conodonts became one of the most important index fossils from the late Cambrian to the Late Triassic, providing a powerful tool for stratigraphic subdivision and correlation (Ziegler, 1962; Sweet, 1988; Ziegler & Sandberg, 1990; Ferretti et al., 2020; Corradini et al., 2024b).

During the Devonian, conodonts reached the peak of their evolutionary and ecological diversity. Important radiations occurred within genera such as *Icriodus*, *Polygnathus*, and *Palmatolepis* (Klapper & Johnson, 1980; Sandberg, 1976). Platform elements showed an unprecedented degree of morphological differentiation, especially during the Famennian, which has been regarded as the "Golden Age" of conodont evolution (Dzik, 2006). The wide distribution and rapid evolution of these taxa provided the foundation for the development of high-resolution

global zonation schemes (Ziegler & Sandberg, 1990; Ferretti et al., 2020). In addition, the biological composition and geochemical characteristics of conodont elements, such as the Color Alteration Index (CAI; Epstein et al., 1977; Rejebian et al., 1987) and stable isotope data (Joachimski & Buggisch, 2002; Joachimski et al., 2009), offer key evidence for evaluating thermal maturity and paleo-ocean chemistry. At the same time, the spatial and temporal variation of conodont biofacies is equally important, reflecting different ecological environments ranging from deep pelagic to shallow high-energy settings (Sandberg, 1976; Sandberg & Ziegler, 1979; Sandberg & Dreesen, 1984; Sandberg et al., 1988). Together, these aspects provide valuable insights into biodiversity patterns and paleoecological structures.

Based on these understandings, the following sections will focus on the high-resolution biostratigraphic framework of Late Devonian conodonts and the paleoecological and paleoenvironmental significance of different conodont biofacies.

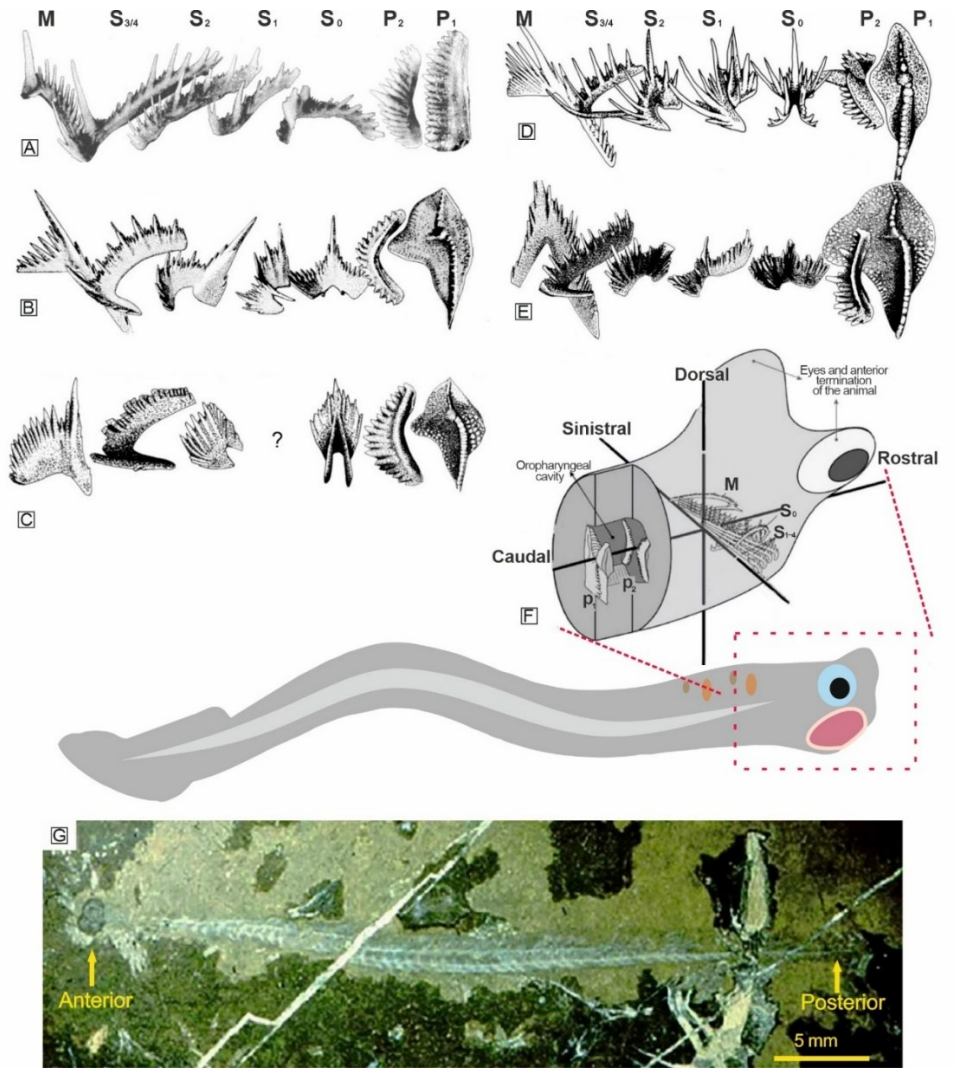

Fig. 2. Morphological characteristics of conodont animals and the morphology and positional arrangement of their apparatus. **A–E.** Morphology of elements filling the principal apparatus positions (left to right: M, $S_{3/4}$, S_2, S_1, S_0, P_2, P_1; illustration from Donoghue, 2001); **A.** *Mehlina gradata* (Branson & Mehl, 1934) (from Uyeno in Norris et al., 1982); **B.** *Palmatolepis winchelli* (Stauffer, 1938) (from van den Boogaard & Kuhry, 1979); **C.** *Palmatolepis quadrantinodosalobata* Sannemann, 1955a (from Metzger, 1994); **D.** *Palmatolepis minuta minuta* Branson & Mehl, 1934 (from Metzger, 1994); **E.** *Palmatolepis bogartensis* (Stauffer, 1938) (from Klapper & Foster, 1993). **F.** Apparatus location in the conodont animal (modified after Jain, 2020). **G.** Photograph of a conodont animal impression from the Lower Carboniferous, kept in the National Museum of Scotland (from Zhang et al., 2025).

1.2.1 High-resolution biostratigraphy

High-resolution conodont studies refine the temporal and spatial ranges of (sub)species and morphotypes, yielding a much finer time resolution for global correlation. Since 1973, the Subcommission on Devonian Stratigraphy has used conodont biostratigraphy to define the boundaries of Devonian series and stages (Becker et al., 2020); as a result, the conodont-based Devonian stratigraphic framework now provides a robust and reliable basis for dating and correlation. Building on this framework, I now review the Late Devonian conodont zonation, outlining the current zonal scheme and its present status (Fig. 3).

Frasnian biostratigraphy

Two biostratigraphic schemes are commonly used for the Frasnian. First, building on Ziegler's original framework (1962, 1971), successive revisions by Sandberg et al. (1988, 1989) culminated in Ziegler and Sandberg (1990) formalizing the "Late Devonian Standard Conodont Zones" (hereafter, the Standard Zonation), which has since been widely used. In parallel, Klapper (1989) proposed the "Montagne Noire Zonation" (hereafter, MN), a widely validated and progressively refined scheme with demonstrated global applicability (Klapper & Foster, 1993; Klapper et al., 1996, 2004; McLean & Klapper, 1998; Girard et al. 2005; Klapper, 2007a; Klapper & Kirchgasser, 2016).

To reconcile these two schemes, Klapper and Becker (1998) resampled the Martenberg section in the Rhenish Slate Mountains, one of the key reference sections of the Standard Zonation in Ziegler & Sandberg (1990). Their work provided a systematic alignment between the MN and the Standard Zonation. Unlike approaches that emphasize only pelagic genera such as *Palmatolepis* and *Mesotaxis*, Klapper's framework also uses taxa reliable in shallower settings, including *Ancyrodella* and *Ancyrognathus*, and employs their First Appearance Datum (FAD) to define boundaries. Klapper and Kirchgasser (2016) referred to this integrated framework as the Frasnian Conodont Zonation (FZ) and listed the index fossils for each zone in detail.

Overall, the Frasnian Conodont Zonation (FZ, previously known as the Montagne Noire Zonation) comprises thirteen zones, with Zone 13 further subdivided into subzones 13a, 13b, and 13c (Klapper et al., 2004; Girard et al., 2005). Compared with the nine-zone of "Standard

Zonation", the "FZ" provides higher biostratigraphic resolution. In sections with dense sampling and rich faunas, graphic correlation can tease out more than fifteen subdivisions, which has helped make the FZ a widely used working standard for the Frasnian (Spalletta et al., 2017).

It should be noted that commonly used standard schemes rely primarily on pelagic genera, especially *Palmatolepis*, which can limit direct application in shallow-water settings. Addressing this gap, Ovnatanova and Kononova (2001, 2008) established a shallow-water biostratigraphy for the eastern European Platform, with index fossils mainly represented by the shallow-water genus *Polygnathus*. Although strongly regional and not always straightforward to correlate with the FZ, this work provides essential anchors for shallow-water correlations and facilitates multi-section integration.

Famennian biostratigraphy

The Famennian conodont biostratigraphic framework was first proposed by Ziegler (1962) and was subsequently revised by Sandberg and Ziegler (1973), Sandberg et al. (1978, 1989), and Ziegler and Sandberg (1984). Ziegler and Sandberg (1990) then formalized the "Late Devonian Standard Conodont Zonation" (hereafter, the Standard Zonation) and argued that a zone may be recognized by a distinctive association of conodont elements even in the absence of the nominal diagnostic taxon. This recommendation facilitated the widespread application of the Famennian part of their scheme over recent decades.

Despite its widespread use, the "Standard Zonation" poses challenges in practical application. Two of its biozones have lower boundaries defined by the Last Appearance Datum (LAD) of *Palmatolepis* species. The Upper *rhomboidea* Zone begins at the extinction of *Palmatolepis poolei* Sandberg & Ziegler 1973, but this species is rare and missing in many sections from the Carnic Alps, Germany, the Montagne Noire, and Morocco, making the boundary hard to identify. The Middle *praesulcata* Zone is tied to the extinction of *Palmatolepis gracilis gonioclymeniae* Müller, 1956, which is likewise difficult to recognize in practice (Over, 1992; Kürschner et al., 1993; Perri & Spalletta, 2000; Kaiser, 2005). Consequently, some authors suggested alternative proposals (Corradini, 2008; Kaiser et al., 2009; Corradini et al., 2016).

In order to minimize stratigraphic ambiguities and improve consistency, Spalletta et al. (2017) revised the Famennian part of the "Late Devonian Standard Conodont Zonation". The new

framework comprises twenty-two zones, each defined by the first appearance datum of a species or subspecies with a well-constrained stratigraphic range and wide geographic distribution; each zone is named after the taxon whose First Appearance Datum (FAD) marks its base. In addition, the authors also provided a detailed comparison with the previous zonation and compiled range charts for Famennian conodont species. This revision offers higher biostratigraphic resolution and greater ease of application in practice.

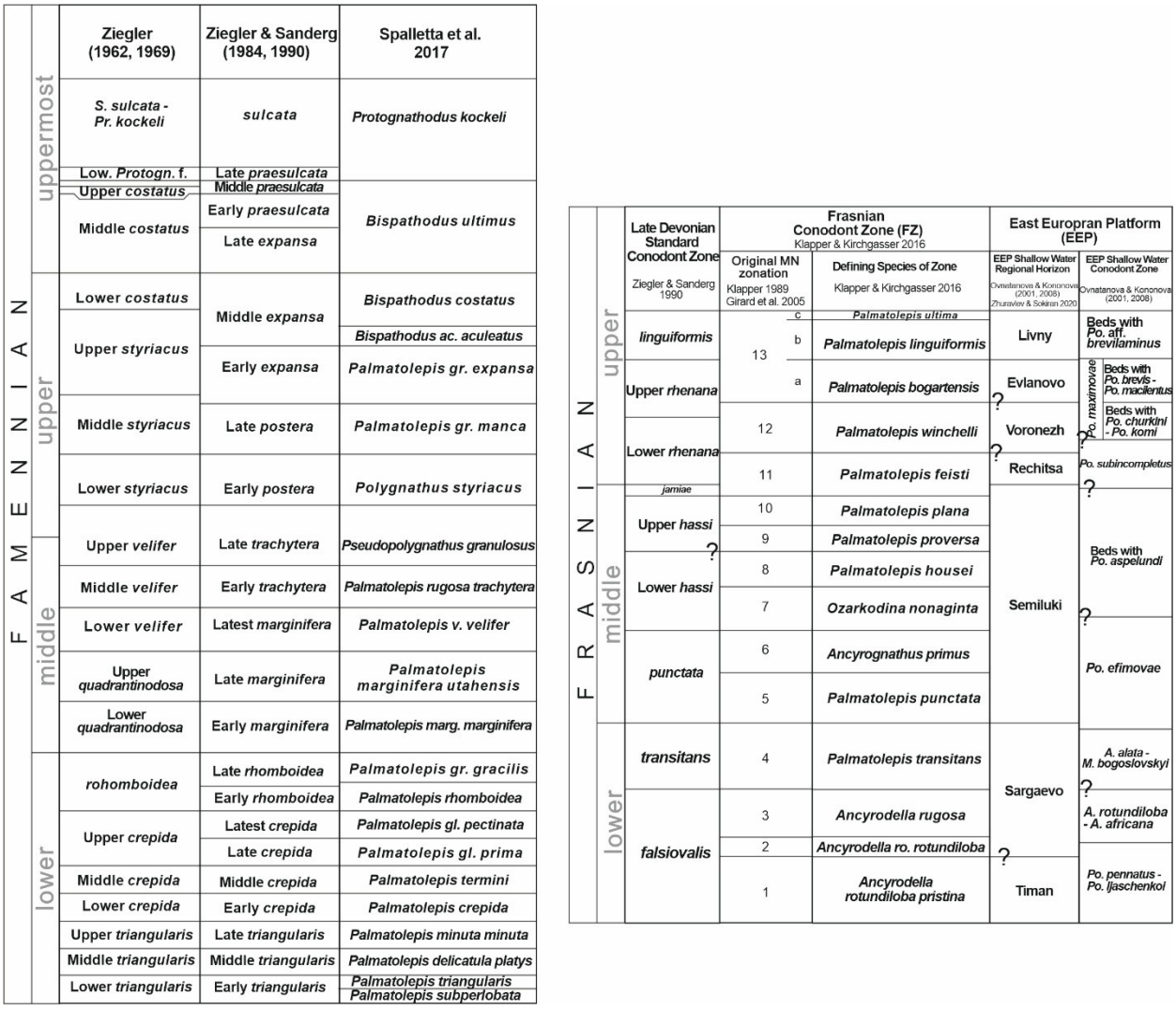

Fig. 3. Correlation of conodont biozones in the Late Devonian.

1.2.2 Conodont biofacies and paleoenvironmental implications

Conodont biofacies are generally defined as characteristic assemblages dominated by one or two genera. Variations in their relative abundances are used to reflect differences in paleoenvironmental conditions (Seddon & Sweet, 1971; Sandberg et al., 1976; Sandberg & Dreesen, 1984; Ziegler & Sandberg, 1984; Sandberg et al., 1989; Ziegler & Sandberg, 1990). Although this approach is influenced by ecological differences within genera and by processes such as storm reworking and sedimentary mixing (Weary & Harris, 1994; Krumhardt et al., 1996; Purnell & Donoghue, 2005; Lüddecke et al., 2017), it has long been regarded as an effective tool for reconstructing paleoecological and paleoenvironmental evolution.

Ecological differentiation among conodont genera became particularly evident during the Late Devonian. The genus *Palmatolepis* is a typical representative of a deep-water pelagic habitat and commonly occurs in outer-basin or open-marine deposits, forming the basis of the "Late Devonian Standard Conodont Zonation" (Sandberg, 1976; Sandberg et al., 1988; Ziegler & Sandberg, 1990). In contrast, the genus *Icriodus* is typically associated with shallow water, high energy nearshore or platform settings (Sandberg & Dreesen, 1984; Dreesen et al., 1986). In several early Famennian levels in Sardinia, palmatolepid-icriodid biofacies was documented, but the *icriodid* component is almost entirely *Icriodus olivieri* Corradini, 1998, which Corradini (1998, 2003) interpreted as more offshore than other congeners. These reports indicate that, although certain species may occur farther offshore, *Icriodus* as a genus remains a reliable indicator of shallow, higher energy environments (Sandberg & Dreesen, 1984; Dreesen et al., 1986; Savoy & Harris, 1993). Some *Polygnathus* species, such as *Polygnathus dubius* Ziegler, 1958 and *Polygnathus pollocki* Klapper, 1969, thrived in well-oxygenated, illuminated, and wave-agitated shallow waters, whereas others extended into upper-slope environments, reflecting their wide ecological range (Sandberg, 1976; Pisarzowska et al., 2006).

Based on these distributional characteristics, Late Devonian conodont assemblages have been subdivided into several composite biofacies that reflect ecological zonation along paleotopographic and bathymetric gradients (Sandberg & Dreesen, 1984; Dreesen et al., 1986; Ziegler & Sandberg, 1990; Savoy & Harris, 1993). Typical examples include the *Palmatolepid* biofacies, representing deep and open-marine settings; the *Palmatolepid-Polygnathid* biofacies, corresponding to the outer shelf to upper slope transition; and the *Polygnathid-Icriodid* biofacies,

which characterizes platform-margin and shallow-shelf high-energy environments. The successive alternation of these biofacies records not only changes in water depth and hydrodynamic energy but also ecological differentiation controlled by multiple environmental factors, such as temperature, oceanic circulation, paleolatitude, and substrate conditions. As emphasized by the "Seddon–Sweet model" (Seddon & Sweet, 1971), depositional environmental factors often play a more decisive role than depth alone in determining the spatial distribution of conodont assemblages. Therefore, recognizing the relative abundance patterns and characteristic combinations of these genera provides an effective means for reconstructing the paleoecological framework and marine evolution of platform, slope, and basin systems during the Late Devonian.

1.3 Stable carbon and oxygen isotopes

On geological timescales, the global carbon cycle operates near steady state, regulated by processes that modulate atmospheric CO_2 and climate (Archer, 2010; Sarmiento & Gruber, 2006; Sundquist & Visser, 2011). Key fluxes include continental weathering, carbonate deposition and recycling, organic carbon burial, and volcanic and mid-ocean ridge degassing (Berner, 2004). This balance is occasionally disrupted during critical intervals, when major biotic crises and environmental change drive strong carbon-cycle perturbations recorded as anomalous $\delta^{13}C$ excursions in oceanic total dissolved inorganic carbon (DIC; Saltzman & Thomas, 2012; Schobben et al., 2019).

The $\delta^{13}C$ value is defined as:

$$\delta^{13}\mathrm{C} = \left[\frac{(\mathrm{C}^{13}/\mathrm{C}^{12})_{\mathrm{sample}}}{(\mathrm{C}^{13}/\mathrm{C}^{12})_{\mathrm{standard}}} - 1\right] \times 1000‰$$

where the standard is typically Vienna Pee Dee Belemnite (VPDB).

The $\delta^{13}C$ value reflects the relative proportions of heavy carbon (^{13}C) and light carbon (^{12}C). Biological processes preferentially use ^{12}C; therefore, organic matter is typically enriched in ^{12}C ($\delta^{13}C \approx -25‰$), whereas carbonate carbon is generally close to 0‰ (about +1‰ in most marine samples). Extensive burial of organic carbon removes ^{12}C from the ocean–atmosphere reservoir, enriching the residual DIC in ^{13}C and increasing carbonate $\delta^{13}C$. Conversely, volcanic degassing or oxidation of organic matter introduces ^{12}C-rich CO_2, lowering $\delta^{13}C$ (Hayes et al., 1999; Kump & Arthur, 1999).

On a global scale, variations in the $\delta^{13}C$ of marine DIC can be described by a mass-balance relationship between carbon inputs and organic carbon burial (Kump & Arthur, 1999; Kump, 2013):

$$\frac{\mathrm{d}\delta_{\mathrm{o}}}{\mathrm{d}t} = \frac{F_{\mathrm{in}}(\delta_{\mathrm{in}} - \delta_{\mathrm{o}}) - F_{\mathrm{org}}\Delta}{M} \qquad [1]$$

where F_{in} is the combined inorganic carbon input from weathering and volcanism (mol yr^{-1}); δ_{in} is its isotopic composition; Δ is the isotopic difference between contemporaneous sedimented organic carbon (δ_{org}) and carbonate carbon (δ_{carb}) approximately –25% (i.e., $\Delta = \delta_{\mathrm{org}} - \delta_{\mathrm{carb}} \approx -25‰$); and M is the combined oceanic and atmospheric inorganic carbon reservoir size (mol).

When considering values representative of long (million years) intervals of Earth history, steady state can be assumed, and δ_o can then be expressed as:

$$\delta_o = \delta_{in} - \frac{F_{org}}{F_{in}}\Delta \qquad [2]$$

Equations (1)-(2) indicate that marine $\delta^{13}C$ is highly sensitive to variations in external carbon inputs (e.g., volcanic degassing) and carbon sinks (e.g., changes in organic carbon burial rate) (Kump & Arthur, 1999; Kump, 2013). Therefore, $\delta^{13}C$ records can serve as a reliable tracer of global carbon-cycle perturbations.

Similar to carbon isotopes, oxygen isotopes ($\delta^{18}O$) in carbonate systems also record variations in climate and hydrological conditions. In primary marine carbonates, the $\delta^{18}O$ values of carbonates are primarily controlled by water temperature and the isotopic composition of the ambient water, typically showing lower (more negative) values during warming and higher (more positive) values during cooling (O'Neil et al., 1969). Because bulk-rock $\delta^{18}O$ values in carbonates are often overprinted by diagenesis, calcite can exchange ^{16}O and ^{18}O with pore waters via dissolution–reprecipitation (Carmichael & Ferry, 2008). Therefore, carbonate $\delta^{18}O$ datasets are commonly used to assess the degree of diagenetic modification of $\delta^{13}C$ rather than to estimate original seawater composition (Carmichael et al., 2019). Nevertheless, recent work indicates that globally coeval, paired negative excursions in $\delta^{13}C$ and $\delta^{18}O$, even when documented solely in carbonates, most likely record primary volcano-climatic (greenhouse) signals and can serve as proxies for volcanic forcing of the global carbon cycle (Pisarzowska & Racki, 2020).

The Late Devonian represents a critical interval in the geological record characterized by profound fluctuations in the global carbon cycle and biosphere. During this period, the Earth system experienced multiple rapid changes in carbon sources and sinks, leading to pronounced biogeochemical instability (Racki, 2005; Buggisch & Joachimski, 2006; Pisarzowska & Racki, 2020). Consequently, carbon-isotope chemostratigraphy has become a key tool for identifying and correlating Devonian global events (Weissert et al., 2008; Saltzman & Thomas, 2005). In cases where the biological evidence is ambiguous, $\delta^{13}C$ variations provide independent constraints on the timing and nature of environmental perturbations (Becker et al., 2016).

Across the Frasnian–Famennian (F–F) boundary crisis, $\delta^{13}C$ records derived from carbonates (including brachiopod calcite and bulk rock) as well as from organic matter have been

widely reported (Joachimski & Buggisch, 1993; Van Geldern et al., 2006). However, significant intra- and inter-regional variations remain a major focus and challenge in current research (Pisarzowska & Racki, 2020). Through systematic analyses of stable carbon and oxygen isotopes ($\delta^{13}C$ and $\delta^{18}O$) in carbonate rocks, the evolution of marine environments and perturbations in the carbon cycle during the key interval of the Late Devonian are examined. The analysis focuses on both positive and negative shifts in $\delta^{13}C$ and $\delta^{18}O$ values and their correlations, to identify potential external carbon input events and related climatic responses. The results may provide geochemical constraints for understanding the coupling between volcanic activity and the carbon cycle during the Frasnian–Famennian (F–F) event.

1.4 Core Objectives of the Study

Research on shallow-water sections remains insufficient, with most attention focused on deep-water records. However, the environmental characteristics of shallow-water settings are still important. The identification of the Frasnian–Famennian (F–F) boundary in shallow-water sections has largely relied on biostratigraphic frameworks established in deep-water successions. How exactly this boundary should be recognized in shallow-water sections, and how these compare with deep-water counterparts, remains an open question. High-resolution biostratigraphy may provide valuable assistance in resolving these issues.

In the context of global events, the adaptive strategies of conodonts during times of crisis may reveal evolutionary patterns. It is necessary to investigate both deep-water and shallow-water sections to understand their respective responses.

Furthermore, research should not be limited to a single region or intracratonic setting. Instead, comparisons across different tectonic plates and global datasets are needed to evaluate whether carbon isotope excursions show consistent patterns worldwide. It is also important to assess whether shallow- and deep-water environments display different isotopic responses, and to determine the specific role of carbon isotopes in constraining stratigraphic correlations.

Building on these research gaps, the present study focuses on newly investigated sections from two distinct paleocontinental settings—Peri-Gondwana and South China. The Peri-Gondwanan section is located in the Carnic Alps, where previous studies have reported the occurrence of the Frasnian–Famennian (F–F) boundary (Pramosio A and Freikofel T, Farabegoli et al., 2023). However, while the Carnic Alps are regarded as an important region for studying the Kellwasser Event, black shale deposits, which are characteristic of this interval elsewhere, have not yet been documented in this area. In contrast, the section from South China is situated in the Longmenshan area. Although isotope anomalies have been recorded there (Zheng & Liu, 1997; Huang et al., 2002), the section represents a shallow-water depositional environment, where conodont data are lacking, and thus the exact position of the F–F boundary remains uncertain. High-resolution biostratigraphic and sequence stratigraphic analyses of both sections are therefore essential. Such investigations will help to accurately identify the F–F boundary in shallow-water carbonates and to test the applicability of biostratigraphic frameworks established in deep-water

successions. Moreover, because both regions have substantial prior research, they provide a solid basis for intra- and inter-regional comparisons.

Accordingly, this study aims to: (1) establish high-resolution stratigraphic and biostratigraphic frameworks for both sections; (2) refine the recognition of the Frasnian–Famennian (F–F) boundary in shallow-water carbonate; (3) evaluate differences in carbon-isotope responses between shallow- and deep-water environments.

2. Geological settings

During the Devonian, global geography was shifting toward a proto-Pangea that would not be complete until the Permian (Scotese, 2021). Gondwana lay at mid- to high southern latitudes near the South Pole and was separated from Laurussia by the Rheic Ocean (Nance et al., 2014). Along Gondwana's northern passive margin, Peri-Gondwanan terranes—rifted fragments and arcs that include the Carnic Alps—were developing (Schönlaub, 1998; Franke et al., 2017). Laurussia spanned equatorial to low northern latitudes, while Siberia occupied mid- to high northern latitudes and drifted toward the Arctic (Blakey, 2016). Independent microcontinents such as South China, North China, and Tarim were dispersed between the Paleo-Tethys and Paleo-Asian oceans, forming a mosaic of arcs, microplates, and marginal seas (Metcalfe, 2013; Blakey, 2016; Fig. 4).

Fig. 4. Late Devonian global palaeogeographic map, modified after Blakey (2016). The red star represents the locations of the Proto-Alps (Carnic Alps) and Proto-Longmenshan.

2.1 Carnic Alps (Peri-Gondwana)

The Carnic Alps are located south of the Periadriatic Line, across the Austrian-Italian border (Fig. 5). The investigated section belongs to the non- to low-metamorphic Pre-Variscan sequence of the Carnic Alps, spanning from the Middle Ordovician to the Early Pennsylvanian (Schönlaub, 1985; Brime et al., 2008; Corradini et al., 2015, 2016; Suttner et al., 2017). Regionally, the Pre-Variscan evolution reflects a rift–drift history along the northern Gondwanan margin that opened the Rheic Ocean and dispersed peri-Gondwanan terranes, recorded in the Carnic Alps by extensive passive-margin carbonate successions. Despite intense deformation associated with the Variscan and Alpine orogeneses, the stratigraphic framework remains relatively well-preserved, allowing for high-resolution palaeogeographic and biostratigraphic analyses (Corradini & Suttner, 2015).

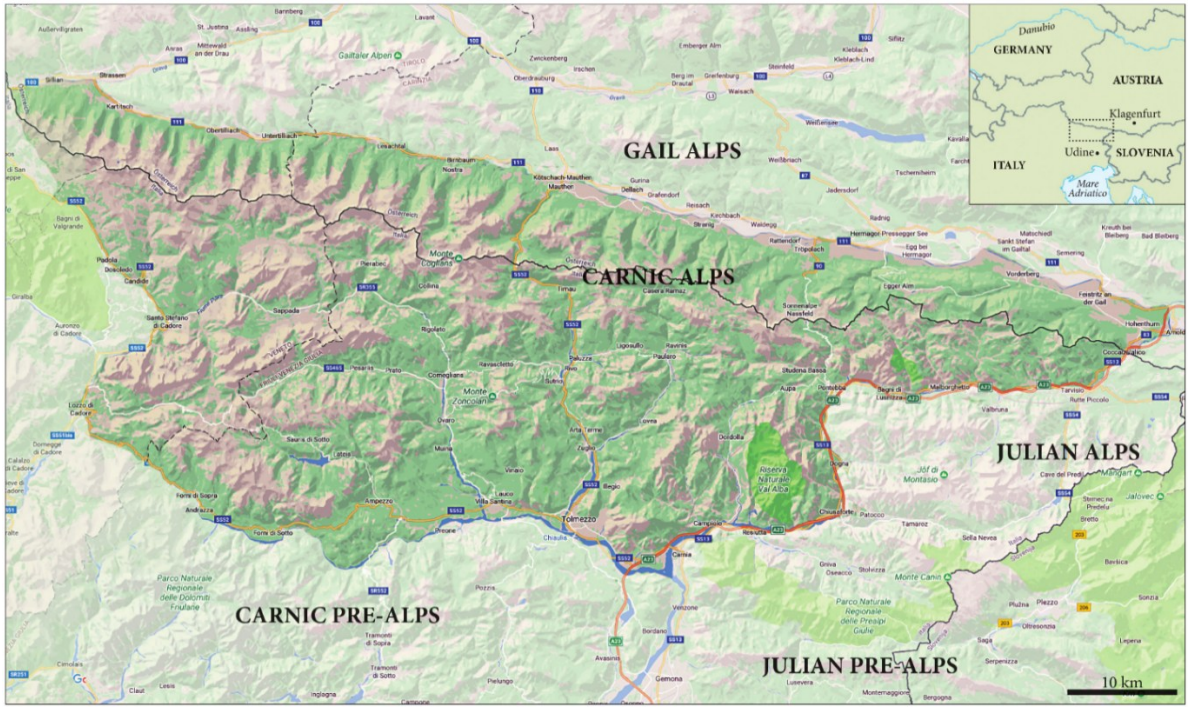

Fig. 5. Location map of the Carnic Alps (from Spalletta & Corradini, 2018)

During the Palaeozoic, the Carnic Alps were part of the Galatian terranes (von Raumer & Stampfli, 2008), a group of microcontinents that drifted northward from the Gondwana margin during the Ordovician at a faster rate than the main continent. Their migration from 50°S in the

Late Ordovician to 35°S in the Silurian and eventually into the southern tropical belt during the Devonian is reflected by distinct lithofacies and biofacies transitions (Schönlaub, 1992). By the Late Devonian, the Carnic microplate was positioned at approximately 30°S (Fig. 4; Schönlaub, 1992; Blakey, 2016). The depositional environments during the Middle and Late Devonian were primarily influenced by the develop of the largest Devonian reefs of Europe, followed by their disappearance, resulting in a range of facies from shallow-water carbonate platforms to pelagic, but not deep, basin (Schönlaub, 1992; Corradini & Suttner, 2015; Suttner et al., 2017, Corradini & Pondrelli, 2021).

These sedimentary variations are well-expressed in the stratigraphic record of the Frasnian in the Carnic Alps (Fig. 6), where different formations reflect distinct depositional environments (Corradini & Suttner, 2015). These units are here briefly presented from shallow to deeper environments. At the shallowest part of the system, the Polinik Formation (Pohler et al, 2015) represents a lagoonal setting, characterized by dark gray limestone interbedded with dolomitic layers, indicative of high salinity conditions and episodic storm deposits. High salinity conditions and storm deposits (tempestites) indicate episodic environmental fluctuations. The Kellergrat Formation (Kido et al., 2015) represents a high-energy reefal environment, dominated by massive reefal limestone with abundant stromatoporoids and corals, indicative of active reef growth and carbonate production. The Freikofel Formation (Pondrelli et al., 2015a) deposited at the slope of a carbonate apron, where floatstone, rudstone, and grainstone were deposited mainly through turbidity currents and mass transport processes, reflecting increasing water depths and periodic sediment gravity flows, with sporadic intervals of pelagic mudstone (Pas et al., 2014; Pondrelli et al., 2020). At the toe-of-slope of a carbonate apron, the Hoher Trieb Formation (Pondrelli et al., 2015b) deposited: it consists of well-bedded packstone, grainstone, and laminated black shales, put in place by density and turbidity flows embedded within a record of pelagic and hemipelagic sediments, sometimes deposited under temporary anoxic and dysoxic conditions (Pondrelli et al., 2015b, 2020; Suttner et al., 2017). Starting from the late Frasnian, the collapse of the reef system resulted in the previously diverse depositional environments being transformed into a more uniform pelagic environment, as recorded in the widely distributed Pal Grande Formation (Spalletta et al., 2015b). Only in a small area west of Passo di Monte Croce Carnico, the Creta di Collina Formation (Spalletta et al., 2015a), represented by dark limestone rich in brachiopods,

unconformably deposited above the Kellergrat Fm. during the late Frasnian to middle Famennian (Corradini et al., 2025).

The Pal Grande Formation primarily consists of gray well-bedded mudstone and wackestone; at place nodular levels are present, and the color changes from gray to moderate pink and red. It deposited in a pelagic, not deep, environment, with localized gravity-driven deposits in the lower part of the unit (Spalletta et al., 2015b; Corradini et al., 2025). In the central part of the Carnic Alps, close to the section studied in this work, two localities (Kronhof Graben and Plan di Zermula A; Schönlaub et al., 1992; Perri & Spalletta, 2001; Spalletta et al., 2021) expose a black shale interval at the Devonian-Carboniferous boundary, interpreted as equivalent to the Hangenberg Shale. The fossil content of the Pal Grande Formation includes cephalopods, trilobites, ostracods, radiolarians, and conodonts, along with less frequent occurrences of echinoderms, bivalves, brachiopods, and fish remain (Spalletta et al., 2015b). Biostratigraphic analysis based on conodont data indicates that this unit spans from the FZ 9 to the lowermost Visean (Spalletta et al., 2015b).

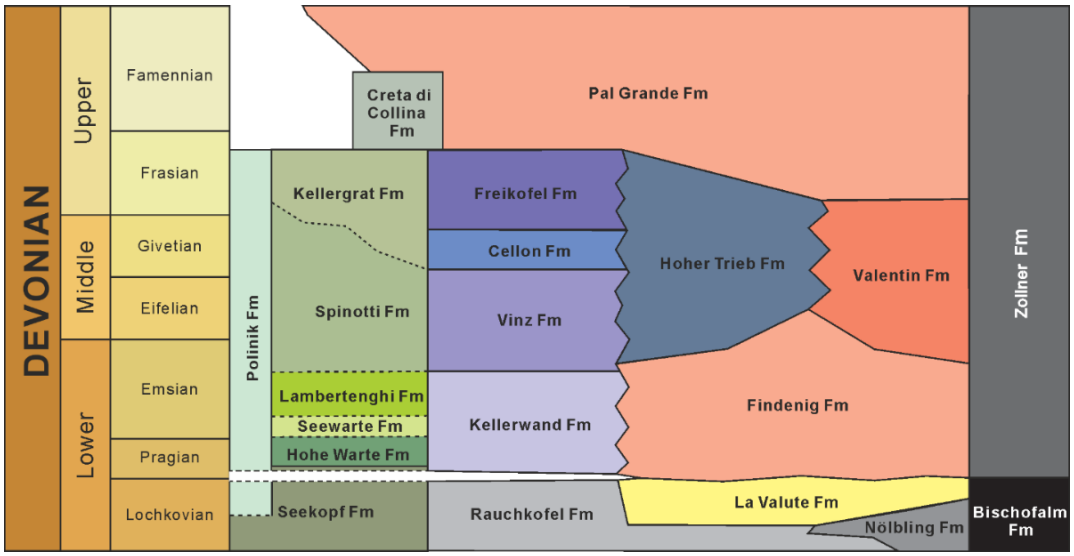

Fig. 6. The stratigraphic scheme of the Devonian part of Pre-Variscan sequence of the Carnic Alps (after Corradini et al. 2015, modified according to Corradini et al. 2024a).

2.2 Longmenshan (South china)

The Longmenshan area is located in the transitional zone between the Sichuan Basin and the eastern margin of the Tibetan Plateau and represents one of the most prominent thrust–nappe structural belts in this area (Zheng et al., 2016). The main body of the Longmenshan belt extends along the northwestern margin of the Upper Yangtze Block (part of the South China Block) in a NE–SW direction. It connects northward with the Qinling Orogen belt and southward with the Kangding Complex, and is bounded by the Songpan–Ganze terrane to the west (Fig. 7; Yan et al., 2018). From the Late Paleozoic to the Early–Middle Triassic, this margin behaved as an extensional passive continental margin and is a product of Hercynian–Indosinian extensional tectonism The Devonian succession in the Longmenshan area is complete and very thick; depositional facies are diverse, fossils are abundant, and the stratigraphic record is continuous, making it an excellent setting for sedimentological and stratigraphic studies (Zheng et al., 2016).

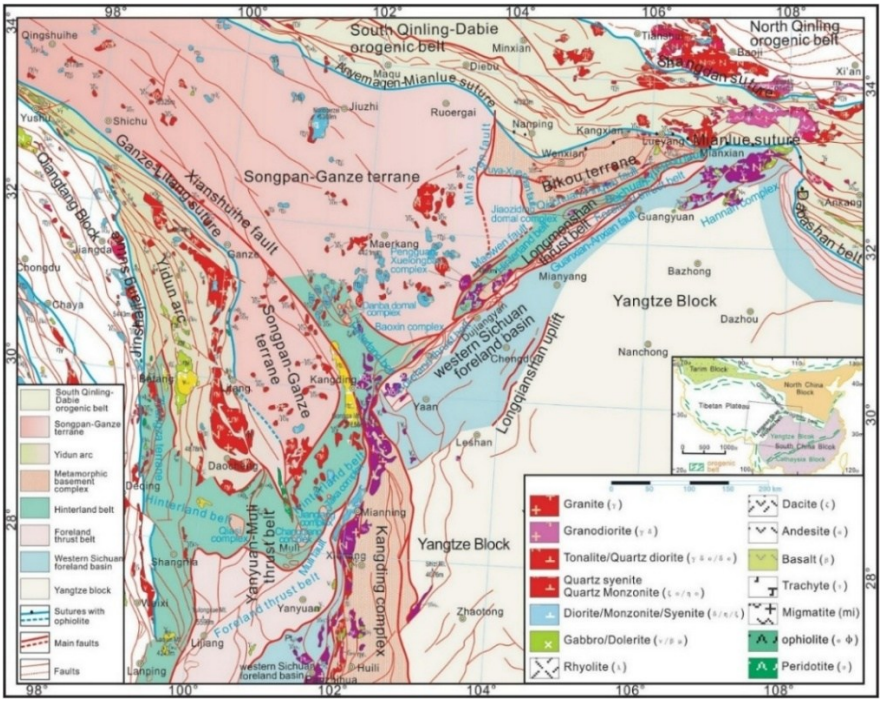

Fig. 7. Division for the tectonic units of the Longmenshan Tectonic Complex and its adjacent: Songpan-Ganze terrane; western Sichuan Basin; and SW-Qinling orogenic belt in the northeast margin of the Tibet Plateau (from Yan et al., 2018).

At the scale of the South China realm, suturing of Cathaysia Block and Yangtze Block during the late Silurian–Early Devonian assembled the South China Block. From the late Emsian to the Eifelian–Givetian, widespread NE- and NW-trending synsedimentary faults developed; during the Devonian, the region represented a passive continental margin (Zhang, 2019). During the Late Devonian, South China resided near the equator under a tropical, humid climate (De Vleeschouwer et al., 2014; Blakey, 2016). Paleogeographically, southern margin of South China multiple isolated carbonate platforms bordered by intraplatform basins produced a mosaic configuration; carbonate platforms also occurred sporadically along the western to northwestern margins (Fig. 8). Such paleogeographic configuration might be attributed to the N-NE migration of the South China Block since the Middle Devonian (Cui et al. 2021).

Following two major Devonian transgressions that advanced toward the N, the area on the southern margin of South China (now mostly in Guangxi and Guizhou) developed a "checkerboard" pattern of alternating platforms and fault-bounded intraplatform troughs (Wu et al., 1997; Zhang, 2019). This pattern reflects the typical filling and reactivation of extensional rift basins, and most previous studies have focused on this area (e.g. Lali section, Nandong section, and Yangdi section; Fig. 8).

By contrast, the Longmenshan area lie across the transition from the platform edge to the basin margin along the NW Upper Yangtze (part of the South China) during the Devonian (Zheng et al., 2016). Water was generally shallow, and sediments were mainly shallow-marine carbonates and siliciclastic deposits from the shoreface. The distribution of facies was closely controlled by small changes in relief along the platform edge and by faults that were active during deposition. These controls caused short-lived shifts between more restricted inner-platform settings and more open platform-margin conditions. During the Late Devonian, the Shawozi and Maoba formations were deposited in here. Detailed descriptions are provided below

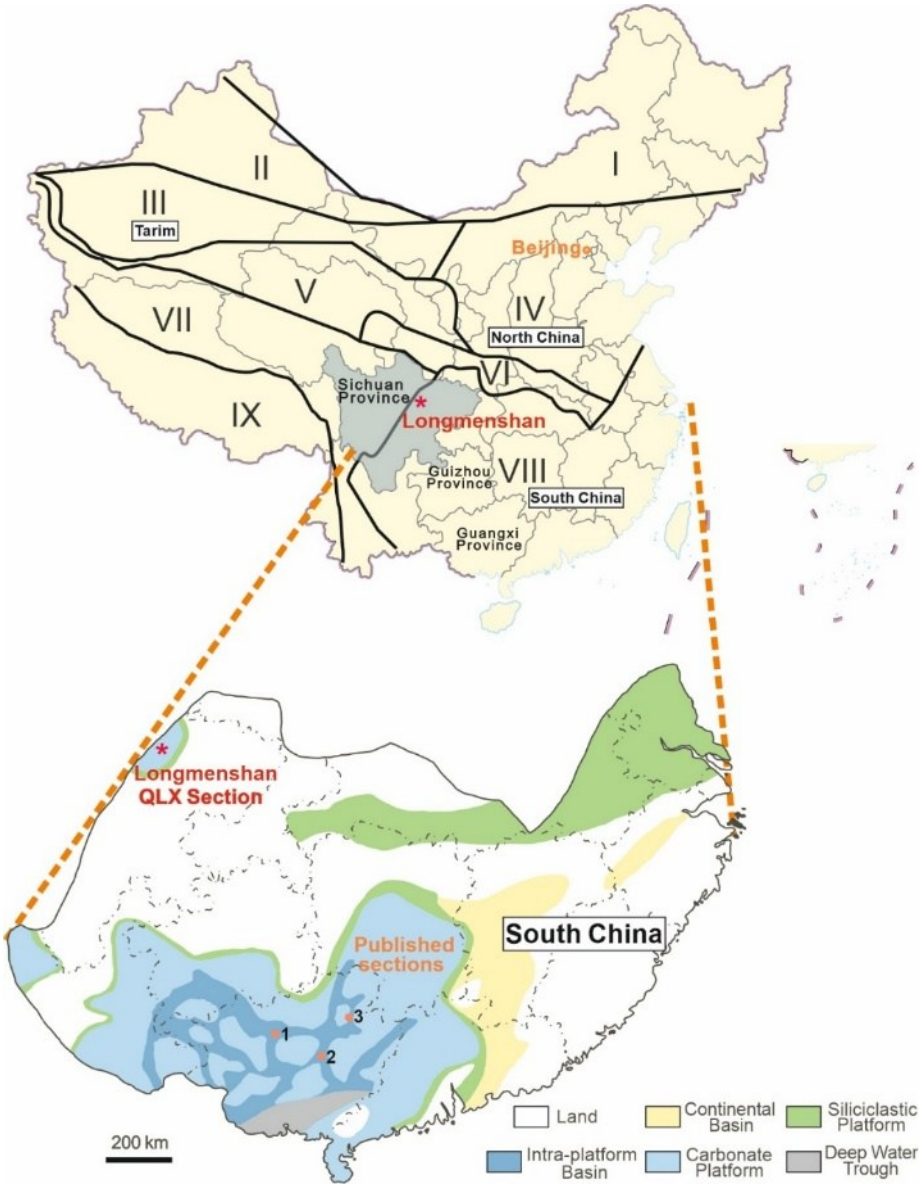

Fig. 8. Devonian Tectonic–Stratigraphic Zonation and Palaeogeographic Reconstruction in South China (modified from Qie et al., 2020). I. Altai-Hinggan; II. Junggar; III. Tarim; IV North China; V. Qilian-Kunlun; VI. Qinling; VII. Qiangtang-Three Rivers; VIII. South China; IX. Himalaya-western Yunnan; The red star Qinglongxia (QLX) section in Sichuan province; 1. Lali section (Ji & Ziegler, 1993; Zhang et al., 2019); 2. Nandong section (Huang et al. 2018b); 3. Yangdi section (Huang et al. 2018a).

The Shawozi Formation primarily consists of gray thin-bedded argillaceous to dolomitic limestone and white to light-gray massive dolostone interbedded with bioclastic micritic limestone or peloidal limestone; in the northeastern Longmen area it is dominated by thin-bedded micritic limestone. The formation represents a shallow-marine carbonate platform environment. Common fossils include brachiopods (*Tenticospirifer, Camarotoechia, Cyrtospirifer*), corals (*Disphyllum, Pseudodazaphrenis*), stromatoporoids (*Hermatostroma, Stachyodes*), spongiomorph (*Amphipora*) and ostracods. Conodonts are rare in this interval, and the conodont zonation is still being refined; the unit is approximately Frasnian (based on other types of fossils). Jiang et al. (1993) attempted to establish a conodont zonation; however, the proposed assemblage zones are broad in temporal range, incomplete, and leave the Frasnian–Famennian boundary unresolved. The absence of illustrated plates further hampers independent verification and inter-regional correlation, rendering the results of limited significance. The unit conformably overlies the Maoba Formation.

The Maoba Formation primarily consists of light gray to gray medium- to thick-bedded wackestone and packstone, and locally containing oolitic or peloidal limestone. The formation represents a shallow-marine carbonate platform environment. Common fossils include rugose corals (*Guerichiphyllum, Siphonophylloides, Beichuanophyllum, Neobeichuanophyllum*) and stromatoporoids (*Cystostroma, Stylostroma, Labechia, Pachystylostroma*), and brachiopods. Conodonts are rare in this interval, and the conodont zonation is still being refined; the unit is approximately Famennian (based on other types of fossils). Xiong et al. (1988) established the *Polygnathus znepolensis–Polygnathus changtanziensis* Zone at the top of this formation. Correlation with *Polygnathus znepolensis* Spassov, 1965 indicates an age from the *Palmatolepis gracilis expansa* Zone to the *Bispathodus ultimus* Zone. *Polygnathus changtanziensis* Ji, 1988 was described as a new species from this locality.

3. Materials and Methods

This study is based on detailed fieldwork and systematic sampling conducted in sections from two distinct regions — the Carnic Alps in Italy and the Longmenshan area in Sichuan, China. It integrates conodont biostratigraphy, microfacies analysis, and stable carbon and oxygen isotope analyses to investigate the Frasnian–Famennian (F–F) boundary interval (detailed geological background and lithological characteristics, see Sections 2, 4.1.1, and 4.2.1). Dense, repeated supplementary sampling across the boundary interval was undertaken to improve stratigraphic (biostratigraphic and chemostratigraphic) resolution.

Conodont biostratigraphy

Rock samples for conodont extraction weighed 1–3 kg, and conodonts were recovered using conventional acid-leaching and sieving procedures. In the laboratory, samples were weighed, rinsed, and immersed in 4% formic acid, with regular acid replacement to ensure complete reaction of carbonate material. The entire leaching process was carried out in an ASEM-brand fume cabinet. Insoluble residues were sieved using a two-step mesh system with 2 mm and ~100 μm screens to retain conodont-enriched fractions. Residues were air-dried at room temperature and manually picked under an OPTIKA stereo microscope equipped with WF10X/22 eyepieces and a zoom range of 0.7× to 4.5×. All sample preparation and conodont picking were conducted at the University of Trieste. SEM micrographs of selected elements were taken at the Interdepartmental Center for Advanced Microscopy of Trieste University.

All conodont specimens recovered in this study are housed in the Palaeontological collection of Department of Mathematics, Informatics and Geoscience, University of Trieste, (DMGTS). Catalogue numbers of figured elements are given in the caption of the figures.

Taxonomic identification was based on well-preserved and morphologically recognizable P1 conodont elements. Identifiable specimens were assigned to species, subspecies, or genus level, and recorded in distribution tables along with the weight of dissolved rock per sample. Broken elements confidently assigned to a genus were marked as “genus + sp.”, and juvenile specimens were recorded as “genus + sp. juv.”. In accordance with the recommendations of previous studies (Girard et al., 2022), the three subspecies of *Icriodus alternatus* (*I. alternatus alternatus* Branson & Mehl, 1934, *I. alternatus helmsi* Sandberg & Dreesen, 1984, and *I. alternatus mawsonae* Yazdi,

1999) were not distinguished in this work, and all specimens were retained under *Icriodus alternatus* at the species level to avoid artificially inflating biodiversity estimates.

The Frasnian conodont biozonation applied in this study follows the revised framework proposed by Klapper and Kirchgasser (2016), hereafter abbreviated as "FZ" (Frasnian Conodont Zones). The Famennian zonation is based on the scheme of Spalletta et al. (2017).

Microfacies analysis

Thin sections were prepared at the University of Trieste. Each slide was examined under a polarizing microscope. We noted grain type and size, matrix and cement, fossil content, and sedimentary structures. Diagenetic features such as recrystallization, pressure-solution seams, and vein cement were also recorded. Microfacies were identified with reference to Flügel (2010), Standard Microfacies (SMF), Carozzi (1989) Ramp Microfacies (RMF), microfacies characteristics and examples from the comprehensive carbonate depositional models of Tucker (1981). Because the PZD section in the Carnic Alps is relatively short and shows uniform lithological characteristics, only a brief description is provided (see Section 4.1.1).

Field observations were then compared with the thin-section results. We related the identified microfacies to lithology, color, sedimentary structures in the outcrop. On this basis, we reconstructed a vertical microfacies succession for the carbonate interval and interpreted the evolution of the depositional environment.

Chemostratigraphic

During field sampling, to preserve the original seawater isotopic signal, fresh rocks were collected while avoiding veins, recrystallized zones, and porous areas. The standard sampling interval was about 1 m, reduced to 20–30 cm near the boundary beds. Each sample weighed more than 100 g and was stored in an individual sealed plastic bag to prevent contamination or mixing. Samples were rinsed and ground to 200 mesh using an agate mortar or handheld drill, then analyzed at the University of Ferrara. Following Spangenberg and Herlec (2006), ~0.5 mg of carbonate powder was reacted with orthophosphoric acid (H_3PO_4) at 70 °C for ~2 h in an automated carbonate preparation system coupled online to an isotope ratio mass spectrometer (IRMS). Carbonate $\delta^{13}C$ and $\delta^{18}O$ values are reported in δ notation relative to Vienna Pee Dee Belemnite (VPDB) and standardized via calibration of reference gases against International Atomic Energy

Agency (IAEA) working standards. The analytical precision, based on replicate analyses of the MAQ-1 standard, is better than ±0.02‰ for $\delta^{13}C$ and ±0.04‰ for $\delta^{18}O$.

Afterward, we plotted whole-rock $\delta^{13}C$ and $\delta^{18}O$ values against each other, a common criterion for assessing diagenetic alteration in carbonates (Hudson, 1977; Brasier et al., 1990). The underlying principle is that, during diagenesis, meteoric or groundwater fluids infiltrate pore spaces and interact with carbonate minerals (Dyer et al., 2015). Unstable minerals such as aragonite or high-Mg calcite may dissolve and reprecipitate as more stable low-Mg calcite. Since meteoric water typically has lower $\delta^{18}O$ values than contemporaneous seawater and may also carry isotopically light carbon (^{12}C) derived from the oxidation of organic matter, both $\delta^{13}C$ and $\delta^{18}O$ values of the host carbonate tend to decrease during such alteration. Consequently, diagenetic overprinting is commonly expressed as a linear positive correlation between $\delta^{13}C$ and $\delta^{18}O$. In contrast, when data points show weak or no linear correlation, the isotope compositions are considered to have retained near-primary signatures (Bathurst, 1972; Knauth & Kennedy, 2009).

4. Studied section

4. 1 The Plan di Zermula D Section in Carnic Alps

4. 1. 1 Fieldwork and sampling

The Plan di Zermula D (PZD) section is located along the road connecting Paularo to Passo del Cason di Lanza in northeastern Italy, at coordinates 46°34′32.104″N, 13°06′42.481″E, at an elevation of approximately 1015 m (Fig. 9). It is measured in a small, abandoned quarry situated just above the steep cliffs of the Rio Chiarsò canyon, providing convenient field access for geological investigations (Fig. 10).

Fig. 9. Location map of the Plan di Zermula D (PZD) section

The section exposes a short, tectonically disturbed interval of the Pal Grande Formation, with a total thickness of approximately 5 meters (Fig. 11). It is overturned, being located along the side of an overturned macrofold constituting the Mt Zermula massif (Venturini, 1991). The lithology is dominated by gray to brownish-gray thin- to medium-bedded micritic limestone, with no significant lateral facies changes or lithologic transitions. A distinctive feature is a ~25 cm-thick dark pelitic layer developed at approximately 1.4 m above the base of the section. This layer is correlative with one of the two Kellwasser type horizons, likely the Upper Kellwasser, testifying the globally significant interval of widespread anoxia and extinction.

The fine-grained texture, absence of high-energy structures, and weak bioturbation support deposition in a basin far from any land, but not deep, and in well oxygenated water. The presence of the black pelitic level could be explained with the physiographic characteristic of the Plan di Zermula area during the Late Devonian and early Carboniferous when the area was probably a narrow and deeper trough that favoured restricted water circulation on the bottom (Spalletta et al. 2021). Microfacies analysis show that the section is composed predominantly of fine-grained

micritic limestone with very limited bioturbation and sparse occurrences of thin-shelled bioclasts (Fig. 10D). Thin sections of samples PZD 5 and PZD 6, which lie immediately above the black shale layer, are characterized by a dense network of bright, sparry calcite-filled fractures and stylolitic sutures (Fig. 10E).

Fig. 10. Field views of the PZD section (A-C) and selected microfacies (D-E). A. panoramic view of the section with indication of samples. B. close view of the black shale interval and of the Frasnian/Famennian boundary. C. detail of the upper part of the section. D. microfacies of sample PZD 3 (FZ 13b) showing micritic matrix with sparse thin-shelled bioclasts. E. microfacies of sample PZD 5 (*Pa. subperlobata* Zone) showing sparry calcite-filled fractures and stylolites.

4. 1. 2 Conodont Data

The collected samples yielded 2,192 identifiable conodont P1 elements, with sample-specific abundances ranging from 8 to 237 elements per kilogram of rock (Tab. 1). The state of preservation is in general quite good, even if some elements are incomplete and partly broken. The Color Alteration Index (CAI) is 4-4.5.

In total, 44 taxa (species, subspecies, and morphotypes) were identified, belonging to seven genera: *Ancyrodella*, *Ancyrognathus*, *Icriodus*, *Mehlina*, *Palmatolepis*, *Pelekysgnathus*, and *Polygnathus* (Tab.1). Among these, *Palmatolepis*, *Polygnathus*, and *Icriodus* were the most common.

4. 1. 2. 1 Biostratigraphy

Seven consecutive conodont zones spanning the late Frasnian to early Famennian (from the FZ 13b to the *Palmatolepis crepida* Zone) have been identified in the PZD section (Fig. 11). Below the biostratigraphic criteria, key index taxa, and local occurrences for each of these zones are described in detail.

Frasnian Zone (FZ) 13b

Frasnian Zone (FZ) 13b corresponds to the *Palmatolepis linguiformis* Zone proposed by Ziegler and Sandberg (1990). The base of this zone is marked by the First Appearance Datum (FAD) of *Palmatolepis linguiformis* Müller, 1956, and covers the entire stratigraphic range of *Pa. linguiformis* (Sandberg et al., 1988; Klapper & Kirchgasser, 2016). In the PZD section, this zone has been discriminated in the lower part of the section, from the base to the bed of sample PZD 3, where conodonts are well preserved and biodiversity is relatively high.

In addition to the index fossil *Palmatolepis linguiformis*, associated species include *Pa. bogartensis*, *Pa. boogaardi*, *Pa. winchelli*, *Pa. juntianensis*, *Pa. rhenana*, *Polygnathus decorosus*, *Po. lodinensis*, *Po. mirificus*, *Po. elegantulus*, *Po. aequalis*, *Po. webbi*, *Ancyrodella hamata*, *Anc. curvata*, *Ancyrognathus.* cf. *asymmetricus*, *Pelekysgnathu planus*, and *Icriodus alternatus*. Among

these, *Ancyrodella hamata*, *Ancyrognathus* cf. *asymmetricus*, and *Polygnathus elegantulus* became extinct within this zone.

The abundances of *Palmatolepis linguiformis*, *Pa. bogartensis*, *Po. lodinensis*, and *Polygnathus decorosus* are relatively high. It is noteworthy that *Polygnathus decorosus* shows a high abundance at its initial occurrence in the lower part of the zone but rapidly decreases toward the top of FZ 13b, indicating a brief bloom event, as already reported for the same biozone in Farabegoli et al. (2023).

Frasnian Zone (FZ) 13c

Frasnian Zone (FZ) 13c corresponds to the upper part of the *Palmatolepis linguiformis* Zone by Sandberg et al. (2002) and represents the uppermost biozone of the Frasnian. In the PZD section, the base of this zone is approximated by the FAD of the index species *Palmatolepis ultima* Ziegler, 1958 (Klapper, 2007b; Farabegoli et al., 2023), identified in sample PZD 4 immediately beneath the black shale interval. The association reflects what was already observed in the other two sections of the Carnic Alps recording the F-F boundary (Freikofel T and Pramosio A; Farabegoli et al., 2023).

In addition to *Palmatolepis ultima*, the identified taxa mainly include *Pa. boogaardi*, *Pa. winchelli*, *Pa. juntianensis*, *Pa. bogartensis*, *Pa. linguiformis*, *Pa. rhenana*, *Pa. beckeri*, *Polygnathus brevis*, *Po. decorosus*, *Po. lodinensis*, *Po. mirificus*, *Po. aequalis*, *Po. macilentus*, *Po. webbi*, *Ancyrodella curvata*, and *Icriodus alternatus*.

It is noteworthy that *Palmatolepis linguiformis*, *Pa. juntianensis*, *Pa. boogaardi*, and *Ancyrodella curvata* are still present in Zone 13c, although only in very low abundance. This pattern is consistent with previous reports from nearby Carnic Alps sections (Farabegoli et al., 2023), where these taxa have been interpreted as potential late survivors or representatives of ecological refugia during this interval.

Furthermore, rare occurrences of *Palmatolepis beckeri* (1 specimen) and *Polygnathus brevis* (3 specimens), taxa typically restricted to the underlying FZ 13b (Klapper, 2007b; Klapper & Kirchgasser, 2016), were recorded slightly above their conventional Last Appearance Datum (LAD) in the PZD section. While the precise cause remains uncertain, these occurrences are

considered part of the faunal assemblage of Zone 13c based on the stratigraphic position of the samples and the FAD of *Palmatolepis ultima*.

Palmatolepis subperlobata Zone

The *Palmatolepis subperlobata* Zone represents the first biozone of the Famennian, and is defined by the first appearance of *Palmatolepis subperlobata* Branson & Mehl, 1934, following the zonation proposed by Spalletta et al. (2017). The level of sample PZD 5 is assigned to this zone by the presence of the index species.

In several nearby sections within the Carnic Alps (e.g., PRA and FRKT), the FAD of *Palmatolepis subperlobata* is typically accompanied by a marked flood occurrence of *Pa. ultima* (Farabegoli et al., 2023). This flood event was previously proposed by Klapper et al. (2004) and Klapper (2007b) as a biostratigraphic marker for defining the Frasnian–Famennian boundary. However, this pattern is not observed in the PZD section, where *Palmatolepis ultima* is only sporadically present and in very low abundance.

Additionally, the conodont assemblage from the PZD section displays extremely low taxonomic diversity. Only three species have been identified: the index taxon *Palmatolepis subperlobata*, *Mehlina gradata*, and a few specimens of *Pa. ultima*. The faunal composition reflects a markedly simplified conodont community following the extinction event. *Palmatolepis ultima* is the only species of *Palmatolepis* that crosses the boundary and continues into this zone.

Palmatolepis triangularis Zone

The base of the *Palmatolepis triangularis* Zone is defined by the FAD of *Palmatolepis triangularis* sensu Klapper in Klapper et al. (2004). In the PZD section, this zone has been identified in beds of samples PZD 5A and PZD 5B.

In addition to the index fossil *Palmatolepis triangularis*, the conodont assemblage of this zone includes *Icriodus alternatus*, *Pa. ultima*, *Pa. subperlobata*, *Pa. delicatula delicatula*, *Polygnathus brevilaminus*, and *Po. praecursor*. The assemblage composition is consistent with

that observed in adjacent sections (Farabegoli et al., 2023), although overall taxonomic diversity remains low.

Palmatolepis delicatula platys Zone

The base of the *Palmatolepis delicatula* platys Zone is defined by the FAD of *Pa. delicatula platys* Ziegler & Sandberg, 1990. In the PZD section, this zone has been recognized in level of sample PZD 6, by the entry of the index taxon.

The conodonts association of this zone includes *Icriodus alternatus*, *Palmatolepis ultima*, *Pa. subperlobata*, *Pa. triangularis*, *Pa. protorhomboidea*, *Polygnathus brevilaminus*, The LAD of *Palmatolepis ultima* is consistent with previous studies reporting its extinction at the top of this zone.

Palmatolepis minuta minuta Zone

The base of the *Palmatolepis minuta minuta* Zone is defined by the FAD of *Pa. minuta minuta* Branson & Mehl, 1934. In the PZD section, this zone has been identified in samples PZD 6A and PZD 7.

The conodont assemblage from these samples includes *Palmatolepis minuta minuta*, *Pa. delicatula delicatula*, *Pa. delicatula platys*, *Pa. subperlobata*, *Pa. triangularis*, *Pa. clarki*, *Pa. protorhomboidea*, *Polygnathus brevilaminus*, *Po. praecursor*, *Po. procerus*, *Icriodus alternatus, and Icr. cornutus*.

Notably, *Polygnathus procerus* is recorded for the first time in this interval, in agreement with previously established biostratigraphic range (Spalletta et al., 2017). The specimens identified in this study conform to the original species concept and diagnosis of *Polygnathus procerus* as established by Sannemann (1955a), based on the holotype. We do not adopt the broader morphological interpretation illustrated by Schülke (1999, Pl. 13, figs. 12–18), which is considered inconsistent with the type diagnosis.

Palmatolepis crepida Zone

The base of the *Palmatolepis crepida* Zone is defined by the FAD of *Palmatolepis crepida* Sannemann, 1955. In the PZD section, it occurs in the upper part of the section, from samples PZD 8 through PZD 12.

In addition to the index taxon *Palmatolepis crepida*, the identified fauna includes *Ancyrognathus cryptus, Icriodus alternatus, Icr. cornutus, Icr. iowaensis iowaensis, Mehlina gradata, Palmatolepis clarki, Pa. delicatula delicatula, Pa. delicatula platys, Pa. lobicornis, Pa. minuta minuta, Pa. protorhomboidea, Pa. quadrantinodosalobata, Pa. regularis, Pa. robusta, Pa. spathula, Pa. subperlobata, Pa. tenuipunctata, Pa. triangularis, Pa. werneri, Pelekysgnathus planus, Polygnathus brevilaminus, Po. eoglaber, Po. nodocostatus nodocostatus, Po. praecursor, Po. procerus*. Additionally, this zone records several first and last occurrences. *Palmatolepis delicatula delicatula*, *Pa. triangularis*, *Pa. delicatula platys*, and *Pa. clarki* are not found above this interval, while *Pa. spathula* reaches its last occurrence at the top of the zone. *Pa. quadrantinodosalobata* enters at the base of the zone, and *Polygnathus nodocostatus nodocostatus* is first recorded in the middle part.

It is noteworthy that a marked increase in taxonomic diversity and abundance is observed in this zone. Compared to the underlying intervals, the species composition is richer, and several taxa that were previously rare or poorly preserved become more frequent and more easily identifiable.

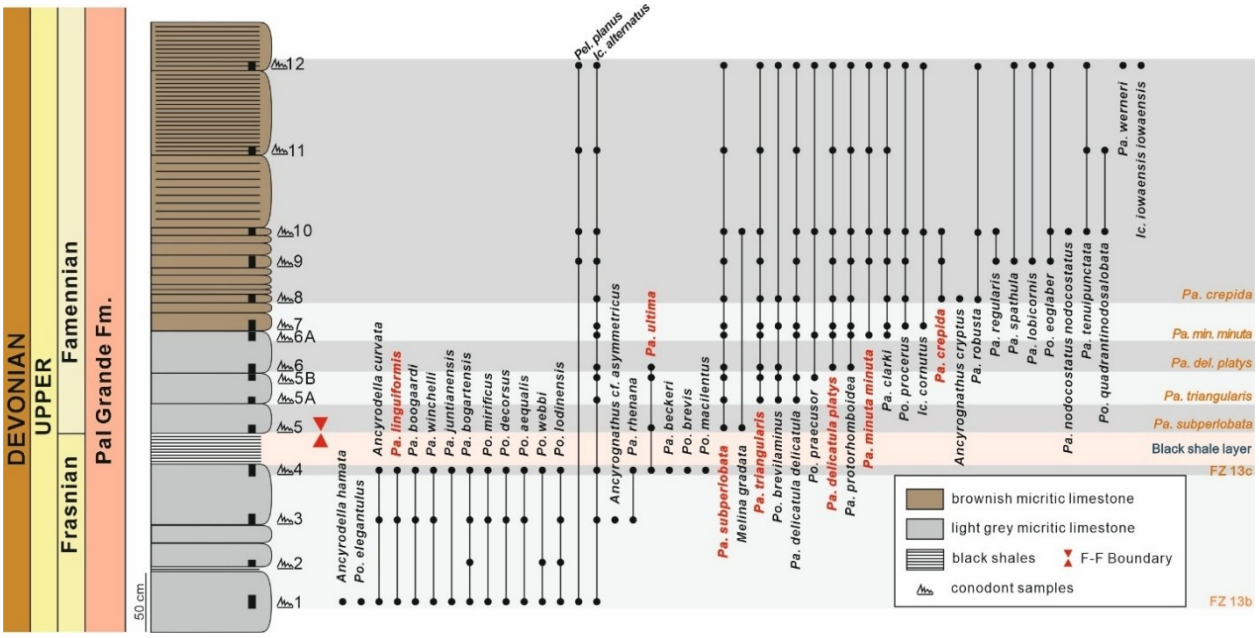

Fig. 11. Stratigraphic column and occurrence of conodonts in PZD section. From Left to right: Chronostratigraphy (Period, Series, Stage), stratigraphic column, conodont sample position, occurrence of conodont taxa, Biozones. Abbreviations: *Ic.* - *Icriodus*, *Pa.* - *Palmatolepis*, *Pel.* - *Pelekysgnathus*, *Po.* - *Polygnathus*.

4. 1. 2. 2 Conodont Biofacies

We conducted genus-level statistical analysis of the conodont data from the PZD section, focusing on both overall conodont abundance and the percentages of genera within each sample. A total of seven genera were identified: *Ancyrodella*, *Ancyrognathus*, *Icriodus, Mehlina*, *Palmatolepis*, *Pelekysgnathus,* and *Polygnathus*, with *Palmatolepis***,** *Polygnathus*, and *Icriodus* being the most common. To identify the biofacies types and reflect water depth changes we used the conodont biofacies model of Ziegler and Sandberg (1990). A higher threshold of 75% (instead of the usual 70%) was applied to improve classification accuracy and reduce the impact of mixed assemblages.

The figure illustrates the abundances of the dominant genera (*Palmatolepis*, *Polygnathus*, and *Icriodus*) and the percentages of genera (Fig. 12). The results show that most samples from the PZD section (PZD 3, and PZD 5A to PZD 11) are assigned to the palmatolepid biofacies, with the relative abundance of *Palmatolepis* exceeding 75% in most samples. This trend is consistent with the observations of Farabegoli et al. (2023) from nearby sections (such as PRA and FRKT), where *Palmatolepis* generally accounts for 70–80% of the assemblage from the late Frasnian 13c Zone to the early Famennian *Pa. minuta minuta* Zone. In the other samples (PZD 1, PZD 2, PZD 4, and PZD 12), a decrease in *Palmatolepis* abundance is accompanied by an increase in *Polygnathus*, with the latter reaching as high as 54.55% in PZD 2. These samples are therefore assigned to the palmatolepid-polygnathid biofacies.

In addition, although *Icriodus* generally occurs at low frequencies, it displays a marked increase in a few samples, such as PZD 5A (16.67%), PZD 5B (10.53%), and PZD 12 (18.43%). The distribution of this genus commonly overlaps with *Palmatolepis*, but rarely coincides with high abundances of *Polygnathus* (also reported by Farabegoli et al. 2023). However, since the combined abundances of *Polygnathus* and *Icriodus* remain low throughout the section, no samples from the PZD section can be clearly assigned to the polygnathid–icriodid biofacies as defined by Ziegler and Sandberg (1990). A palmatolepid-icriodid biofacies was discriminated in a few levels of early Famennian age in Sardinia by Corradini (1998, 2003), but the genus *Icriodus* was represented almost exclusively by *Icr. olivieri* Corradini, 1998, that the author supposed to live more far from the coast than the other representative of the genus.

In summary, genus-level conodont data from the PZD section reveal the dominance of open sea taxa (*Palmatolepis*) throughout the study interval, with only minor increases of *Icriodus* and *Polygnathus* at certain horizons.

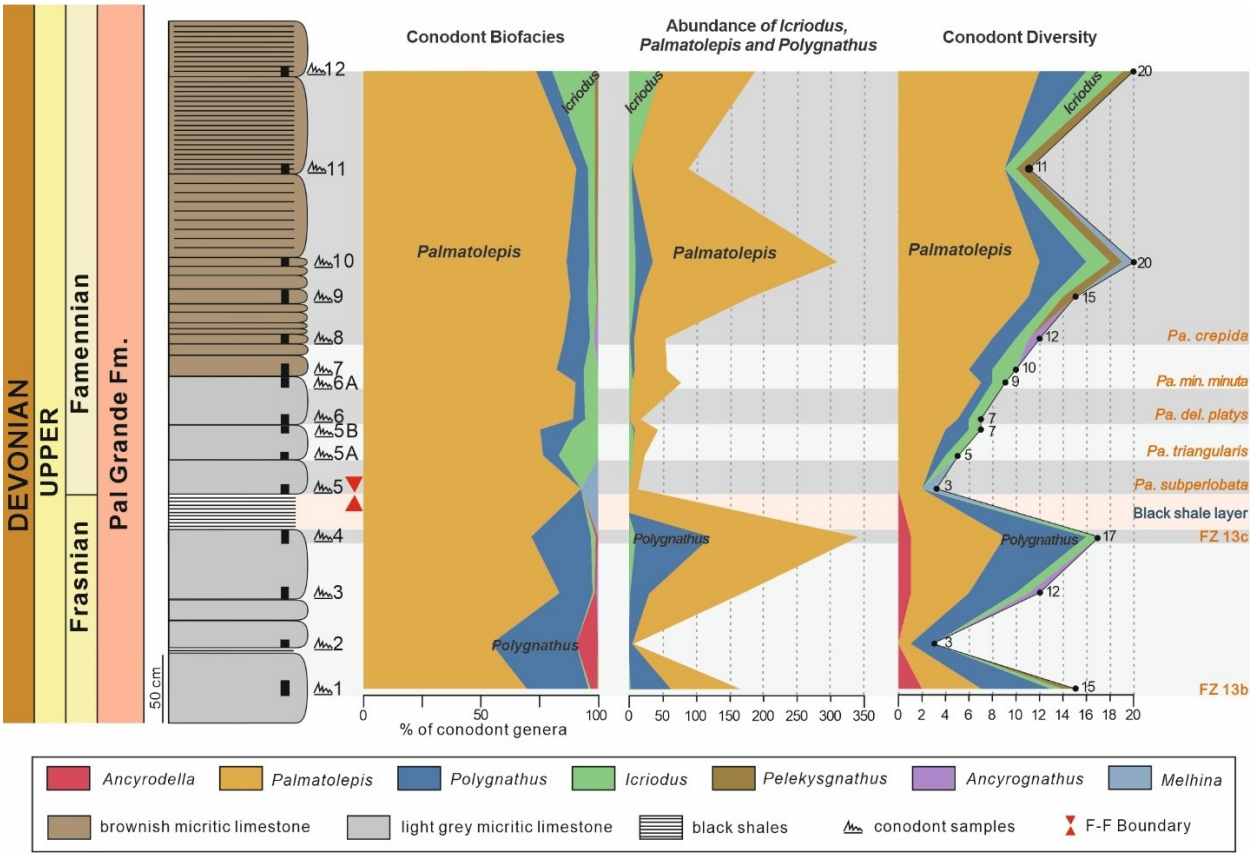

Fig. 12. Conodont biofacies, Abundance of P1 elements and species diversity in the PZD section.

Conodont zones	FZ 13b			FZ 13c	Pa. subpe	Pa. triangularis		Pa. del.pla.	Pa. minuta minuta		Pa. crepida					Tot.
Sample name	PZD-01	PZD-02	PZD-03	PZD-04	PZD-05	PZD-5A	PZD-5B	PZD-06	PZD-06A	PZD-07	PZD-08	PZD-09	PZD-10	PZD-11	PZD-12	
Sample weight (Kg)	0.9993	1.0513	1.1062	2.569	1.8304	0.8604	0.7692	1.1514	0.9321	1.0055	1.5302	1.157	1.6004	0.4298	1.305	
Ancyrodella curvata	2		2	3												5
Ancyrodella hamata	3															0
Icriodus alternatus	2		1	10		5	4	1	3	2	1	6	8	3	41	85
Palmatolepis bogartensis	24	3	7	7												17
Palmatolepis boogaardi	10		8	12												20
Palmatolepis juntianensis	11			10												10
Palmatolepis linguiformis	8		19	23												42
Palmatolepis winchelli	5		2	5												7
Pelekysgnathus planus	1											1	3	1	3	8
Polygnathus aequalis	3		2	7												9
Polygnathus decorosus	24		1	1												2
Polygnathus elegantulus	2															0
Polygnathus ladinensis	12	1	16	69												86
Polygnathus mirificus	3		2	7												9
Polygnathus webbi	1	1		3												4
Ancyrognathus cf. asymmetricus			1													1
Palmatolepis rhenana			1	3												4
Palmatolepis beckeri				3												3
Palmatolepis ultima				1	2		4	3								10
Polygnathus brevis				1												1
Polygnathus macilentus				4												4
Mehlina gradata					1								1			2
Palmatolepis subperlobata					5	5	14	1	4	4	3	15	37	10	17	115
Palmatolepis delicatula delicatula						5	6		5	4	6	17	14	10	25	92
Palmatolepis triangularis						2	2	2	3	4	1	2	16	3	12	47
Polygnathus brevilaminus						1	3	1		1	2				1	9
Polygnathus praecursor							3		1				14		1	19
Palmatolepis delicatula platys								3	5	3	4	7	11	11	5	49
Palmatolepis protorhomboidea								1	5	3	5	5	11	4	2	36
Palmatolepis clarki									2	2	7	7	14	1	10	43
Palmatolepis minuta minuta									2			6	8	3	2	21
Icriodus cornutus										1			1		1	3
Polygnathus procerus										4	3	7	5		8	27
Ancyrognathus cryptus											1					1
Palmatolepis crepida											5	2	2			9
Palmatolepis robusta											2		2		2	6
Palmatolepis labicornis												1			4	5
Palmatolepis regularis												2	8			10
Palmatolepis spathula												3			10	13
Polygnathus eoglaber												2	2		5	9
Palmatolepis quadrantinodosalobata													2	1		3
Palmatolepis tenuipunctata													5	3	4	12
Polygnathus nodocostatus nodocostatus													1			1
Icriodus iowaensis iowaensis															1	1
Palmatolepis werneri															2	2
Ancyrodella sp.		1		1												2
Ancyrodella sp. juv.	1															1
Icriodus sp.							2		2	1		2			4	11
Palmatolepis sp.	64	3	83	195	6	10	17	7	45	36	19	113	166	43	77	884
Palmatolepis sp. juv.	44		50	84		1			6		2	9	15		16	227
Polygnathus sp.	15	2	7	17		1	2		1	3	2	1	10	4	2	67
Polygnathus sp. juv.	2		1	13					1			6	3	1		27
Total	237	11	203	479	14	30	57	19	85	68	63	214	359	98	255	2192

Table 1 Numerical distribution of P1 conodont elements in Plan di Zermula D (PZD) section.

4. 1. 2. 3 Diversity Trends Across the F–F Boundary

The conodont assemblage of the PZD section clearly records the extinction and recovery processes across the Frasnian–Famennian (F–F) boundary. Figure 12 shows variation in total abundance of the association and diversity. The abundance is normalized per kg of rock, and the diversity is counted at specific level.

Phase 1 (Late Frasnian High Diversity)

In the late Frasnian (samples PZD 1 to PZD 4), the conodont fauna shows high taxonomic diversity ranging between 14 and 17 identified species and subspecies per sample. Sample PZD 1 records the highest abundance of 237 elements per kilogram. During this phase, assemblages were characterized by dominant genera such as *Palmatolepis* (e.g., *Pa. linguiformis*, *Pa. bogartensis*), and *Polygnathus* (e.g., *Po. decorosus*, *Po. lodinensis*), accompanied by subordinate occurrences of *Icriodus* and *Ancyrodella*. The uppermost Frasnian sample (PZD 4, FZ 13c) is still characterized by a relatively high diversity with 17 species/subspecies identified, indicating a stable, diverse, and productive ecological system prior to the extinction event.

Phase 2 (Basal Famennian Low Diversity Minimum)

At the base of the Famennian (sample PZD 5), just above the black shale interval and the extinction event, conodont diversity sharply decreased to only three identified taxa, reflecting a drastic diversity loss of approximately 80% compared to the immediately underlying sample (PZD 4). Only a few opportunistic taxa, notably *Icriodus alternatus*, and scarce representatives of *Palmatolepis ultima*, persisted through this interval at very low abundance (8 elements/kg), and *Palmatolepis subperlobata* (marking the base of its biozone) enters. Unlike contemporaneous records from neighbouring sections (Farabegoli et al., 2023), no occurrence of the flood of *Pa. ultima* was observed at this interval, suggesting possible differences in local environmental conditions affecting productivity and preservation.

Phase 3 (Early Famennian Gradual Recovery):

Conodont diversity began a gradual but clear recovery during the early Famennian, initially remaining relatively low (5–10 taxa per sample) from the *Pa. triangularis* through the *Pa. minuta minuta* zones (samples PZD 5A-7) zones. A significant increase in diversity became evident in the subsequent *Pa. crepida* Zone (samples PZD 8-12), with samples PZD 10 and PZD 12 reaching a

peak of approximately 20 taxa. This diversity increase coincided with notable recovery in genus-level abundance, particularly among the genera *Palmatolepis* and *Polygnathus*, suggesting ecosystem stabilization and renewed availability of ecological niches.

Overall, the detailed data from the PZD section clearly illustrate a strong ecological response associated with the F–F extinction event: an abrupt decline in biodiversity at the boundary, followed by a protracted and gradual recovery of conodont communities during the early Famennian.

4. 1. 3 Carbon and oxygen isotope records

All carbonate samples in this study were collected from the PZD section, belonging to the same stratigraphic unit, the Pal Grande Formation. The succession is well exposed and lithologically continuous, allowing reliable stratigraphic correlation. A detailed reliability assessment of the carbon and oxygen isotope data was performed.

The $\delta^{13}C_{carb}$ values from the PZD section range from +1.41‰ to +3.31‰ (VPDB), while $\delta^{18}O_{carb}$ values vary between -5.61‰ and -4.64‰ (Fig. 14). In the lower part of the section (samples PZD 1-4), $\delta^{13}C_{carb}$ values remain relatively low and stable, averaging around +1.5‰. From PZD 5 upward, $\delta^{13}C_{carb}$ values gradually increase, reaching +2.97‰ at PZD 5A and with a peak of +3.31‰ at PZD 8. Above this level, values remain high (mostly between +3.0‰ and +3.3‰) before showing a slight decrease to +2.59‰ at the topmost sample (PZD 12). Overall, the upper part of the section records a distinct positive excursion of approximately +1.8‰ (from +1.5‰ to +3.3‰).

In contrast, $\delta^{18}O_{carb}$ values display only minor variations (within ~1.4‰) throughout the succession and show no systematic stratigraphic trend. The weak covariance between $\delta^{13}C_{carb}$ and $\delta^{18}O_{carb}$ (Pearson's $r = -0.220$; $r^2 = 0.048$) indicates minimal diagenetic overprinting and supports the reliability of the carbon isotope dataset (Fig. 13).

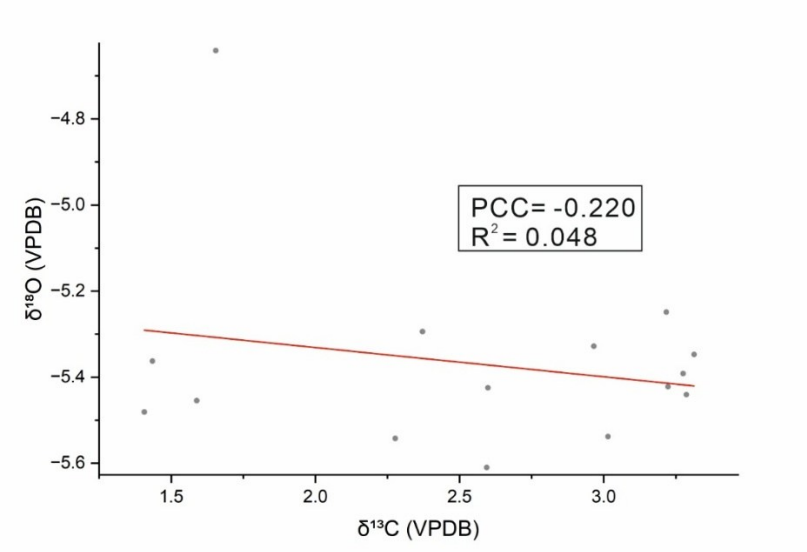

Fig. 13. Cross plot of carbon and oxygen isotope data from the PZD section. PCC=Pearson Correlation Coefficient.

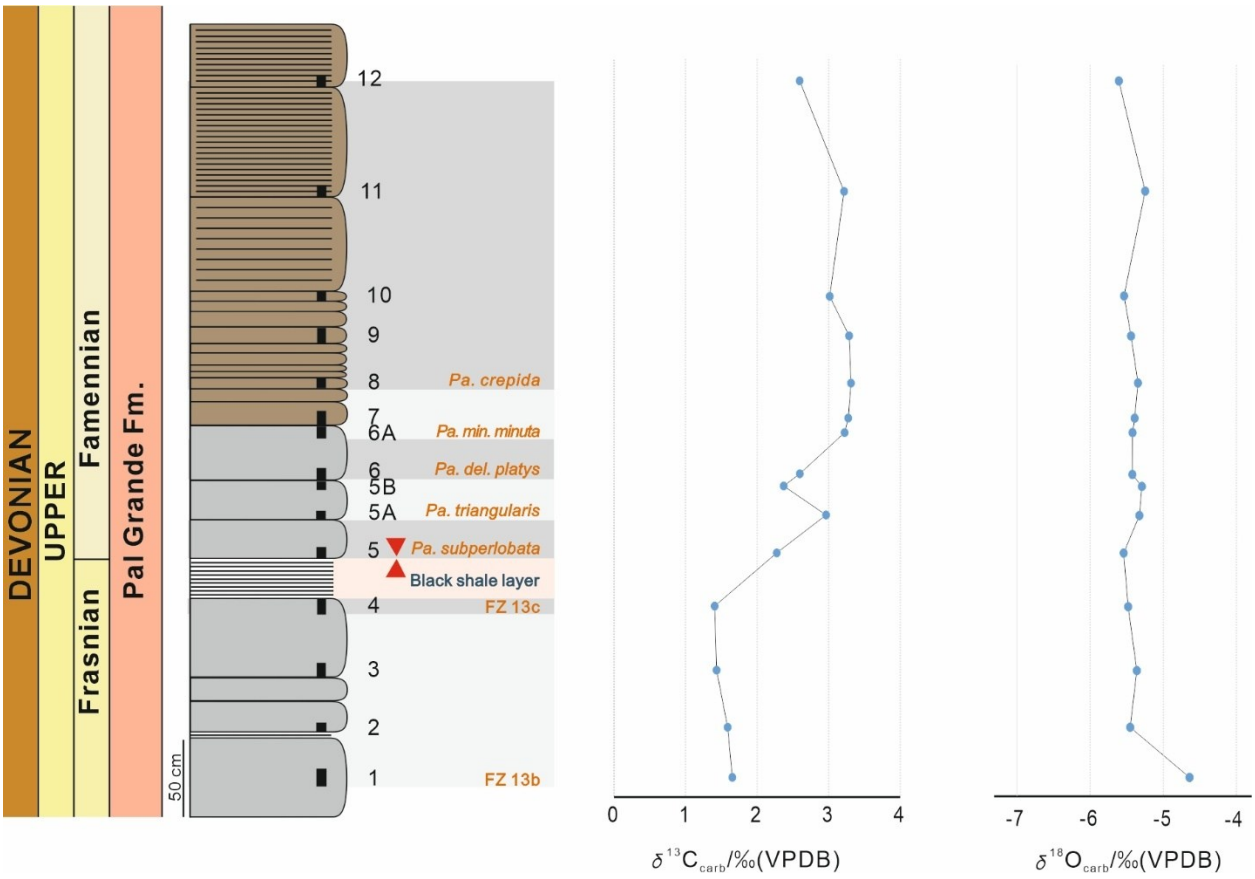

Fig. 14. $\delta^{13}C_{carb}$ and $\delta^{18}O_{carb}$ profiles of the PZD section showing the Frasnian–Famennian boundary interval.

4. 2 The Qinglongxia Sections in Longmenshan

4. 2. 1 Fieldwork and sampling

The Qinglongxia sections are located about 100 m southwest of Maobazi in Jingyuan Township, Jiangyou City, Sichuan, China (Fig. 15). The outcrops lie directly beside Provincial Road S209 and the Qingshui River, approximately 4 km northwest of Yanmen Town. The exposure is excellent and continuous, making the site ideal for field investigation. Two stratigraphic sections, Qinglongxia A (QLX A) and Qinglongxia B (QLX B), were measured in this area. The two sections are separated by a fault, and the outcrops are largely covered by dense vegetation (Fig. 15B). The overall folding structures indicate a regional compressional deformation pattern. Detailed descriptions of the two sections are presented below.

The Qinglongxia A (QLX A) section is located at 30°14′17.51″ N, 105°09′31.39″ E. The section is continuously exposed along a road cut and a hillside for approximately 160 m. The lower part (0–120 m) belongs to the Shawozi Formation and consists mainly of dark gray to black micritic limestone and wackestone, which are thin- to medium-bedded and well-lithified. Bedding planes are generally straight and display good lateral continuity. Alternating light and dark bands, together with several thin marly or clay-rich interbeds, are visible. Small calcite veins and occasional joints are present locally. The upper part (120–160 m) corresponds to the Maoba Formation and is composed of gray, medium- to thick-bedded limestone. In outcrop, the contact between the two formations appears conformable, showing continuous. Conodont biostratigraphy ranges from the FZ 3 Zone to the *Palmatolepis gracilis expansa* Zone (see Section 4.2.2.1), spanning the Frasnian–Famennian boundary. However, the section lacks the typical lithological features commonly developed at this boundary, such as black, organic-rich shales.

The Qinglongxia B (QLX B) section is located at 30°14′20.95″N, 105°09′27.42″E, with a total thickness of approximately 40 m. The succession is dominated by medium- to thick-bedded gray to light-gray grainstones, interbedded with thin layers of micritic limestone or dark-colored laminae. Locally, broken, rolled, or torn structures are observed, indicating short-term high-energy events or reworking processes along a carbonate shoal margin. Hand specimens of the grainstones are uniformly light gray and compact, with evenly distributed grains and a sparkling appearance on fresh surfaces due to abundant fine ooids, representing a typical high-energy shoal facies. The

entire sequence belongs to the Shawozi Formation. Conodont biostratigraphy ranges from the the *Palmatolepis marginifera utahensis* Zone to the *Bispathodus costatus* Zone (see Section 4.2.2.2).

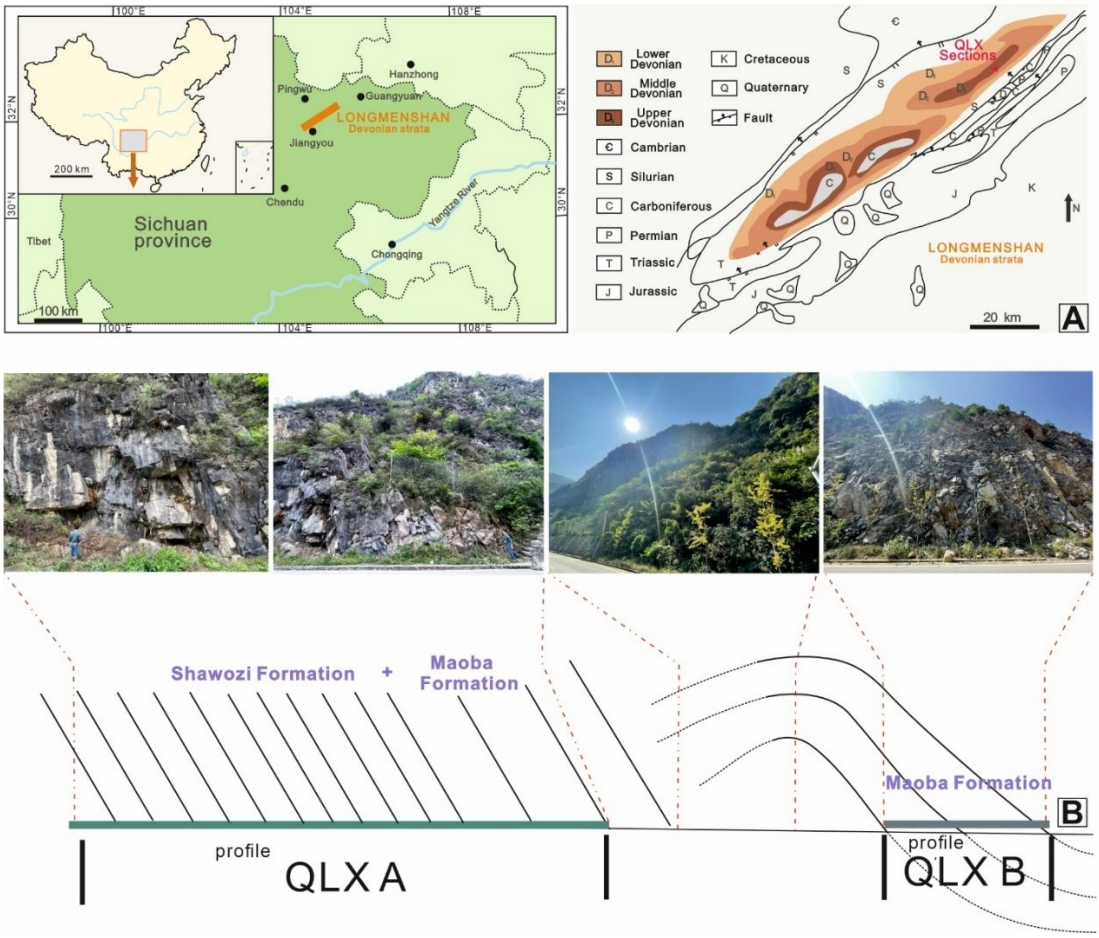

Fig. 15. A. Location map of the Qinglongxia (QLX) sections; B. Schematic diagram illustrating the spatial relationship between the QLX A and QLX B sections.

4. 2. 2 Conodont Data

The collected samples yielded 891 identifiable conodont P1 elements, with sample-specific abundances ranging from 0.3 to 45 elements per kilogram of rock (Tabs. 2-3). The state of preservation is in general quite good, even if some elements are incomplete and partly broken. The Color Alteration Index (CAI) is 4-4.5.

In total, 19 taxa (species, subspecies, and morphotypes) were identified, belonging to four genera: *Branmehla, Mehlina, Polygnathus, Pseudopolygnathus* (Tabs. 2-3). Among these, *Polygnathus* were the most common.

4. 2. 2. 1 Biostratigraphy in QLX A section

In the QLX A section, one well-defined and several conodont zones are recognized, spanning the Frasnian to Famennian. From bottom to top, these are: FZ 3–FZ 4, FZ 5, FZ 6–FZ 11, FZ 12–FZ 13a, FZ 13b–*Palmatolepis crepida*, *Palmatolepis termini–Palmatolepis velifer velifer*, and *Palmatolepis rugosa trachytera–Palmatolepis gracilis expansa* (Fig. 16).

FZ 3–FZ 4 (undifferentiated)

This zone represents the lowermost unit of the QLXA section. The conodont assemblages from samples QLXA C1, QLXA C2, QLXA C3, and QLXA C5 are characterized by very low abundances, yielding only 0.3-2 identifiable P1 elements per kilogram of rock. The faunal composition is exclusively represented by two genera, *Polygnathus* and *Mehlina*. The identified species include *Mehlina gradata* (Branson & Mehl, 1934), *Polygnathus alatus* Huddle, 1934, and *Polygnathus xylus* Stauffer, 1940.

According to the ranges summarized by Ovnatanova et al. (2017), *Polygnathus alatus* occurs from FZ 1 to FZ 5, *Polygnathus xylus* from the Givetian to FZ 5/6, and *Mehlina gradata* extends from FZ 3 to the *Palmatolepis marginifera marginifera* Zone. The succeeding sample (QLXA C6) contains *Polygnathus decorosus*, whose first occurrence lies within the FZ 5/6 (Ovnatanova et al., 2017). Taken together, these overlapping ranges constrain the QLXA C1-C5 interval to FZ 3–FZ 4 Zone, pending the first appearance of *Po. decorosus* at FZ 5/6.

FZ 5

In the QLX A section, samples QLXA C6 and QLXA C6A yield approximately 3 identifiable P1 elements per kilogram of rock. The assemblage is again restricted to *Polygnathus* and *Mehlina*, comprising *Mehlina gradata*, *Polygnathus alatus*, *Polygnathus xylus*, *Polygnathus decorosus* Stauffer, 1938, and *Polygnathus zinaidae* Kononova, Alekseev, Barskov & Reimers, 1996.

Among these species, *Polygnathus decorosus* first appears in this interval, which indicates entry into FZ 5. Most of the other taxa also have ranges consistent with FZ 5. In addition, *Polygnathus alatus* (FZ 1–FZ 5) and *Polygnathus xylus* (Givetian–FZ 5/6) both disappear above this level. Considering all these lines of evidence, the interval is assigned to FZ 5. The only notable mismatch concerns *Polygnathus zinaidae*, whose range from FZ 7/8–FZ 11/12 (Ovnatanova & Kononova, 2008). Its occurrence here may indicate a slightly longer stratigraphic range in this succession than previously reported.

FZ 6–FZ 11 (undifferentiated)

In the QLXA section, the zone includes samples QLXA C6D-C12A. The conodont abundance ranges from 1 to 10 identifiable elements per kilogram of rock. The assemblage comprises *Mehlina gradata*, *Polygnathus mosquensis* Litvinova, 1996, *Polygnathus praepolitus* Kononova, Alekseev, Barskov & Reimers, 1996, *Polygnathus zinaidae*, and *Polygnathus* cf. *zinaidae*.

Both *Polygnathus mosquensis* and *Polygnathus praepolitus* make their first appearances in this zone. According to Ovnatanova et al. (2017), *Po. mosquensis* ranges from FZ 5 to FZ 11, and the other species fall within the FZ 6–FZ 11 range. Considering all this evidence, this zone is therefore assigned to FZ 6–FZ 11. In the uppermost sample (QLXA C11), a shape very similar to *Polygnathus zinaidae* is present and is assigned to *Polygnathus* cf. *zinaidae*. This taxon differs from *Po. zinaidae* by its distinct ornamentation along the inner platform margins (see discussion in Chapter 7).

FZ 12–FZ 13a (undifferentiated)

In the QLX A section, this zone includes samples QLXA C13-C13B. The conodont abundance ranges from 3 to 25 identifiable elements per kilogram of rock. The assemblage comprises *Mehlina gradata*, *Polygnathus decorosus*, *Polygnathus krestovnikovi* Ovnatanova, 1969, *Polygnathus macilentus* Kuzmin, 1993, *Polygnathus zinaidae*, and *Polygnathus* cf. *zinaidae*.

Both *Polygnathus krestovnikovi* and *Polygnathus macilentus* make their first appearances in this zone. These two species provide practical guidance for locating the Frasnian–Famennian (F–F) boundary. According to Ovnatanova and Kononova (2008), *Po. krestovnikovi* ranges from FZ 11/12–FZ 13b/13c, while *Po. macilentus* is documented from FZ 12–FZ 13c (Ovnatanova et al., 2017); both taxa become extinct before the boundary and do not cross it. In the overlying zone, *Polygnathus brevilaminus* appears and crosses the F–F boundary, ranging from FZ 13b/13c to the *Pseudopolygnathus granulosus* Zone (Schülke, 1995; Spalletta et al., 2017).

FZ 13b–*Palmatolepis crepida* (undifferentiated)

In the QLX A section, this zone includes samples QLXA C14-C14A. The conodont abundance ranges from 17 to 24 identifiable elements per kilogram of rock. The assemblage comprises *Mehlina gradata*, *Polygnathus brevilaminus* Branson & Mehl, 1934, *Polygnathus zinaidae*, and *Polygnathus* cf. *zinaidae*.

Polygnathus brevilaminus makes its first appearance in this zone. This species is important around the Frasnian–Famennian (F–F) boundary: although its stratigraphic range is relatively long (FZ 13b/13c–*Pseudopolygnathus granulosus*), it is one of the few species that crosses the F–F boundary. In the overlying zone, *Mehlina strigosa* (Branson & Mehl, 1934) first appears in the lowest sample; this species ranges from *the Palmatolepis termini* Zone to the Tournaisian (Spalletta et al., 2017).

Considering these occurrences and ranges, these beds are assigned to FZ 13b–*Palmatolepis crepida* Zone, and the F–F boundary passes through this zone.

***Palmatolepis termini–Palmatolepis velifer velifer* (undifferentiated)**

In the QLX A section, this zone includes samples QLXA C15-C17. The abundance yield ranges from 20 to 45 identifiable elements per kilogram of rock. The assemblage comprises *Mehlina strigosa* (Branson & Mehl, 1934), *Polygnathus zinaidae*, and *Polygnathus* cf. *zinaidae*.

This zone is characterized by a very simple conodont assemblage, in which the genus *Polygnathus* is represented only by *Polygnathus zinaidae* and *Polygnathus* cf. *zinaidae*. Among them, *Po.* cf. *zinaidae* shows a gradual increase upward (Tab. 2). *Mehlina strigosa* makes its first appearance in this zone; this species ranges from the *Palmatolepis termini* Zone to the Tournaisian (Spalletta et al., 2017). In the overlying zone, *Polygnathus subirregularis* Sandberg & Ziegler, 1979 first appears in the lowest sample. This species ranges from the *Palmatolepis rugosa trachytera* Zone to the *Palmatolepis gracilis expansa* Zone (Spalletta et al., 2017).

***Palmatolepis rugosa trachytera–Palmatolepis gracilis expansa* (undifferentiated)**

In the QLX A section, this zone includes samples QLXA C18-C19. The conodont abundance ranges from 10 to 25 identifiable elements per kilogram of rock. The assemblage comprises *Mehlina strigosa*, *Polygnathus subirregularis* Sandberg & Ziegler, 1979, *Polygnathus zinaidae*, and *Polygbathus* cf. *zinaidae*.

This zone represents the uppermost unit of the QLX A section. *Polygnathus zinaidae* and *Polygbathus* cf. *zinaidae* continue to occur in this zone, with *Po.* cf. *zinaidae* showing a marked increase in abundance. *Polygnathus subirregularis* makes its first appearance in this zone. Based on the known stratigraphic range of *Po. subirregularis*, which extends from the *Palmatolepis rugosa trachytera* Zone to the *Palmatolepis gracilis expansa* Zone, this zone is assigned to the *Palmatolepis rugosa trachytera–Palmatolepis gracilis expansa*. This zone lies within Famennian.

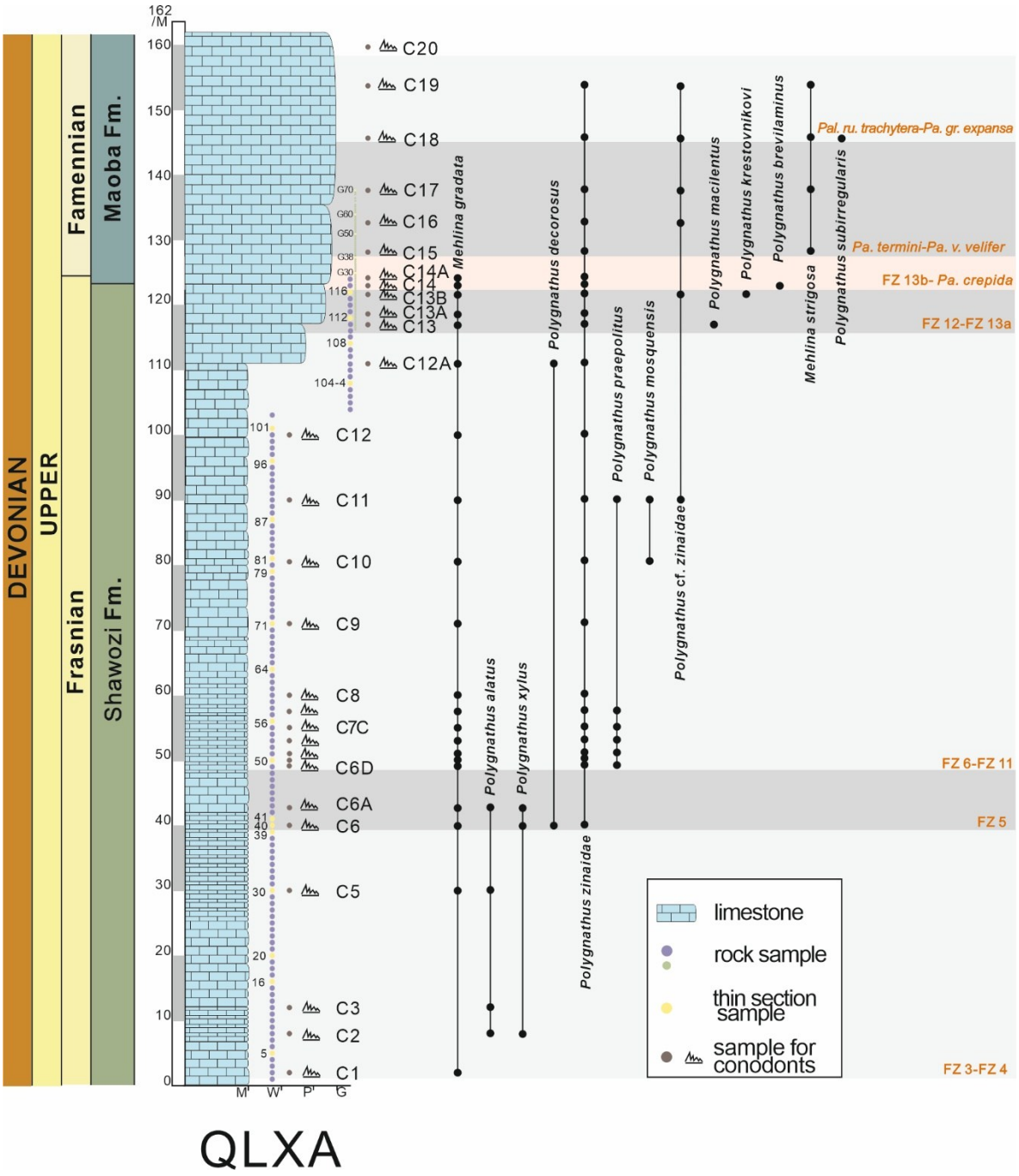

Fig. 16. Stratigraphic column, occurrence of conodonts, and biostratigraphy in QLX A section. From Left to right: Chronostratigraphy (Period, Series, Stage), stratigraphic column, sample position, occurrence of conodont taxa, Biozones, conodont biofacies. Abbreviations: *Pa.* - *Palmatolepis*, *Pa. v.* - *Palmatolepis velifer*, *Pa. ru.* - *Palmatolepis rugosa*, *Pa. gr.* - *Palmatolepis gracilis*

Conodont zones	FZ 3-FZ 4				FZ 5		FZ 6-FZ 11											
Sample name	QLXA C1	QLXA C2	QLXA C3	QLXA C5	QLXA C6	QLXA C6A	QLXA C6D	QLXA C7	QLXA C7A	QLXA C7B	QLXA C7C	QLXA C7D	QLXA C8	QLXA C9	QLXA C10	QLXA C11	QLXA C12	QLXA C12A
Sample weight (g)	3340	3286.3	3009.7	3384.5	3352.1	2560.3	2925	3825.3	2338.2	2768.1	2484.4	2427.5	3766.9	3595.2	3345.2	3372.8	3354.6	1941.1
Mehlina gradata	1			4	5	3	1	1	3	1	7	1	1	1	7	6	1	5
Polygnathus alatus		1	4	2		2												
Polygnathus xylus		1			2	1												
Polygnathus decorosus					1													1
Polygnathus zinaidae					3		5	3	8	6	1	2	35	27	12	18	10	1
Polygnathus praepolitus							2		1	2	2	1				1		
Polygnathus mosquensis															1	1		
Polygbathus cf. zinaidae																1		
Polygnathus macilentus																		
Polygnathus krestovnikovi																		
Polygnathus brevilaminus																		
Mehlina strigosa																		
Polygnathus subirregularis																		
Pseudopolygnathus sp.																		
Mehlina sp.																		
Mehlina sp. juv.																		
Polygnathus sp.			1	1		2							5					1
Polygnathus sp. juv.														1				
Tot.	1	2	5	7	11	8	8	4	12	9	10	4	41	29	20	27	11	8

Conodont zones	FZ 12-FZ 13a			FZ 13b- *Pa. crepida*		*Pa. termini-Pa. v.velifer*			*Pal. ru. trachytera-Pa. gr. expansa*		
Sample name	QLXA C13	QLXA C13A	QLXA C13B	QLXA C14	QLXA C14A	QLXA C15	QLXA C16	QLXA C17	QLXA C18	QLXA C19	Tol.
Sample weight (g)	3340	2205.6	3519	2095.9	2400.6	2547.5	2875.8	2622.7	2564.3	2379.7	
Mehlina gradata	1	9	9	2	1						70
Polygnathus alatus											9
Polygnathus xylus											4
Polygnathus decorosus											2
Polygnathus zinaidae	9	34	63	47	31	91	57	60	39	16	578
Polygnathus praepolitus											9
Polygnathus mosquensis											2
Polygbathus cf. zinaidae			4	2	2	5	1	7	12	2	36
Polygnathus macilentus	1										1
Polygnathus krestovnikovi			1								1
Polygnathus brevilaminus				1							1
Mehlina strigosa						1		1	3	2	7
Polygnathus subirregularis									1		1
											0
Pseudopolygnathus sp.								2			2
Mehlina sp.						7		2	1		10
Mehlina sp. juv.					1		1				2
Polygnathus sp.		9	12		6	11	1		7	3	59
Polygnathus sp. juv.		1									
Tot.	11	53	89	52	41	115	60	72	63	23	794

Table 2 Numerical distribution of P1 conodont elements in Qinglongxia A (QLX A) section.

4. 2. 2. 2 Biostratigraphy in QLX B section

In the QLX B Section, two conodont zones are recognized within the Famennian: *Palmatolepis marginifera utahensis–Palmatolepis gracilis manca*, and *Palmatolepis gracilis expansa–Bispathodus costatus* (Fig. 17).

***Palmatolepis marginifera utahensis–Palmatolepis gracilis manca* (undifferentiated)**

In the QLX B section, this zone includes samples QLXB C1-C2. The conodont abundance ranges from 1 to 4 identifiable elements per kilogram of rock. The assemblage comprises *Branmehla inornata* (Branson & Mehl, 1934), *Mehlina strigose*, *Polygnathus* cf. *zinaidae*, *Polygnathus experplexus* Sandberg & Ziegler, 1979, *Polygnathus perplexus* Thomas, 1949.

This zone represents the lowermost unit of the QLX B section. *Branmehla inornata* makes its first appearance in this zone; this species ranges from the *Palmatolepis marginifera utahensis* Zone to Tournaisian (Spalletta et al., 2017). In the overlying zone, *Polygnathus znepolensis* Spassov, 1965 first appears in the lowest sample. This species from the *Palmatolepis rugosa trachytera* Zone to the *Palmatolepis gracilis expansa* Zone (Spalletta et al., 2017). Meanwhile, other species exhibits ranges that overlap *the Palmatolepis marginifera utahensis–Palmatolepis gracilis mancarange* interval.

This zone lies within Famennian; *Polygnathus* cf. *zinaidae* still persists, while *Polygnathus zinaidae* is no longer recorded.

***Palmatolepis gracilis expansa–Bispathodus costatus* (undifferentiated)**

In the QLX B section, this zone includes samples QLXB C4-C6. The conodont yield ranges from 0.8 to 15 identifiable elements per kilogram of rock. The assemblage comprises *Branmehla inornata*, *Mehlina strigose*, *Polygnathus* cf. *zinaidae*, *Polygnathus experplexus*, *Polygnathus margaritatus* Schäfer, 1976, *Polygnathus perplexus*, *Polygnathus znepolensis* Spassov, 1965.

This zone represents the uppermost unit of the QLX B section. *Polygnathus znepolensis* makes its first appearance at the base of the zone; this species ranges from the *Palmatolepis gracilis expansa* Zone (Spalletta et al., 2017). *Polygnathus margaritatus* makes its last appearance in the *Bispathodus costatus* Zone (Spalletta et al., 2017). Meanwhile, other species exhibits ranges that overlap the *Palmatolepis gracilis expansa–Bispathodus costatus* interval.

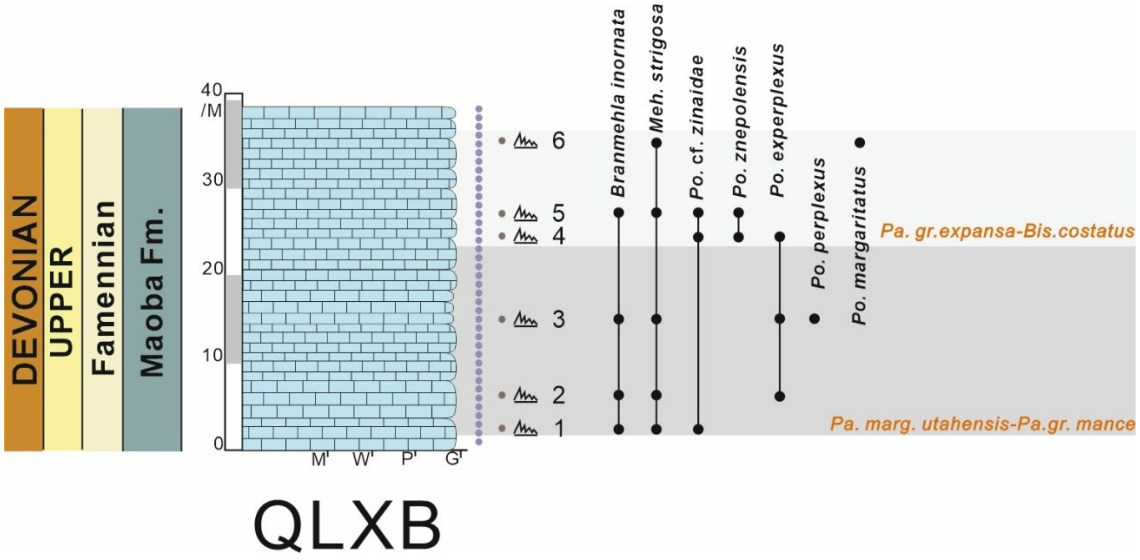

Fig. 17. Stratigraphic column, occurrence of conodonts, and biostratigraphy in QLX B section. From Left to right: Chronostratigraphy (Period, Series, Stage), stratigraphic column, sample position, occurrence of conodont taxa, Biozones, conodont biofacies. Abbreviations: *Bis.* – *Bispathodus*, *Meh.* -*Mehlina*, *Pa.* - *Palmatolepis*, *Pa. gr.* - *Palmatolepis gracilis*, *Pa. marg.* - *Palmatolepis marginifera*, *Po.* – *Polygnathus*.

Conodont zones	*Pa. marg. utahensis-Pa. gr. Manca*			*Pa. gr. expansa- Bi. costatus*			
Sample name	QLXB C1	QLXB C2	QLXB C3	QLXB C4	QLXB C5	QLXB C6	
Sample weight (Kg)	3.49	3.18	3.45	3.62	3.36	3.55	Tol.
Branmehla inornata	1	3	3		7		14
Mehlina strigosa	1	2	6		8	1	18
Polygnathus cf. zinaidae	1			6	5		12
Polygnathus znepolensis				2	20		22
Polygnathus experplexus		3	2	1			6
Polygnathus perplexus			1				1
Polygnathus margaritatus						1	1
							0
Mehlina sp.						1	1
Polygnathus sp.	1	3	3	2	11		20
Tol.	4	11	15	11	51	3	95

Table 3 Numerical distribution of P1 conodont elements in Qinglongxia B (QLX B) section.

4. 2. 2. 3 Conodont Biofacies and abundance

We conducted genus-level statistical analysis of the conodont data from the QLX sections, focusing on both overall conodont abundance and the percentages of genera within each sample (Figs.18-19). A total of four genera were identified: *Branmehla*, *Mehlina*, *Polygnathus*, *Pseudopolygnathus*, with *Polygnathus* being the most common.

In the QLX A section, identifiable conodont P_1 elements display abundances ranging from 0.3 to 45 elements per kilogram of rock. Abundance is very low in the lower part of the section (C1–C7D), generally less than 5 elements per kilogram. Between C8 and C11, a slight increase is observed, although values remain below 10. The abundance then drops again (C12–C13) less than 5 elements per kilogram. A pronounced rise occurs from C13A to C14, reaching about 25 elements per kilogram, followed by a sudden decline to approximately 17 at C14A. Above this level, conodont yield rises again, with most samples exceeding 20 elements per kilogram, and the maximum value of 45.1 elements per kilogram recorded at C15. The assemblages are overwhelmingly dominated by *Polygnathus*, with minor *Mehlina* and extremely rare *Pseudopolygnathus*. *Polygnathus* occurs consistently throughout the section and shows a distinct upward increase in abundance, paralleling the overall trend in total conodont yield. *Mehlina* appears sporadically but is present at nearly all levels, generally representing only a minor proportion of the assemblage. Ziegler and Sandberg (1990) recognized several major conodont biofacies but did not define a distinct *Polygnathus* biofacies. In the QLX A section, *Polygnathus* constitutes more than 80% of the total assemblage, whereas other genera are minor or absent.

In the QLX B section, identifiable conodont P_1 elements display abundances ranging from 0.8 to 15 elements per kilogram of rock. The lowest value is recorded in QLXB C6 (0.84 elements/kg), whereas the highest occurs in QLXB C5 (15.18 elements/kg). Similar to the QLX A section, the QLX B section contains a low-diversity conodont assemblage that is strongly dominated by *Polygnathus*, with subordinate *Mehlina* and rare *Branmehla*. The overall conodont abundance increases in parallel with the rising abundance of *Polygnathus*.

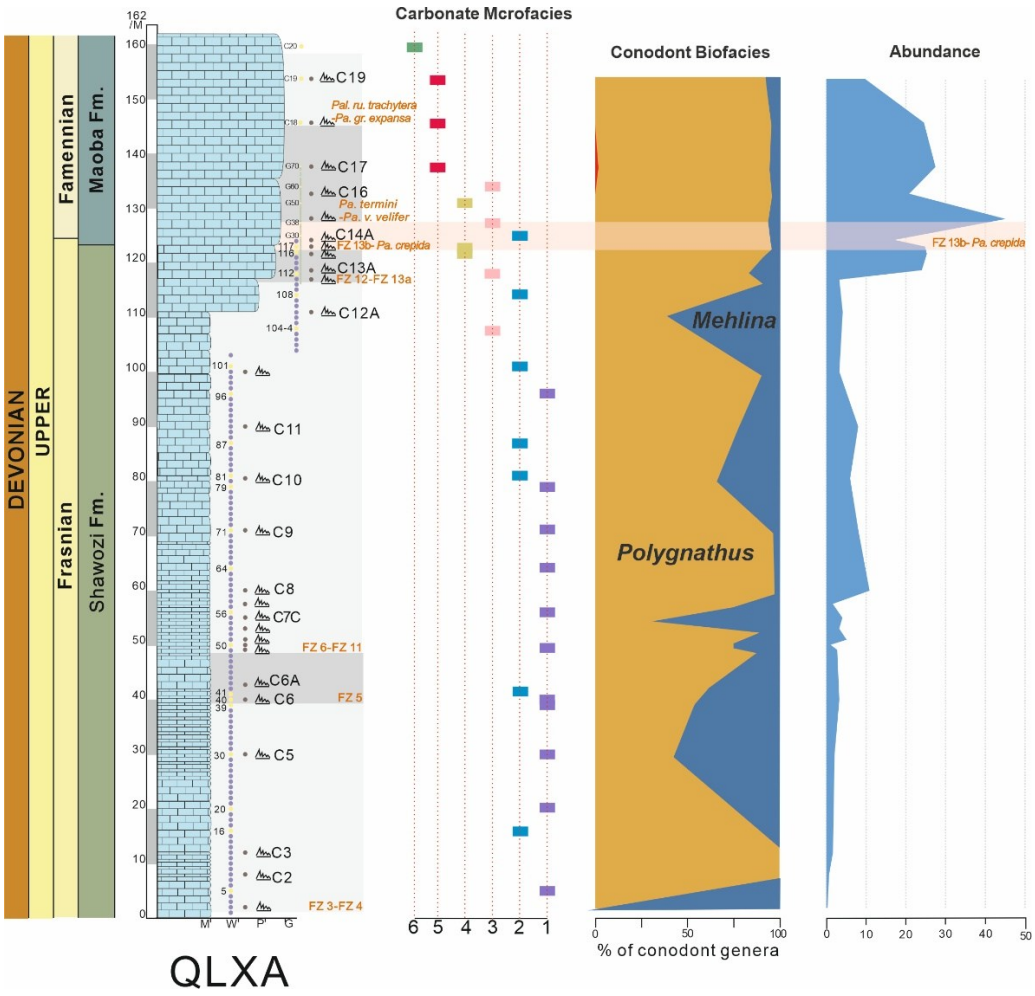

Fig. 18. Carbonate Mcrofacies, Conodont biofacies, and Abundance of P1 elements in the QLX A section

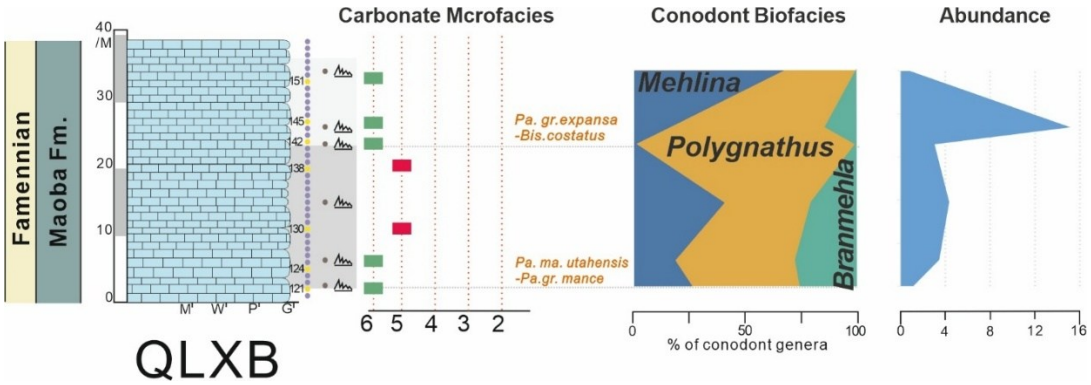

Fig. 19. Carbonate Mcrofacies, Conodont biofacies, and Abundance of P1 elements in the QLX B section

4. 2. 3 Carbonate microfacies

We analyzed 36 thin sections from two QLX sections. Assemblages of sponge spicules, ooids, intraclasts, and other bioclasts indicate a shallow carbonate platform within the photic zone, recording alternating low–high energy conditions driven by waves, tides, and storm reworking. From lower to higher energy, six microfacies (Fig. 18-20) are distinguished as follows:

M1 Laminated spiculitic micritic limestone

Matrix supported, fine micritic limestone with sponge spicules. The matrix is dominantly micritic; allochems generally <10%, locally grading to wackestone where bioclastic higher. Dominated by sponge spicules that are commonly aligned parallel to laminae (Fig. 20A), with minor thin-shelled bivalves, brachiopods, small crinoid fragments, few peloids; grains are very fine. Bioturbation is absent to very weak, with locally scattered rhombic dolomite.

Interpretation: Based on the bioclastic assemblage dominated by sponge spicules with minor thin-shelled bivalves, brachiopods, and crinoids, this facies was deposited in a low energy shallow subtidal environment (inner-platform) within the photic zone (Scholle & Ulmer-Scholle, 2003; Franseen, 2006; Flügel, 2010). Situated below the fair-weather wave base (FWWB) and near to, or slightly beneath, the storm wave base (SWB), sedimentation was dominated by suspension settling, with only weak traction during waning storms or gentle bottom currents that locally aligned spicules parallel to laminae. The prevalence of spicules together with micrite indicates a well-oxygenated water column and low sedimentation rates (Franseen, 2006).

Representative samples: QLXA 5, QLXA 20, QLXA 30, QLXA 39, QLXA 40, QLXA 50, QLXA 56, QLXA 64, QLXA 71, QLXA 79, QLXA 96.

M2 Bioclastic wackestone

Matrix-supported micritic limestone with ~25% allochems, locally grading to packstone; weakly laminated, and bioclastic grains are coarser than M1. The bioclastic assemblage consists mainly of thin-shelled bioclasts (bivalves, brachiopods, and rare bryozoans), accompanied by a few peloids, scattered sponge spicules, and large fragments primarily of crinoids (Fig. 20B).

Interpretation: Deposited below the FWWB and near the SWB in a quiet to weakly agitated inner-platform setting, where suspension settling predominated with minor traction during waning storms (Franseen, 2006; Flügel, 2010). The assemblage resembles Facies M1, but the occurrence of locally larger bioclasts indicates slight storm reworking in a low to moderate energy shallow-marine environment (Flügel, 2010).

Representative samples: QLXA 16, QLXA 41, QLXA 81, QLXA 87, QLXA 101, QLXA 108, QLXA G30.

M3 Intraclastic wackestone to packstone

Matrix-supported with ~30–45% allochems; micrite remains dominant, but thin grain-supported laminae are common. Bioclasts are broken and difficult to identify, possibly including some crinoid fragments; Irregular micritic aggregates with diffuse internal lamination, possibly algal lumps; micritic matrix still relatively abundant.

Interpretation: Deposited in a fore-shoal to shoal-toe setting below but close to the FWWB, where storm-induced currents and weak winnowing locally produced thin, grain-supported laminae (Franseen, 2006; Flügel, 2010). The increased proportion of intraclasts (Fig. 20C) together with local development of grain-supported packstone laminae, indicates higher energy and shallower conditions than M2, reflecting episodic storm agitation and partial winnowing within a moderate-energy subtidal environment (Flügel, 2010).

Representative samples: QLXA 104-4， QLXA 112, QLXA G38, QLXA G60

M4 Shoal-margin intraclastic–bioclastic packstone

Grain-supported packstone with >50% allochems, mainly dark gray irregular to sub-rounded intraclasts; contains highly fragmented bioclasts, probably from bivalves, brachiopods, and crinoids, with minor peloids; matrix mainly of micritic calcite (Fig. 20D).

Interpretation: Deposited above the FWWB on the lower shoal margin to shoal toe. Grains are generally irregular to sub-rounded, partly semi-rounded, indicating short-distance

transport or local reworking under moderate-energy conditions (Flügel, 2010). The environment is shallower than M3.

Representative samples: QLXA 116, QLXA 117, QLXA G50

M5 Lump–bioclastic packstone to grainstone

Grain-supported packstone with >60% allochems, locally grading to grainstone. Contains irregular micritic aggregates with diffuse internal lamination, possibly algal lumps (Fig. 20E), and large crinoid fragments in some samples. Some part are cleaner and approach a grainstone texture, with little micritic matrix and local sparry calcite cement. The micritic matrix locally sparse, with sparry calcite cement present in the interparticle pores.

Interpretation: Deposited above the FWWB on the lower shoal margin, where strong light favored algal–skeletal growth. Influenced by waves, currents, and intermittent storms, the energy was moderate to high but lower than that of the shoal crest (Franseen, 2006; Flügel, 2010).

Representative samples: QLXA G70, QLXA C18, QLXA C19, QLXB 130, QLXB 138

M6 Ooidal grainstone

Ooidal grainstone dominated by ooids (Fig. 20F), with minor algal lumps, intraclasts, and scattered skeletal debris; skeletal framework is rare. Fabric is strongly grain-supported, well sorted, and well rounded, with virtually no micritic matrix.

Interpretation: Deposited in an oolitic shoal under persistently high-energy conditions dominated by waves and tides, representing the shoal crest and associated channels (Franseen, 2006; Flügel, 2010).

Representative samples: QLXB C20, QLXB 121, QLXB 124, QLXB 142, QLXB 145, QLXB 151

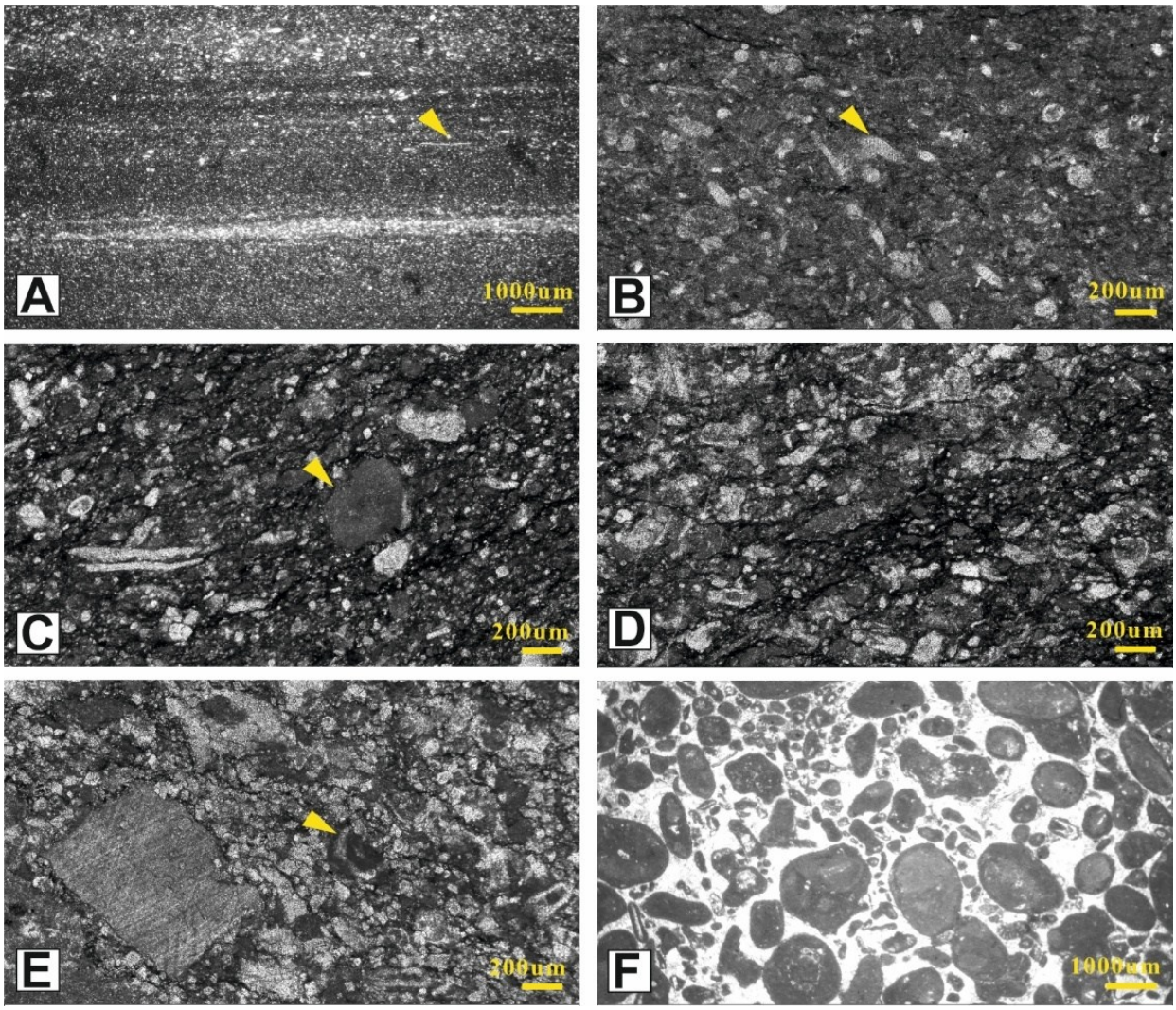

Fig. 20. Microfacies characteristics in the QLX sections. A. M1 Laminated spiculitic micritic limestone, yellow arrows indicate sponge spicules; B. M2 Bioclastic wackestone**,** yellow arrows indicate crinoid fragments; C. M3 Intraclastic wackestone to packstone, yellow arrows indicate intraclasts; D. M4 Shoal-margin intraclastic–bioclastic packstone; E. yellow arrows indicate algal lumps; F. M6 Ooidal grainstone

4. 2. 4 Carbon and oxygen isotope records

A total of 98 carbonate samples from the QLX A section, spanning from the top of the FZ 6–FZ 11 Zone (sample QLXA 91) to the top of the *Palmatolepis gracilis* expansa–*Bispathodus costatus* Zone (sample QLXA C20), were analyzed for stable carbon and oxygen isotopes. Most samples were collected at a standard spacing of approximately 1 m, while closer sampling intervals of 20–25 cm were applied at key stratigraphic levels. The $\delta^{13}C_{carb}$ values range from 1.62‰ to 3.46‰ (VPDB), with most samples clustering between 2.7‰ and 3.3‰. The $\delta^{18}O_{carb}$ values vary between -6.87‰ and -3.94‰, generally showing limited fluctuation within a narrow interval of approximately 2-2.5‰ for most of the section (Fig. 22).

Through the section, $\delta^{13}C_{carb}$ values remain on a relatively high baseline but begin to fluctuate and decline above sample QLXA G22, reaching the lowest value at QLXA G29 (1.62‰), where a negative excursion can be identified. Above the sample QLXA G29, $\delta^{13}C_{carb}$ gradually returns toward the baseline. Despite these local perturbations, there is no systematic positive covariance between $\delta^{13}C_{carb}$ and $\delta^{18}O_{carb}$ (Pearson Correlation Coefficient = 0.391; r^2 = 0.153), suggesting limited diagenetic overprint and preservation of near-primary isotopic signals (Fig. 21).

Overall, the $\delta^{13}C_{carb}$ curve shows a generally stable high beseline with a minor negative excursion near the inferred Frasnian–Famennian boundary. The possible causes of this negative shift are discussed in detail in Chapter 5.

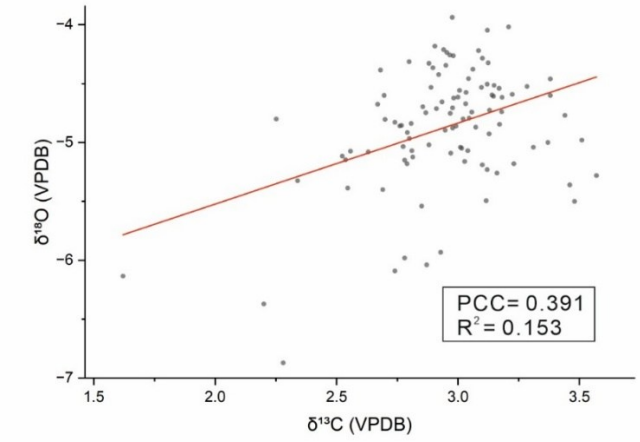

Fig. 21. Cross plot of carbon and oxygen isotope data from the QLX A section. PCC=Pearson Correlation Coefficient.

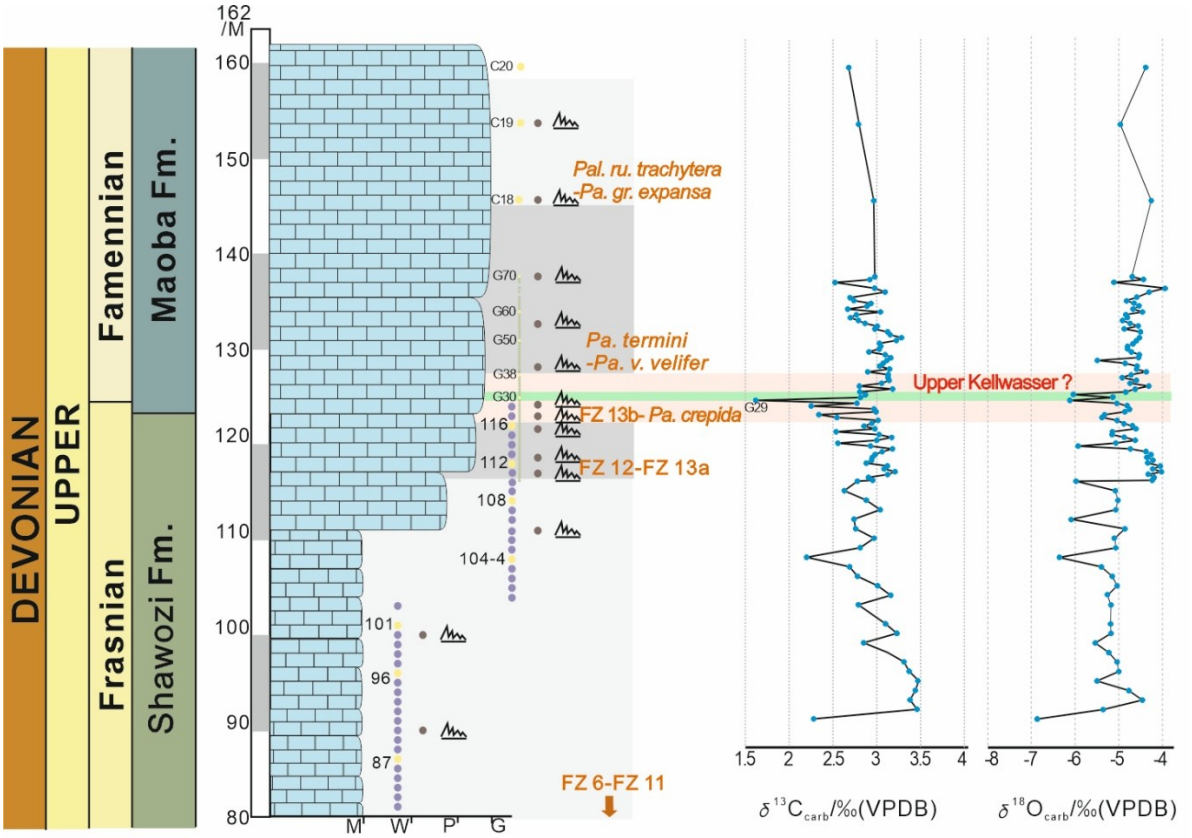

Fig. 22. $\delta^{13}C_{carb}$ and $\delta^{18}O_{carb}$ profiles of the QLX A section showing the Frasnian–Famennian boundary interval.

5 Discussion

We integrate biostratigraphy, carbonate microfacies, and stable-isotope geochemistry from newly investigated successions in the Carnic Alps (Italy) and the Longmenshan area (Sichuan, China). Our material comprises the Plan di Zermula D (PZD) section in the Carnic Alps and the Qinglongxia A (QLX A) section in Longmenshan, both spanning the Frasnian–Famennian (F–F) boundary. In Longmenshan, a second complementary section (QLX B) records only Famennian strata; although it does not cross the boundary, it constrains over-boundary stratigraphic architecture and lateral facies variability. Despite their shared focus on the F–F transition, the two records differ markedly in depositional character, biostratigraphic markers, and geochemical signatures. The first F–F boundary with black shale in the Carnic Alps, and the first confirmed section spanning the boundary in Longmenshan. Accordingly, our discussion is organized around three themes: (5.1) boundary recognition and correlation, (5.2) Carbon isotope characteristics and controlling mechanisms, and (5.3) biotic responses and ecological differentiation.

5.1 Frasnian–Famennian Boundary Recognition in Different Sedimentary Settings

5.1.1 Deep water Section: Carnic Alps

Microfacies analysis shows that the PZD section in the Carnic Alps is composed predominantly of fine-grained micritic limestone with very limited bioturbation and sparse thin-shelled bioclasts, indicating deposition in a low-energy, deep-water environment (Flügel, 2010). Conodont biofacies dominated by open-marine taxa (*Palmatolepis*) further support a deep-water setting. In comparison with adjacent Carnic Alps F–F boundary sections that lack black-shale deposition (e.g., Pramosio A and Freikofel T; Farabegoli et al., 2023), the PZD locality was likely situated in a deeper and more topographically restricted part of the Carnic basin.

The Frasnian–Famennian (F–F) boundary in this section is precisely located immediately above a ~25 cm-thick dark pelitic layer by the First Appearance Datum (FAD) of *Palmatolepis superlobata*. This placement is corroborated by a continuous, high-resolution conodont zonation spanning seven conodont zones: FZ 13b, FZ 13c, the *Palmatolepis subperlobata* Zone, the *Palmatolepis triangularis* Zone, the *Palmatolepis delicatula platys* Zone, the *Palmatolepis minuta minuta* Zone, and the *Palmatolepis crepida* Zone. The completeness and clarity of this framework

are fully consistent with the revised global F–F conodont zonation and updated taxonomy (Klapper & Kirchgasser, 2016; Spalletta et al., 2017).

Carbon isotope data further substantiate this placement. Across the F–F interval, $\delta^{13}C_{carb}$ exhibits a distinct positive excursion, rising from an average of 1.52‰ below the dark pelitic layer (FZ 13b – FZ 13c) to 2.83‰ above it (from the *Pa. subperlobata* to the *Pa. crepida* Zone), and attaining a peak of 3.31‰ at PZD 8, slightly above the boundary. Although the subsequent return toward baseline is not fully captured within the exposed section, the magnitude and trajectory of the positive shift are diagnostic and concordant with the Upper Kellwasser excursion documented from multiple regions worldwide (Buggisch & Joachimski, 2006; George et al., 2014; De Vleeschouwer et al., 2017; Zhang et al., 2019).

The conodont abundance and diversity shows a marked decline across the boundary interval. Immediately above the dark pelitic layer, standing abundance and taxonomic richness of *Icriodus*, *Palmatolepis*, and *Polygnathus* collapse, delineating the extinction horizon. Both metrics remain depressed until the *Pa. crepida* Zone, where a gradual recovery becomes evident. Although some successions document earlier recovery phases (e.g., within the *Pa. termini* Zone; Farabegoli et al., 2023), the PZD section clearly shows that faunal rebound occurred subsequent to the extinction event.

Overall, the integrated lithological, biostratigraphic, and geochemical dataset shows that the PZD section preserves a typical and stratigraphically complete deep-water expression of the Frasnian–Famennian boundary. A continuous high-resolution conodont zonation, a well-developed positive $\delta^{13}C_{carb}$ excursion linked to the Upper Kellwasser, and a marked reduction in conodont abundance and diversity, allow confident Frasnian–Famennian boundary recognition.

5.1.2 Shallow-water Section: Longmenshan

Assemblages of sponge spicules, ooids, intraclasts, and other bioclasts (thin-shelled bivalves, brachiopods, and crinoids) indicate deposition on a shallow carbonate platform within the photic zone (Flügel, 2010), and the conodont biofacies dominated by *Polygnathus* further supports a shallow-marine (upper-slope to platform) environment.

At the QLX A section, the Frasnian–Famennian (F–F) boundary can be coarsely constrained within the FZ 13b – *Palmatolepis crepida* undifferentiated interval. From base to top,

the conodont zonation FZ 3–FZ 4, FZ 5, FZ 6– FZ 11, FZ 12–FZ 13a, FZ 13b–*Pa. crepida*, *Pa. termini–Pa. velifer velifer,* and *Pa. rugosa trachytera–Pa. gracilis expansa*. Although a precise boundary horizon cannot be fixed in this section, the biostratigraphic sequence is internally consistent and complete. In addition, no erosional surfaces, hardgrounds, or lag deposits are observed, and bed thickness and microfacies vary gradually rather than abruptly, indicating a conformable shallow-water record.

In contrast to the deep-water PZD section, which shows little microfacies change across the boundary, QLX A records shallowing across the base of the FZ 13b–*Palmatolepis crepida* undifferentiated interval and through its lower part. Samples 116–117 correspond to M4, interpreted as deposits above the fair-weather wave base (FWWB) on the lower shoal margin to shoal toe. This facies is shallower than the underlying M1–M3 microfacies, which formed at or below, but not exceeding, the fair-weather wave base (FWWB), and thus indicates a regressive trend prior to the boundary.

We interpret this regression as the "*linguiformis* regression." Bond and Wignall (2008) placed this regressive pulse immediately preceding the Upper Kellwasser interval; similarly, Zhuang (2019) identified a regression at FZ 13b in the Lali section. Consistent with this placement, the Baisha section shows elevated abundances of *Polygnathus* within FZ 13b relative to adjacent intervals (Chang et al., 2019). Our zonal scheme and facies shift at QLX A align with these observations, suggesting that the *linguiformis* regression drove the local shallowing recorded here. Higher in the interval, at sample G30, microfacies shift from M4 to M2, recording a deepening (transgressive) pulse. We tentatively correlate this deepening with the Upper Kellwasser interval, which has been widely regarded as a phase of relative transgression in many place (Bond & Wignall, 2008; Bond et al., 2013; Zhang, 2019). Above this level, the section shallows again, completing a regression–transgression–renewed regression pattern across the F–F transition, consistent with globally compiled, continuously refined reconstructions of eustatic sea-level change (Johnson et al., 1985; Whalen & Day 2008, 2010).

Unlike the globally reported positive $\delta^{13}C$ excursion associated with the Upper Kellwasser, our section records a negative shift within the FZ 13b–*Palmatolepis crepida* undifferentiated interval at QLXA, with a minimum at sample G29 ($\delta^{13}C_{carb}$ =1.62‰). The elevated baseline (≈2.96‰) is consistent with the generally heavier $\delta^{13}C_{carb}$ values typical of shallow-water

carbonates, although minor diagenetic effects may influence the absolute magnitude of this offset (Swart, 2008; Saltzman & Thomas 2012).

Although the precise position of the Frasnian–Famennian boundary cannot be fixed in the shallow-water QLX A section, it can be roughly constrained within the FZ 13b–*Palmatolepis crepida* undifferentiated interval. Nevertheless, this section is relatively sensitive to global sea-level fluctuations, which helps refine the boundary interpretation. The $\delta^{13}C_{carb}$ record exhibits an anomalous negative shift, the potential causes of which will be discussed in Section 5.2.2.

5.2 Carbon isotope comparison and implications

Based on the global chemostratigraphic record, the Kellwasser events were global in extent, yet carbon cycling and redox dynamics vary regionally; $\delta^{13}C$ excursions are predominantly positive, many European basinal sections in Laurussia and Gondwana, whereas several North American and South China sections show negative excursions or muted signals, indicating that indicating that the isotopic expressions of the Kellwasser Event display marked regional variability (Joachimski et al., 2002; Buggisch & Joachimski, 2006; George et al., 2014; Hillbun et al., 2015; De Vleeschouwer et al., 2017; Carmichael et al., 2019; Zhang et al., 2019; Pisarzowska & Racki, 2020; Fig. 23). Instead, we interpret these differences as reflecting subtle paleogeographic and environmental controls on the timing of global carbon-cycle perturbations, rather than independent local events.

5.2.1 Positive $\delta^{13}C$ excursions

The carbon isotope record from the PZD section shows a pronounced positive excursion of approximately +1.8‰, which is consistent with the positive $\delta^{13}C$ shifts documented in classic German sections across the Frasnian–Famennian (F–F) transition (e.g., Kellwasser events). This agreement suggests that the PZD section preserves a reliable global signal rather than a local diagenetic artifact.

Paleogeographic reconstructions for the Late Devonian (Fig. 4) indicate that most sections in Europe, North America, and North Africa were situated on shallow epeiric shelves. The convergence of Laurussia and Gondwana led to the closure of the Rheic Ocean and the narrowing of the southwestern Paleotethys seaway (Keppie & Ramos, 1999; Stampfli et al., 2002; Torsvik et al., 2012). Under the influence of regression and orogenic activity, these shallow-marine settings were susceptible to terrigenous input and oxygen-deficient conditions, both of which could locally alter the composition of dissolved inorganic carbon (DIC). Such environmental factors may have enhanced the positive $\delta^{13}C$ excursions, producing patterns comparable to those observed in the PZD section.

The overall isotopic trend in our section closely resembles that of the Carnic Alps, which, like the German reference sections, developed in a comparable paleogeographic and depositional setting, resulting in a similar carbon-isotope evolution. In contrast, the Canning Basin of Australia

was influenced by fewer tectonic and terrigenous factors. The carbonate platform on the Lennard Shelf remained well connected to open-marine conditions during the Late Devonian (Carpenter et al., 1991), and no significant orogenic activity was recorded in western Australia at that time (Plumb, 1979; Forman & Wales, 1981). Consequently, the observed differences in the timing and magnitude of the Upper Kellwasser positive excursion between the Australian records and other regions are likely related to contrasts in paleogeographic and depositional settings.

5.2.2 What caused the negative $\delta^{13}C$ excursion?

The most common cause of changes in $\delta^{13}C$ records is meteoric diagenesis (Marshall, 1992). Such diagenetic alteration generally results in lower $\delta^{13}C$ values of carbonates, as ^{12}C-rich carbon derived from the oxidation of soil organic matter is incorporated into the carbonates (Allan & Matthews, 1982; Joachimski, 1994; Lohmann, 1988). Therefore, negative carbon isotope excursions are commonly interpreted as a signature of diagenetic modification.

In our QLX A section, a distinct negative $\delta^{13}C$ shift occurs within the FZ 13b–*Palmatolepis crepida* undifferentiated interval; meanwhile, other sections in South China also record negative $\delta^{13}C$ excursions during the F–F interval (Wang et al., 1991; Yan et al., 1993; Ma & Bai, 2002; Gharaie et al., 2007), suggesting that this feature is not an isolated phenomenon. However, Racki (2020) and Schobben et al. (2019a, b) argued against interpreting the negative $\delta^{13}C$ anomalies of the Frasnian–Famennian (F–F) interval solely as products of diagenetic alteration or productivity collapse. These hypotheses can explain local variability but fail to account for the globally synchronous negative excursions and their systematic links to volcanic activity, climate fluctuations, and oceanic anoxia.

Our case may fit better with the Retallack/Racki–Schobben (R&S) hypothesis (Racki, 2020; Schobben et al., 2019a), which interprets the Late Devonian $\delta^{13}C$ negative excursions not as diagenetic artifacts but as the initial response to massive volcanic CO_2 degassing and greenhouse warming. Subsequent enhanced organic carbon burial would have led to a positive $\delta^{13}C$ excursion, marking the peak of the Kellwasser Event. In this scenario, a minor negative perturbation typically precedes the positive excursion, as also observed by Chen et al. (2005) immediately before the $\delta^{13}C$ rise.

In our section, however, no clear positive shift follows the negative excursion. This may be because the section represents a shallow-water environment with relatively high baseline $\delta^{13}C$ values (Swart, 2008), which could have masked the positive excursion. Thus, while we cannot exclude the influence of diagenesis entirely, the observed pattern is still consistent with the initial volcanic signal predicted by the R&S model.

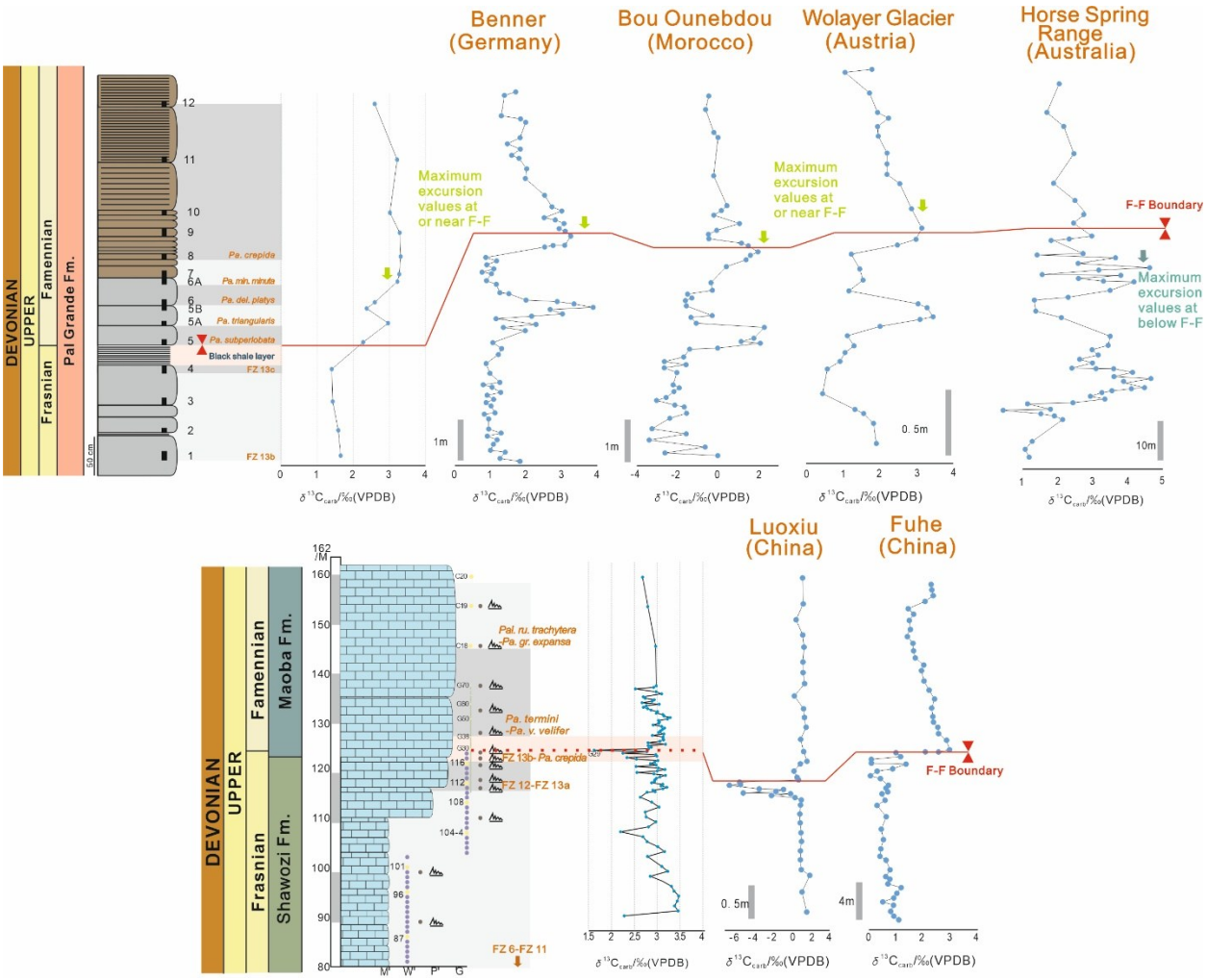

Fig. 23. Comparsion of $\delta^{13}C_{carb}$ for Frasnian–Famennian (F-F) boundary from Benner Quarry, Genmany (Joachimski & Buggisch, 1993), Bou Ounebdou, Morocco (Joachimski et al., 2002), Wolayer Glacier, Austria (Buggisch & Joachimski, 2006), Horse Spring Range, Austrialia (Hillbun et al., 2015), Luoxiu , China (Yan et al., 1993), Fuhe, China (Chen et al., 2005)

5.3 Ecological selectivity and opportunistic recovery

While the global trigger is widely attributed to Kellwasser-related anoxia and climatic stress (Bond & Wignall, 2008; Joachimski & Buggisch, 1993; Carmichael et al., 2014), the tempo and mode of biotic recovery were strongly shaped by regional paleoenvironmental factors.

5.3.1 Stepwise recovery of conodont in PZD

The genus analysis of conodont assemblages across the PZD section highlights the ecological selectivity of the F–F crisis. In the upper Frasnian (FZ 13b–13c), the fauna was diverse and dominated by *Palmatolepis* and *Polygnathus*, indicating stable open-marine ecosystems. At the base of the Famennian, diversity collapsed by ~80%. The immediate post-boundary assemblage at PZD 5 is extremely depauperate and consists of three recorded taxa: the incoming (FAD) *Palmatolepis subperlobata*, *Mehlina gradata*, and scarce *Pa. ultima*. In terms of boundary crossers, however, the PZD dataset shows that *Pelekysgnathus planus*, *Icriodus alternatus*, and *Palmatolepis ultima* range beyond FZ 13c into the Famennian; some of these survivors are absent or very rare immediately above the boundary but reappear slightly higher in the section. This pattern underscores a severe, selective extinction pulse rather than a random loss of diversity (Racki, 2005; Bond & Wignall, 2008; McGhee et al., 2013; Bush et al., 2015).

The role of *Icriodus alternatus* is particularly significant. Although never dominant in the PZD section, its relative abundance increases notably in PZD 5A, 5B, and 12—not at the first post-boundary level (PZD 5) but in the immediately overlying beds and again higher in the section. Such short-lived expansions are consistent with the interpretation of *Icriodus alternatus* as an opportunistic taxon able to exploit stressed, unstable conditions where competition was reduced (Sandberg et al., 1989; Corradini, 2003; Purnell & Donoghue, 2005). Its distribution often overlaps with *Palmatolepis* but rarely coincides with *Polygnathus* dominance, supporting the view that *Icriodus alternatus* occupied ecological niches distinct from those of more typical shallow-water conodonts. Similar opportunistic abundance increases have been documented in other F–F boundary sections worldwide (Farabegoli et al., 2023), while in some cases opportunistic responses manifested instead as body-size reduction and morphological variation (Girard & Renaud, 1996).

The extinction record of the PZD section reveals a gradual yet stepwise recovery of conodont biodiversity during the early Famennian. Immediately above the extinction horizon, diversity remained extremely low (from the *Pa. triangularis* to *Pa. minuta minuta* zones), with assemblages dominated by a few taxa (e.g., *Palmatolepis subperlobata*, *Pa. ultima*, *Icriodus alternatus*) and very low absolute abundances. This protracted low-diversity interval is comparable to the "survival phase" described for earliest Famennian ecosystems in other fossil groups, particularly brachiopods (Baliński, 2002), although conodont evidence for this phase remains scarce.

A notable turning point occurs in the *Pa. crepida* Zone, where species richness rose significantly, reaching nearly 20 taxa in samples PZD 10 and PZD 12. This rebound was driven both by the appearance of new forms (e.g., *Palmatolepis quadrantinodosalobata*, *Polygnathus nodocostatus*) and the re-expansion of previously rare taxa. Comparable recovery dynamics are reported regionally: in southern Poland, brachiopod assemblages show a survival interval in the *Pa. triangularis* Zone followed by a marked diversity increase in the *Pa. crepida* Zone (Baliński, 2002). In the Carnic Alps, the recovery in the PZD section is substantially slower than in the other sections in the area (Farabegoli et al., 2023) where anoxic conditions did not develop at the Frasnian-Famennian boundary. This is likely due to the peculiar local physiographic settings at the area of PZD section, where a through developed in the sea-bottom, generating a less efficient water circulation than the nearby areas.

5.3.2 Facies-controlled opportunistic recovery of conodonts in QLX

In contrast to the open-marine conditions recorded at PZD, the QLX sections represent shallow-water carbonate platform settings, where facies exerted strong control on conodont community composition. Conodont assemblages in the two QLX sections show overall low taxonomic diversity and dominance of shallow-water genera, chiefly *Polygnathus*. Open-marine indicator genera such as *Palmatolepis* are rare or absent. As a result, biostratigraphic resolution is limited, and several intervals must be treated as undifferentiated zones (see Section 4.2.2; Klapper & Kirchgasser, 2016; Spalletta et al., 2017). This low-diversity, single-genus-dominated pattern typifies inner-platform or shallow-shelf environments (Ziegler & Sandberg, 1990) and reflects the ecological filtering effect common in restricted carbonate platforms, where taxa preferring open-marine or upper-water conditions are naturally scarce.

Across and immediately above the inferred F–F boundary (sample C14A), conodont abundance increases markedly, but taxonomic diversity does not. This pattern of high abundance coupled with low diversity indicates that post-extinction recovery did not involve the rapid appearance of new taxa. Instead, a few environmentally tolerant genera, such as *Polygnathus*, proliferated rapidly, occupying ecological niches left vacant by extinct taxa. Such a pattern represents an opportunistic rebound (Sandberg et al., 1989; Corradini, 2003; Purnell & Donoghue, 2005), characterized by rapid numerical recovery but simple community structure. In the PZD section, this mode is expressed by the short-lived expansion of *Icriodus alternatus,* whereas in QLX the same ecological role was played by *Polygnathus*. Both cases indicate that the initial post-extinction phase reflects ecological restructuring rather than genuine taxonomic diversification.

5.3.3 Comparison the sections

The PZD section records a pattern of a severe and selective extinction pulse, followed by a brief opportunistic proliferation and then a stepwise recovery. In contrast, the QLX section represents a shallow, more restricted counterpart with limited faunal information:

Common features: both sections display early post-extinction opportunistic signals (high abundance with low diversity).

Differences: the QLX assemblages are more strongly controlled by facies and ecological filtering, leading to the absence of open-marine indicators, a higher proportion of undifferentiated zones, and a numerical rebound dominated by a single genus.

These observations suggest that, although the global trigger of the crisis is widely attributed to Kellwasser-related anoxia and climatic stress (Bond & Wignall, 2008), regional paleoenvironmental differences strongly modulated the tempo and mode of recovery (Wang & Ziegler, 2002; Baliński, 2002; Farabegoli et al., 2023).

6 Conclusions

The main results of this study may be summarized as follows:

1. Deep-water expression (PZD, Carnic Alps): The Frasnian–Famennian (F–F) boundary is precisely located above a ~25 cm dark pelitic layer marked by the FAD of *Palmatolepis superlobata*, with seven successive conodont zones (FZ 13b–*Pa. crepida*) spanning the interval, providing a complete and globally correlatable record. Black shale and the Upper Kellwasser Event: The PZD black shale represents local development of anoxia linked to the Upper Kellwasser Event. Its occurrence, contrasted with nearby oxic sections, demonstrates strong lateral paleoenvironmental variability within a small region.

Positive $\delta^{13}C_{carb}$ excursion (global signal): The PZD section shows a pronounced positive δ^{13}Ccarb excursion (~+1.3-+1.8‰), rising from ~1.52‰ below to 2.83‰ above the boundary and peaking at 3.31‰. This pattern matches the global Upper Kellwasser positive shift, indicating a primary and not diagenetic signal. Abrupt diversity collapse and delayed recovery: Conodont abundance and diversity dropped by ~80% at the boundary and remained low through the *Pa. triangularis–Pa. minuta minuta* zones. Diversity recovered gradually in the *Pa. crepida* Zone, reaching nearly 20 taxa, reflecting a stepwise, environmentally modulated rebound. Selective survival and opportunistic response: Only stress-tolerant taxa (*Pa. ultima*, *Icriodus alternatus*) survived across the boundary. *I. alternatus* showed short-lived opportunistic increases but never became dominant, confirming that extinction was selective rather than random. Biofacies and setting: the PZD section is dominated by the palmatolepid biofacies, with short-term increases of *Polygnathus* and *Icriodus*, consistent with deposition in a deep, open-marine environment.

2. Shallow-water expression (QLX, Longmenshan): The QLX A section represents a shallow carbonate platform environment dominated by *Polygnathus*. Although the exact F–F boundary cannot be fixed, it lies within the FZ 13b–*Pa. crepida* undifferentiated interval. The section shows high sensitivity to global sea-level fluctuations. Regression–transgression pattern: A regressive pulse ("*linguiformis* regression") is recorded at FZ 13b, followed by deepening near sample G30, interpreted as the Upper Kellwasser transgression, and then renewed shallowing above. This regression–transgression–regression pattern agrees with global sea-level reconstructions.

Negative $\delta^{13}C_{carb}$ excursion and its cause: QLX A records a distinct negative $\delta^{13}C_{carb}$ excursion (minimum ~1.62‰) within the FZ 13b–*Pa. crepida* interval. While meteoric diagenesis cannot be fully excluded, the excursion is more consistent with an early volcanogenic CO_2 input envisaged by the Retallack/Racki–Schobben model. Additional geochemical constraints are required, and high shallow-water baseline $\delta^{13}C$ values may have damped or masked any subsequent positive shift.

Facies-controlled opportunistic recovery: Across and above the inferred boundary, conodont abundance increased while diversity remained low. *Polygnathus* rapidly proliferated as an environmentally tolerant opportunist, mirroring the short-lived expansion of *I. alternatus* in PZD. Recovery was ecological rather than taxonomic.

3. Regional contrast under a global trigger: Both sections show early post-extinction opportunistic peaks (high abundance, low diversity) driven by Kellwasser-related anoxia and climatic stress. However, the expression of isotopic and biotic signals differs systematically between deep-water (positive shift, stepwise recovery) and shallow-water (negative shift, facies-filtered rebound) settings. Itegrated framework for boundary correlation: By combining high-resolution conodont biostratigraphy, microfacies analysis, and carbon-isotope stratigraphy, the F–F boundary can be confidently recognized across contrasting depositional environments. The Famennian QLX B section complements this framework by constraining over-boundary facies changes and stratigraphic architecture.

7 Systematic palaeontology

All conodont specimens collected in this study are stored in the Palaeontological Collection of the Department of Mathematics, Informatics and Geoscience, University of Trieste (DMGTS). Catalogue numbers of the illustrated specimens are listed in the captions of the relevant plates and figures.

Taxonomic work is based exclusively on the P1 elements, as they provide the most reliable characters for species-level identification in the Late Devonian. This practice follows standard usage in conodont studies, since P1 elements show the highest degree of morphological distinction and stratigraphic value.

For suprageneric classification, this study follows the phylogenetic framework outlined by Dzik (1991), which emphasizes evolutionary relationships among Late Devonian conodont lineages and provides the basis for distinguishing the major families. Within this framework, particular attention is given to three genera of primary stratigraphic importance during the Late Devonian: *Icriodus*, *Palmatolepis*, and *Polygnathus*. These genera are discussed in detail based on the studied material, while other taxa (*Ancyrodella*, *Ancyrognathus*, *Branmehla*, *Mehlina*, *Pelekysgnathus*, *Pseudopolygnathus*) are only briefly documented due to their limited occurrence.

Phylum CHORDATA Bateson, 1886

Class CONODONTA Pander, 1856

Order PRIONIODONTIDA Dzik, 1976

Family ICRIODONTIDAE Müller & Müller, 1957

Genus *Icriodus* Branson & Mehl, 1938.

Type species: *Icriodus expansus* Branson & Mechl, 1934a

***Icriodus alternatus* Branson & Mehl, 1934a**

(Pl. 1, fig. 4)

1934a *Icriodus alternatus* n. sp. Branson & Mehl, p. 225-226, pl. 13, figs. 4-6

1967 *Icriodus alternatus* Branson & Mehl – Wolska, pl. 2, fig. 6

1984 *Icriodus alternatus helmsi* n. subsp. Sandberg & Dreesen, p. 159, pl. 2, figs. 1-4, 6-7

1992 *Icriodus alternatus alternatus* Branson & Mehl – Savage, p. 279-280, fig. 4 6-8

1993 *Icriodus alternatus alternatus* Branson & Mehl – Ji & Ziegler, p. 55, pl. 5, figs. 5-8

1993 *Icriodus alternatus helmsi* Sandberg & Dreesen – Ji & Ziegler, p. 55, pl. 4, fig. 5; pl. 5 figs. 3-4

1999 *Icriodus alternatus mawsonae* n. subsp. Yazdi, p. 178-181, pl. 1, fig. 15; pl. 2, figs. 3, 4

2003 *Icriodus alternatus alternatus* Branson & Mehl – Corradini, p. 92, pl. 2, figs. 9-12

2006 *Icriodus alternatus alternatus* Branson & Mehl – Savage et al., p. 180, fig. 5L, 5M

2007 *Icriodus alternatus helmsi* Sandberg & Dreesen – Gholamalian, p. 466-467, fig. 9Q

2013 *Icriodus alternatus alternatus* Branson & Mehl – Bahrami et al., p. 384, 386, fig. 9F-K

2013 *Icriodus alternatus helmsi* Sandberg & Dreesen – Bahrami et al., fig. 9Q-U [Only]

2014 *Icriodus alternatus alternatus* Branson & Mehl – Mossoni, p. 143-144, pl. 1, fig.5

2015 *Icriodus alternatus alternatus* Branson & Mehl – Huang, p. 82-83, pl. 2, figs. 1-3, 7

2015 *Icriodus alternatus helmsi* Sandberg & Dreesen – Huang, p. 83-84, pl. 2, figs. 4-6

2019 *Icriodus alternatus alternatus* Branson & Mehl – Zhang, p. 166, pl. 51, figs. 11-14

2019 *Icriodus alternatus helmsi* Sandberg & Dreesen – Zhang, p. 166-167, pl. 51, figs. 5-9

2022 *Icriodus alternatus alternatus* Branson & Mehl – Girard et al., fig. 3H-J

2022 *Icriodus alternatus helmsi* Sandberg & Dreesen – Girard et al., fig. 3A-C

2022 *Icriodus alternatus mawsonae* Yazdi – Girard et al., fig. 3E-F

2024 *Icriodus alternatus alternatus* Branson & Mehl – Barrera Lahoz et al., p. 27, 29, fig. 5E-F
2024 *Icriodus alternatus mawsonae* Yazdi – Barrera Lahoz et al., p. 29, fig. 5G-H

Description: *Icriodus alternatus* is characterized by an elongate platform with three longitudinal rows of nodes. The median row is generally more elevated than the lateral rows and terminates in posterior cusp, typically aligned with the median row (*Icriodus alternatus alternatus* Branson & Mehl, 1934a), but in some morphotypes aligned with one of the lateral rows (*I. alternatus helmsi* Sandberg & Dreesen, 1984). In certain forms, the median row is only weakly developed, represented by poorly expressed nodes within a shallow trough (*I. alternatus mawsonae* Yazdi, 1999). The basal cavity is narrow and deep beneath the anterior platform, expanding in the posterior part of the element into a wider, rounded depression.

Remarks: In accordance with the recommendations by Girard et al., (2022), the three subspecies of *Icriodus alternatus* (*I. alternatus alternatus* Branson & Mehl, 1934, *I. alternatus helmsi* Sandberg & Dreesen, 1984, and *I. alternatus mawsonae* Yazdi, 1999) reflect ontogenetic and size dependent remodeling within a single species rather than distinct evolutionary units. Therefore, in this study we adopt this view and refer to all material as *Icriodus alternatus*, which also avoids artificial inflation of biodiversity.

Range: From FZ 12 Zone to the *Palmatolepis glabra pectinata* Zone (Ji & Ziegler 1993; Bultynck, 2003; Spalletta et al., 2017)

Studied material: 87 elements from PZD section (samples PZD 1, PZD 3-4, PZD5A-12)

***Icriodus cornutus* Sannemann, 1955b**

(Pl. 1, fig. 5)

1955b *Icriodus cornutus* n. sp. Sannemann, p. 130, pl. 4, figs. 19-21
1966 *Icriodus cornutus* Sannemann – Glenister & Klapper, p. 804-805, pl. 95, figs. 2-3
1984 *Icriodus cornutus* Sannemann – Sandberg & Dreesen, p. 162, pl. 2, fig. 8; pl. 4, figs. 19, 20
2006 *Icriodus cornutus* Sannemann – Dzik, p. 32-33, fig. 11A-B, 11D-F
2013 *Icriodus cornutus* Sannemann – Bahrami et al., fig. 9L-P

2015 *Icriodus cornutus* Sannemann – Huang, p. 84, pl. 2, fig. 14

2019 *Icriodus cornutus* Sannemann – Zhang, p. 167-168, pl.51, figs. 10, 15-18

2020 *Icriodus cornutus* Sannemann – Jafarbeigloo et al., fig. 6.1-3

2024 *Icriodus cornutus* Sannemann – Barrera Lahoz et al., p. 29, fig. 6O

Description: *Icriodus cornutus* is characterized by a dorsally inclined cusp. Additionally, the icrion is narrow, with irregular middle row denticles and sometimes slightly taller than those of the lateral rows, and in some adult specimens these denticles coalesce into irregular transverse ridges.

Remarks: *Icriodus cornutus* differs from *Icriodus alternatus* Branson & Mehl, 1934 by its dorsally inclined cusp.

Range: From the *Palmatolepis delicatula platys* Zone to the *Pseudopolygnathus granulosus* Zone (Spalletta et al., 2017)

Studied material: 3 elements from PZD section (samples PZD 7, PZD 10, PZD 12)

***Icriodus iowaensis iowaensis* Youngquist & Peterson, 1947**

(Pl. 1, fig. 6)

1947 *Icriodus iowaensis* n. sp. Youngquist & Peterson, p. 247, pl. 37, figs. 22-24, 27-29

1966 *Icriodus iowaensis* Youngquist & Peterson – Anderson, p. 406, pl. 52, figs. 8, 9, 13, 17-21

1984 *Icriodus iowaensis iowaensis* Youngquist & Peterson – Sandberg & Dreesen, p. 159-160, pl. 1, figs. 7-11; pl. 2, figs. 9-10

1985 *Icriodus iowaensis iowaensis* Youngquist & Peterson – Klapper & Lane, p. 920, fig. 11.7-11.10

1992 *Icriodus iowaensis iowaensis* Youngquist & Peterson – Savage, p. 280, fig. 2.1-6

1993 *Icriodus iowaensis iowaensis* Youngquist & Peterson – Ji & Ziegler, p. 56, text-fig. 6.8

1995 *Icriodus iowaensis iowaensis* Youngquist & Peterson – Schülke, p. 68, pl. 13, fig. 6

2002 *Icriodus iowaensis* Youngquist & Peterson – Wang & Ziegler, pl. 8, fig. 19

2008 *Icriodus iowaensis iowaensis* Youngquist & Peterson – Gholamalian & Kebriaei, pl. 1, figs. 2, 3, 5-7 [Only]
2011 *Icriodus iowaensis iowaensis* Youngquist & Peterson – Bahrami et al., pl. 2, fig. 18 [Only]
2013 *Icriodus iowaensis iowaensis* Youngquist & Peterson – Bahrami et al., fig. 9V-Z
2013 *Icriodus iowaensis iowaensis* Youngquist & Peterson – Tagarieva, figs. 7R, 8N, 8O
2015 *Icriodus iowaensis iowaensis* Youngquist & Peterson – Huang, p. 86-87, pl. 2, figs. 8-9

Description: *Icriodus. iowaensis iowaensis* is characterized by a low cusp and conspicuous ridges connecting denticles. These ridges link many lateral row denticles to those of the medial row and also connect denticles within the medial row. In lateral view, the posterior cusp and all or most denticles are of about equal height.

Remarks: Sandberg & Dreesen (1984) report on variability of the size of the platform, from broad platform and widely expanded basal cavity tonarrow specimens. Since only one element is present in the studied material, it is not possible determine whether it is broad with a widely expanded basal cavity or narrow.

Range: From FZ 12 to the *Palmatolepis rhomboidea* Zone (Bahrami et al. 2013 ; Spalletta et al., 2017)

Studied material: 1 element from PZD section (samples PZD 12)

Genus *Pelekysgnathus* Thomas, 1949

Type species: *Pelekysgnathus inclinatus* Thomas, 1949

***Pelekysgnathus planus* Sannemann, 1955b**

(Pl. 2, fig. 18)

1955b *Pelekysgnathus planus* n. sp. Sannemann, p. 149, pl. 4, figs. 22-23

1984 *Pelekysgnathus planus* Sannemann – Sandberg & Dreesen, pl. 3, fig. 6

1993 *Pelekysgnathus planus* Sannemann – Matya & Narkiewicz, pl. 4, fig. 13-15, 17

1995 *Pelekysgnathus planus* Sannemann – Schülke, pl. 13, figs. 8-9 [Only]

1999 *Pelekysgnathus planus* Sannemann – Schülke, p. 67, pl. 13, figs. 33-34.

2006 *Pelekysgnathus planus* Sannemann – Dzik, p. 33-34, fig. 12A-Q.

2008 *Pelekysgnathus planus* Sannemann – Gholamalian & Kebriaei, pl. 1, fig. 23

2015 *Pelekysgnathus planus* Sannemann – Huang, p. 107, pl. 12, figs. 1-3

2023 *Pelekysgnathus planus* Sannemann – Farabegoli et al., pl. 3, figs. 11-13

Description: The blade of the P1 element looks straight or only slightly curved in side view, with the cusp not clearly separate from the nearby denticles, or just a bit higher while still almost in line. The basal cavity on the aboral face is nearly symmetrical and occupies the entire aboral face.

Remarks: *Pelekysgnathus planus* occurs from the Frasnian to the Famennian. According to records (Dzik, 2002; Dzik, 2006), elements from the Frasnian and the earliest Famennian show an early form with a nearly straight blade, weak denticulation, and a cusp not separated from nearby denticles. In later, typical forms the cusp is gently inclined and the blade profile is convex, as in the holotype (Sannemann 1955b)

Range: From FZ 11 to the *Palmatolepis glabra prima* Zone (Corradini, 2003; Spalletta et al., 2017)

Studied material: 9 elements from PZD section (samples PZD 1, PZD 9-12)

Order OZARKODINIDA Dzik, 1976

Family PALMATOLEPIDIDAE Bassler, 1925

Genus *Palmatolepis* Ulrich & Bassler, 1926

Type species: *Palmatolepis perlobata* Ulrich & Bassler, 1926

***Palmatolepis beckeri* Klapper, 2007a**

(Pl. 1, fig. 8)

2007a *Palmatolepis beckeri* n. sp. Klapper, p. 517, fig. 5.3-5 (holotype: fig 5.5)

2013 *Palmatolepis beckeri* Klapper – Tagarieva, fig. 7E

Description: The platform has an extremely broad outer lobe, which is the most distinctive feature. The midline of this lobe lies slightly anterior to the central node and trends laterally or a little anteriorly. Shallow anterior and posterior sinuses set off the outer lobe from the main platform. The blade carina is strongly sigmoidal, and in antertior of platform blade very short. Posterior outer and inner margins meet at about a right angle at tip. Platform posterior of central node short. Nodes are fairly uniform, ranging from fine to coarse.

Remarks: *Palmatolepis beckeri* differs from *Palmatolepis bogartensis* (Stauffer, 1938) by its extremely broad outer lobe.

Range: Previously reported from FZ 13a -13b (Klapper, 2007a); based on our material, the range may extend into FZ 13c.

Studied material: 3 elements from PZD section (samples PZD 4)

***Palmatolepis bogartensis* (Stauffer, 1938)**

(Pl. 1, fig. 9)

1938 *Nothognathellab bogartensis* (Stauffer), p. 436, pl.48, fig. 30 (holotype)

1990 *Palmatolepis rotunda* n. sp. Ziegler & Sandberg, p. 62, pl. 10, figs. 1-4

1990 *Palmatolepis subrecta* Miller & Youngquist – Ziegler & Sandberg, pl. 11, fig. 10 [Only]

1993 *Palmatolepis bogartensis* (Stauffer) – Klapper & Foster, p. 17-18, figs. 13.4-16, 19.1-5, 20.1-11

1996 *Palmatolepis bogartensis* (Stauffer) – Klapper et al., p. 140, 143, fig. 8.6

1997 *Palmatolepis bogartensis* (Stauffer) – Over, p. 168, fig. 6.14-15

1998 *Palmatolepis hassi* Müller & Müller – Schindler et al., pl. 4, fig. 23; pl. 5, fig. 31[Only]

1999 *Palmatolepis bogartensis* (Stauffer) – Schülke, p. 30-31, pl. 3, fig. 11-13

2007a *Palmatolepis bogartensis* (Stauffer) – Klapper, p. 517, 521, fig. 1.1-2

2007b *Palmatolepis bogartensis* (Stauffer) – Klapper, p. 70, pl. 1, figs. 1-13

2023 *Palmatolepis bogartensis* (Stauffer) – Farabegoli et al., pl. 4, figs, 4, 8; p. 196-197, pl. 6, 1-12

Description: The outline of platform almost semicircular, which is the most distinctive feature. Margin posterior of the latter strongly convex in a continuous curve to tip. Outer lobe ranges from narrow to wide, its midline lies just anterior to the central node and trends laterally or slightly forward. The anterior sinus varies from shallow to deep, and the posterior sinus is small. The blade and anterior carina clearly cueved; blade-carina sigmoidal. Short blade anterior of platform. Uniform fine nodes.

Remarks: *Palmatolepis bogartensis* (Stauffer, 1938) is the main *Palmatolepis* species of Zone 13c (Girard et al., 2006). Because the margin posterior of the posterior sinus forms convex, *Pa. bogartensis* and *Palmatolepis winchelli* (Stauffer, 1938) are easily confused; however, *Pa. winchelli* may show a small sinus just anterior of the tip (Klapper, 2007a).

Range: FZ 13a, 13b, 13c (Klapper, 1993; Klapper & Kirchgasser, 2016).

Studied material: 41 elements from PZD section (samples PZD 1-4)

***Palmatolepis boogaardi* Klapper & Foster, 1993**

(Pl. 1, fig. 11-12)

1958 *Palmatolepis rhenana (*Bischoff) – Ziegler: p. 64: pl. 5, fig.6?

1987 *Palmatolepis gigas gigas* Miller & Youngquist – Barskov et al., Pl. 7, figs. 26, 27 [Only]

1993 *Palmatolepis boogaardi* n. sp. Klapper & Foster, p. 18,22, figs. 13.3, 14.1-10, 17.1-2, 19.13-15 (holotype: fig. 14.5)
1996 *Palmatolepis boogaardi* Klapper & Foster – Klapper et al., p. 143, fig. 8.9, 8.11-12
2019 *Palmatolepis boogaardi* Klapper & Foster – Zhang, p. 182-183, pl. 4, figs. 4-8, 12
2023 *Palmatolepis boogaardi* Klapper & Foster – Farabegoli et al., pl. 5, figs. 1-6; pl. 6, fig.13

Description: The lobe midline shows a slight but clear anterior orientation, which is the most distinctive feature. Outer lobe well developed and broad; platform with weakly developed to moderately sized nodes; platform outline is triangular, with a pointed tip; deep sinuses demarcate the lobe both anteriorly and posteriorly; margin a strongly convex curve from posterior sinus to tip; sigmoidal median ridge; platform bearing weakly developed to medium-sized nodes.

Remarks: *Palmatolepis boogaardi* differs from *Palmatolepis bogartensis* (Stauffer, 1938) by its an anteriorly directed lobe.

Range: Previously reported from FZ 13a-13b (Klapper, 2007a); based on our material, the range may extend into FZ 13c, consistent with nearby sections (Farabegoli et al., 2023).

Studied material: 30 elements from PZD section (samples PZD 1, PZD 3-4)

***Palmatolepis clarki* Ziegler, 1962**

(Pl. 1, fig. 13-14)

1962 *Palmatolepis marginata clarki* n. subsp. Ziegler, p. 62-65, pl. 2, figs. 20-25. (holotype: pl.2, fig. 22)
1989 *Palmatolepis delicatula clarki* Ziegler – Ji, pl. 2, figs. 11-13
1990 *Palmatolepis clarki* Ziegler – Ziegler & Sandberg, p. 66, pl. 6, fig. 7
1993 *Palmatolepis clarki* Ziegler – Ji & Ziegler, p. 59, pl. 12, figs. 11-15
1994 *Palmatolepis clarki* Ziegler – Wang, p. 100, pl. 5, fig. 11
2007 *Palmatolepis clarki* Ziegler – Over, pl. 13, fig. 18
2008 *Palmatolepis clarki* Ziegler – Ovnatanova & Kononova, pl. 13, fig. 30
2013 *Palmatolepis clarki* Ziegler – Tagarieva, fig. 8I, 8L, 8M

2015 *Palmatolepis clarki* Ziegler – Huang, p. 89, pl. 9, figs. 10-12

2023 *Palmatolepis clarki* Ziegler – Farabegoli et al., pl. 10, figs. 1-5

Description: The platform is long and narrow and bears a short, distinct lobe, which is its most distinctive feature. Platform surface ornamentation is smooth to weakly except the margins that are fortified by node or transverse ridges and fortified outer rostral area. Both the platform and lobe are relatively thicker than in most other sprcise of *Palmatolepis*; anterior and posterior sinuses weakly.

Remarks: Due to their surface ornamentation, *Palmatolepis clarki* is often confused with *Palmatolepis protorhomboidea* Sandberg & Ziegler, 1973, but the presence of a short lobe in *Pa. clarki* and its absence in *Pa. protorhomboidea.*

Range: From the *Palmatolepis delicatula platys* Zone to the *Palmatolepis crepida* Zone (Spalletta et al., 2017)

Studied material: 43 elements from PZD section (samples PZD 6A-12)

***Palmatolepis crepida* Sannemann, 1955b**

(Pl. 1, fig. 15)

1955b *Palmatolepis crepida* n. sp. Sannemann, p. 134, pl. 6, fig. 21.

1989 *Palmatolepis crepida* Sannemann – Ji, pl.3, fig. 26

1993 *Palmatolepis crepida* Sannemann – Ji & Ziegler, p. 59, pl. 22, figs. 1-7

1995 *Palmatolepis crepida* Sannemann – Schülke, p. 32, pl. 9, figs. 14-15

1999 *Palmatolepis crepida* Sannemann – Schülke, p. 31-33, pl. 9, fig. 13

2006 *Palmatolepis crepida* Sannemann – Bardashev et al., pl. 2, fig. 11

2014 *Palmatolepis crepida* Sannemann – Mossoni, p.89, pl. 1, fig. 18

2015 *Palmatolepis crepida* Sannemann – Huang, p. 88, pl. 10, figs. 5-6

2019 *Palmatolepis crepida* Sannemann – Zhang, pl. 25, figs 1-8 [Only]

2023 *Palmatolepis crepida* Sannemann – Farabegoli et al., pl. 9, figs. 10-12, 14-17

2024 *Palmatolepis crepida* Sannemann – Barrera Lahoz et al., p. 4, fig. 4I-J

Description: The drop-shaped platform outline is the most distinctive feature. The lobe is absent or poorly developed, and with relatively straight lateral sides; anterior carina arched with coarse, partly fused denticles; posterior carina short and weak, not reaching the end; posterior platform slightly to strongly elevated, bearing irregularly distributed fine to coarse nodes.

Remarks: *Palmatolepis crepida* differs from *Palmatolepis tenuipunctata* Sannemann by the less developed lobe and wider platform. Compared with *Palmatolepis linguiformis* Müller, *Pa. crepida* has an upturned posterior platform end, a slightly more posterior maximum platform width, and a weaker carina behind the central node.

Range: From the *Palmatolepis crepida* Zone to the *Palmatolepis rhomboidea* Zone (Spalletta et al., 2017)

Studied material: 9 elements from PZD section (samples PZD 8-10)

***Palmatolepis delicatula delicatula* Branson & Mehl, 1934**

(Pl. 1, fig. 16)

1934 *Palmatolepis delicatula delicatula* n. sp. Branson & Mehl, p.237, pl.18 ,figs. 4, 10

1993 *Palmatolepis delicatula delicatula* Branson & Mehl – Ji & Ziegler, p. 59-60, pl. 8, figs. 9-10

1995 *Palmatolepis delicatula delicatula* Branson & Mehl – Schülke, p. 33, pl. 10, figs. 16-19

2015 *Palmatolepis delicatula delicatula* Branson & Mehl – Huang, p. 89-90, pl. 9, figs. 1-3

2017 *Palmatolepis delicatula delicatula* Branson & Mehl – Ovnatanova et al., p. 1068, 1071, pl. 44, figs. 6, 8

2019 *Palmatolepis delicatula delicatula* Branson & Mehl – Zhang, p. 254-255, pl. 16, figs. 5-8

2023 *Palmatolepis delicatula delicatula* Branson & Mehl – Farabegoli et al., pl. 10, figs. 18-22

Description: The absence of a lobe is its most diagnostic feature. Usually shorter and triangular in shape; platform surface smooth lacks ornamentation. An imaginary line drawn from the azygous node to the platform margin divides the inner platform into two equal parts, anterior and posterior.

Remarks: *Palmatolepis delicatula delicatula* is very tiny and difficult to distinguish from juvenile of *Palmatolepis triangularis* Sannemann, 1955. However, *Pa. delicatula delicatula* has a straight platform margin, whereas *Pa. triangularis* is relatively longer and possesses a well-developed lobe that makes it easier to differentiate.

Range: From the *Palmatolepis subperlobata* Zone to the *Palmatolepis crepida* Zone (Spalletta et al., 2017)

Studied material: 92 elements from PZD section (samples PZD 5A-5B, PZD 6A-12)

***Palmatolepis delicatula platys* Ziegler & Sandberg, 1990**

(Pl. 1, fig. 17)

1990 *Palmatolepis delicatula platys* n. subsp. Ziegler & Sandberg, p. 67-68, pl. 17, figs. 4-7

1993 *Palmatolepis delicatula platys* Ziegler & Sandberg – Ji & Ziegler, p. 60, pl. 8, figs. 5-8

1995 *Palmatolepis delicatula platys* Ziegler & Sandberg – Schülke, p. 33-34, pl. 10, figs. 6, 11-12

2006 *Palmatolepis delicatula platys* Ziegler & Sandberg – Bardashev et al., pl. 2, fig. 5

2015 *Palmatolepis delicatula platys* Ziegler & Sandberg – Huang, p. 90, pl. 7, figs. 13-14; pl. 9, figs. 8-9

2017 *Palmatolepis delicatula platys* Ziegler & Sandberg – Ovnatanova et al., p. 1071, pl. 44, fig. 7; pl. 46, figs. 1-2, 4, 7

2019 *Palmatolepis delicatula platys* Ziegler & Sandberg – Zhang, p. 255, pl. 16, figs. 9-12

2023 *Palmatolepis delicatula platys* Ziegler & Sandberg – Farabegoli et al., pl. 10, figs. 12-17, 23

Description: The absence of a lobe is its most diagnostic feature. Usually shorter and approximately triangular in shape; platform surface smooth lacks ornamentation. An imaginary line extending from the azygous node to the platform margin divides the inner platform into two parts; the area of the anterior half is considerably larger than that of the posterior half.

Remarks: *Palmatolepis delicatula platys* differs from *Palmatolepis clarki* Ziegler, 1962 and

Palmatolepis protorhomboidea Sandberg & Ziegler, 1973 by its smooth surface without ornamentation.

Range: From the *Palmatolepis delicatula platys* Zone to the *Palmatolepis crepida* Zone (Spalletta et al., 2017)

Studied material: 49 elements from PZD section (samples PZD 6-12)

***Palmatolepis juntianensis* Han, 1987**

(Pl. 1, fig. 18)

1987 *Palmatolepis juntianensis* n. sp. Han, p.186, pl.1, figs. 15–16 (holotype: pl. 1, fig. 15)

1990 *Palmatolepis juntianensis* Han – Ziegler & Sandberg, p. 52, pl. 14, figs. 6-7

1995 *Palmatolepis juntianensis* Han – Schülke, p. 39-40, pl. 8, figs. 1-2

2008 *Palmatolepis juntianensis* Han – Ovnatanova & Kononova, p. 1092-1093, pl. 12, figs. 13-17

2013 *Palmatolepis juntianensis* Han – Tagarieva, fig. 7F-J

2015 *Palmatolepis juntianensis* Han – Huang, p. 90, pl. 7, figs. 13-14; pl. 9, figs. 8-9

2019 *Palmatolepis juntianensis* Han – Zhang, p. 191-192, pl. 6, figs. 9-12

2004 *Palmatolepis juntianensis* Han – Klapper et al., p. 378, fig. 6.1-3

2023 *Palmatolepis juntianensis* Han – Farabegoli et al., pl. 10, figs. 24-28

Description: The rostral area is elongated, and the posterior part of the platform is very short, with the widest point situated close to the posterior tip. The surface is essentially smooth, but in some larger specimens a slightly raised rim or a few marginal nodes may be observed on one or both sides of the platform.

Remarks: *Palmatolepis juntianensis* differs from *Palmatolepis winchelli* (Stauffer, 1938) by its absence of a distinct lateral lobe.

Range: Previously reported from FZ 13a-13b (Klapper & Kirchgasser, 2016); based on our material, the range may extend into FZ 13c, consistent with records from adjacent Carnic Alps sections (Farabegoli et al., 2023).

Studied material: 21 elements from PZD section (samples PZD 1, PZD 4)

***Palmatolepis linguiformis* Müller, 1956**

(Pl. 2, fig. 1)

1956 *Palmatolepis linguiformis* n. sp. Müller, p. 24, pl. 7, fig. 1–7 (holotype: pl. 7, fig. 4)
1990 *Palmatolepis linguiformis* Müller – Ziegler & Sandberg, p. 59, pl. 14, figs. 8-10
1995 *Palmatolepis linguiformis* Müller – Schülke, p. 40, pl. 8, figs. 6-7
2006 *Palmatolepis linguiformis* Müller – Bardashev et al., pl. 2, figs. 8-9
2008 *Palmatolepis linguiformis* Müller – Ovnatanova & Kononova, p. 1095, pl. 12, figs. 9-12
2013 *Palmatolepis linguiformis* Müller – Tagarieva, fig. 7A, 7B
2015 *Palmatolepis linguiformis* Müller – Huang, p. 97, pl. 5, figs. 7-11
2019 *Palmatolepis linguiformis* Müller – Zhang, p. 205-206, pl. 12, figs. 9-12
2023 *Palmatolepis linguiformis* Müller – Farabegoli et al., pl. 9, figs. 10-12, 14-17

Description: The platform is narrow with nearly parallel sides, resembling an elongated linguiform shape. The posterior part of the platform shows variation, being inclined upward, downward, or remaining flat; the surface bears a few evenly distributed nodes or smooth, and the median ridge is relatively smooth; the lobe is absent, and the free blade is short; strongly compressed nodes are nearly equal in size and form a strongly denticulate anterior platform margin.

Remarks: An earlier record (Ziegler & Sandberg) of this species' surface ornamentation described the diagnostic feature as "the surface bears a few evenly distributed nodes," but subsequent authors (Zhang, 2019) have also reported specimens with smooth oral ornamentation. In our material, both conditions are represented: specimens with nodes and specimens with a smooth surface.

Range: Based on previous reports, the range of *Palmatolepis linguiformis* has been considered restricted to FZ 13b (Girardet al., 2006; Klapper & Kirchgasser, 2016), and Klapper & Kirchgasser, 2016 suggested using *Pa. linguiformis* exctinction as an additional marker for recognizing the onset of FZ 13c. However, based on our material, *Palmatolepis linguiformis* occurs in FZ 13c, as also reported from nearby sections in the Carnic Alps (Farabegoli et al., 2023).

Studied material: 50 elements from PZD section (samples PZD 1, PZD 3-4)

***Palmatolepis lobicornis* Schülke, 1995**

(Pl. 2, fig. 8)

1989 *Palmatolepis subperlobata* Branson & Mehl, 1934 – Ji, pl. 2, figs. 25-27

1976 *Palmatolepis subperlobata helmsi* n. subsp. Ovnatanov, p. 113, pl. 9, fig. 7

1995 *Palmatolepis lobicornis* n. sp. Schülke, p. 40-41, pl. 7, figs. 1–17 (holotype: pl. 7, fig. 4)

2019 *Palmatolepis lobicornis* Schülke – Zhang, p. 242, pl. 20, figs 5-16

2004 *Palmatolepis lobicornis* Schülke – Klapper et al., p. 379, fig. 7.30

2023 *Palmatolepis lobicornis* Schülke – Farabegoli et al., pl. 12, figs. 11-17

2024 *Palmatolepis lobicornis* Schülke – Barrera Lahoz et al., p. 10, fig. 5B

Description: The presence of two anterior sinuses is the most distinctive feature. Slightly upturned posterior end; the inner platform at the carina contact is distinctly higher than the outer; free blade is short or absent. Denticles are elongate-rounded and inward-oriented; carina slightly sigmoid, the median denticle developed, and the posterior carina poorly developed; platform surface is smooth and unornamented.

Remarks: The species was widely referred to as *Palmatolepis subperlobata* in the literature following publications such as Branson & Mehl (1989). However, the platform outline is clearly distinct from that of *Palmatolepis subperlobata* Branson & Mehl, 1934, as discussed under the latter taxon. Helms (1963) subsequently treated this form as a separate subspecies, though only in open nomenclature, and it was later formally named by Ovnatanova (1976). Her designation,

however, proved to be a junior homonym of *Palmatolepis helmsi* Ziegler, 1962. Schülke (1995) therefore introduced *Palmatolepis lobicornis* as an effective replacement name.

Range: From the *Palmatolepis minuta minuta* Zone to the *Palmatolepis rhomboidea* Zone (Spalletta et al., 2017)

Studied material: 5 elements from PZD section (samples PZD 9, PZD 12)

***Palmatolepis minuta minuta* Branson & Mehl, 1934**

(Pl. 2, fig. 2)

1934 *Palmatolepis minuta* n. sp. Branson & Mehl, p. 236, Pl. 18, figs. 1, 6-7 (holotype: pl. 18, fig. 1)

1990 *Palmatolepis minuta minuta* Branson & Mehl – Ziegler & Sandberg, p. 69

1995 *Palmatolepis minuta minuta* Branson & Mehl – Schülke, p. 42-43, pl. 10, figs. 5, 7-9, 13, 21

2003 *Palmatolepis minuta minuta* Branson & Mehl – Corradini, p. 80, pl. 5, figs. 1-6

2014 *Palmatolepis minuta minuta* Branson & Mehl – Mossoni, p. 97-98, pl. 2, fig. 17

2015 *Palmatolepis minuta minuta* Branson & Mehl – Huang, p. 97-98, pl. 10, figs. 9-14, 18

2017 *Palmatolepis minuta minuta* Branson & Mehl – Ovnatanova et al., p. 1092, 1095, pl. 46, figs. 3, 8; pl. 47, fig. 10; pl. 48, figs. 12, 14, pl. 52, fig.1

2019 *Palmatolepis minuta* Branson & Mehl – Zhang, pl. 24, figs. 1-4, 9-16 [Only]

2023 *Palmatolepis minuta minuta* Branson & Mehl – Farabegoli et al., pl. 12, fig. 4

2024 *Palmatolepis minuta minuta* Branson & Mehl – Barrera Lahoz et al., p. 11, 13, fig. 4G-H

Description: Based on the platform outline and lobe features, three morphotypes of this subspecies can be distinguished (Ji & Ziegler,1993): morphotype 1 has a small ovate platform with straight to gently convex anterior and posterior inner margins and lacks lobe; morphotype 2, shows a large, elongate platform with a small, smoothly rounded lobe like protrusion and a well-developed posterior carina that extends to or nearly to the posterior tip of the platform; morphotype 3, inferred to descend from *Palmatolepis minuta minuta* morphotype 1, bears an elongate, narrowly lanceolate platform without an inner lobe.

Remarks: Our material corresponds to *Palmatolepis minuta minuta* morphotype 1; by contrast, *Palmatolepis delicatula platys* Ziegler & Sandberg, 1990 is approximately triangular in shape.

Range: From the *Palmatolepis minuta minuta* Zone to the *Pseudopolygnathus granulosus* Zone (Spalletta et al., 2017)

Studied material: 21 elements from PZD section (samples PZD 6A, PZD 9-12)

***Palmatolepis protorhomboidea* Sandberg & Ziegler, 1973**

(Pl. 2, fig. 6)

1973 *Palmatolepis delicatula protorhomboidea* n. subsp. Sandberg & Ziegler, p. 112, pl. 1, figs. 14-19 (holotype: pl. 1, fig. 14)

1990 *Palmatolepis protorhomboidea* Sandberg & Ziegler – Ziegler & Sandberg, p. 68-69, pl. 17, figs. 8-11

1993 *Palmatolepis protorhomboidea* Sandberg & Ziegler – Ji & Ziegler, p. 68, pl. 11, figs. 12-16

1995 *Palmatolepis protorhomboidea* Sandberg & Ziegler – Schülke, p. 44-45, pl. 10, figs. 1-4

2003 *Palmatolepis protorhomboidea* Sandberg & Ziegler – Corradini, p. 82, pl. 3, figs. 14-15

2015 *Palmatolepis protorhomboidea* Sandberg & Ziegler – Huang, p. 99-100, pl. 9, figs. 4-7

2019 *Palmatolepis* cf. *protorhomboidea* Sandberg & Ziegler – Zhang, pl. 16, figs. 1-4 [Only]

2023 *Palmatolepis protorhomboidea* Sandberg & Ziegler – Farabegoli et al., pl. 10, figs. 6-10

Description: The absence of a lobe is its most diagnostic feature. Usually shorter and triangular in shape. Platform surface ornamentation is diverse; typically, the anterior outer platform bears a few nodes, and the inner anterior platform margin is reinforced, forming a low rim.

Remarks: *Palmatolepis protorhomboidea* differs from *Palmatolepis clarki* Ziegler, 1962 by its shorter platform with a much more reduced and weakly defined lobe. Besides, *Pa. protorhomboidea* differs from *Palmatolepis delicatula platys* Ziegler &Sandberg, 1990 by its surface ornamentation of the platform.

Range: 36 elements from PZD section (samples PZD 6-12)

Studied material: From the *Palmatolepis subperlobata* Zone to the *Palmatolepis rhomboidea* Zone (Spalletta et al., 2017)

***Palmatolepis quadrantinodosalobata* Sannemann, 1955a**

(Pl. 2, fig. 4)

1955a *Palmatolepis quadrantinodosalobata* n. sp. Sannemann, p. 328, pl. 24, fig. 6

1993 *Palmatolepis quadrantinodosalobata* Sannemann – Ji & Ziegler, p. 69, pl. 23, figs. 1-7

2003 *Palmatolepis quadrantinodosalobata* Sannemann – Corradini, p. 83, pl. 5, figs. 7-9

2014 *Palmatolepis quadrantinodosalobata* Sannemann – Mossoni, p. 103-104, pl. 1, fig. 14

2017 *Palmatolepis quadrantinodosalobata* Sannemann – Ovnatanova et al., p. 1104, 1107, pl. 45, figs. 3, 5

2023 *Palmatolepis quadrantinodosalobata* Sannemann – Farabegoli et al., pl. 12, fig. 8

2024 *Palmatolepis quadrantinodosalobata* Sannemann – Barrera Lahoz et al., p. 16, fig. 4E-F

Description: The development of nodes on the anterior part of the platform is the most distinctive feature. Subtriangular platform with a well-developed, elongated lobe aligned with the azygous node; coarse nodose ornamentation is confined to the platform anterior to the azygous node.

Remarks: *Palmatolepis quadrantinodosalobata* is similar to *Palmatolepis subperlobata* Branson & Mehl, 1934 and *Palmatolepis lobicornis* Schülke, 1995 in platform outline and lobe development. It is distinguished by coarse nodose ornamentation on the platform. Three morphotypes are distinguished by platform shape and nodes on the anterior part (Sandberg & Ziegler, 1973; Ji & Ziegler, 1993): Morphotype 1- Broad platform,prominent outer-anterior nodal cluster nearly concentric with the curved carina and slightly converging toward the central node; anterior inner platform nodose; inner lobe much reduced. Morphotype 2 - Most typical; characterized by a broad platform, a well-developed lobe, and nodes on the outer platform. Morphotype 3 - Characterized by a narrow platform; a slightly arched to straight carina, a pointed lobe, and nodes on the outer platform.

Range: M1 from the *Palmatolepis glabra pectinata* Zone to the *Palmatolepis rhomboidea* Zone; M2 from the *Palmatolepis crepida* to the *Palmatolepis rhomboidea* Zone (Spalletta et al., 2017).

Studied material: 3 elements from PZD section (samples PZD 10, PZD 11), our elements closely resemble Morphotype 2.

***Palmatolepis regularis* Cooper, 1931**

(Pl. 2, fig. 3)

1931 *Palmatolepis regularis* Cooper, p. 242, pl. 28, fig. 36 (holotype)
1962 *Palmatolepis* cf. *regularis* Cooper – Ziegler, p. 75-76, pl. 6, figs. 20-24
2004 *Palmatolepis regularis* Cooper – Klapper et al., p. 381, fig. 7.28, 7.31
2014 *Palmatolepis regularis* Cooper – Mossoni, p. 104, pl. 1, fig. 12
2015 *Palmatolepis regularis* Cooper – Huang, p. 100-101, pl. 10, figs. 7-8
2019 *Palmatolepis regularis* Cooper – Zhang, p. 239, pl. 18, figs. 5-8
2023 *Palmatolepis regularis* Cooper – Farabegoli et al., pl. 9, figs. 3-4
2024 *Palmatolepis regularis* Cooper – Barrera Lahoz et al., p. 16-17, fig. 4O-P

Description: The platform is sigmoidal with a parallelogram outline and lacks a lobe, which is the most distinctive character. The anterior inner margin meets the carina more anteriorly than the outer margin; the outer platform is slightly elevated and curved; the anterior carina is strongly arched; the posterior carina, formed by aligned nodules, is straight to slightly oblique and nearly reaches a pointed, upturned posterior end; the free blade is short; the platform surface is shagreen.

Remarks: Because Cooper's (1931) holotype of *Palmatolepis regularis* was embedded in shale, only the lower view was available and the published figure was hand-drawn, making precise comparisons impossible; consequently, subsequent researchers referred comparable forms as *Palmatolepis* cf. *regularis* (Ziegler, 1962). Later Klapper et al. (2004) provided upper views of the paratypes and a description and platform outline consistent with the holotype, ultimately rejecting the cf. attribution, after which precise comparison became feasible.

Range: From the *Palmatolepis minuta minuta* Zone to the *Palmatolepis rhomboidea* Zone (Spalletta et al., 2017)

Studied material: 10 elements from PZD section (samples PZD 9, PZD 10)

***Palmatolepis rhenana* Bischoff, 1956**

(Pl. 2, fig. 7)

1956 *Palmatolepis rhenana* n. sp. Bischoff, p. 129- 130, pl. 8, figs. 26-28, 30, pl. 10, fig. 7 (holotype: pl. 8, fig. 27)

1993 *Palmatolepis rhenana* Bischoff – Klapper & Foster, p. 24, figs. 16.1, 17.3-10, 19.19-20

1996 *Palmatolepis rhenana* Bischoff – Klapper et al., p. 148, fig. 8.7, 8.10, 8.13

2008 *Palmatolepis rhenana* Bischoff – Ovnatanova & Kononova, p. 1101, pl. 7, figs. 9-11; pl. 14, figs. 7-8

2013 *Palmatolepis rhenana* Bischoff – Tagarieva, fig. 6A, AB, AF, AE

2015 *Palmatolepis rhenana* Bischoff – Huang, p. 101, pl. 6, figs. 1-3

2019 *Palmatolepis rhenana* Bischoff – Zhang, pl. 4, figs. 9-11,13-16 [Only]

Description: Platform outline roughly triangular; outer lobe large, laterally wide and longitudinally narrow, directed laterally to posterior; deep anterior and posterior sinuses; margin nearly straight from posterior sinus to tip; carina sigmoidal; platform coarsely nodose; in large specimens the blade forms a high apex just anterior to the platform, overtopping the anterior carina.

Remarks: *Palmatolepis rhenana* Bischoff, 1956 differs from *Palmatolepis boogaardi* Klapper & Foster, 1993 in lobe orientation: lateral to posterior in *Pa. rhenana*, but posteriorly directed in *Pa. boogaardi*.

Range: From FZ 12 - FZ 13 (Klapper, 1993)

Studied material: 4 elements from PZD section (samples PZD 3, PZD 4)

Palmatolepis robusta Schülke, 1995

(Pl. 2, fig. 5)

1962 *Palmatolepis termini* Sannemann – Ziegler, pl. 6, fig. 8-11 [Only]

1995 *Palmatolepis termini robusta* n. subsp. Schülke, p. 54, pl. 7, fig. 1–16 (holotype: pl. 7, fig. 1).

2019 *Palmatolepis robusta* Schülke – Zhang, p. 221, pl. 14, figs. 5-8

2023 *Palmatolepis robusta* Schülke – Farabegoli et al., pl. 12, figs. 18-19

Description: The most distinctive feature is a thick platform with two small, short, rounded lobes, its anterior part densely covered with nodules. The platform is relatively small and bears a short free blade.

Remarks: Based on oral surface ornamentation and morphology, *Palmatolepis robusta* is no longer regarded as a subspecies of *Palmatolepis termini* Sannemann, 1955b. *Pa. robusta* differs from *Palmatolepis triangularis* Sannemann 1955a in two small, short, rounded lobes and platform-surface ornamentation indistinct.

Range: From the *Palmatolepis minuta minuta* Zone to the *Palmatolepis crepida* Zone (Spalletta et al., 2017)

Studied material: 6 elements from PZD section (samples PZD 8, PZD 10, PZD 12)

Palmatolepis spathula Schülke, 1995

(Pl. 2, fig. 11)

1992 *Palmatolepis quadrantinodosalobata* Sannemann – Lazreq, pl. 2, fig. 9

1995 *Palmatolepis spathula* n. sp. Schülke, p. 50-51, pl. 6, figs. 1–17 (holotype: pl. 6, fig. 2).

2019 *Palmatolepis spathula* Schülke – Zhang, p. 221-222, pl. 15, figs. 5-8

2023 *Palmatolepis spathula* Schülke – Farabegoli et al., pl. 12, figs. 20-26

Description: The main feature is the presence of a very long rod-shaped lobe directed anteriorly or laterally. Subtriangular platform with a slightly upturned, pointed posterior end; the free blade

is short. The anterior and posterior sinuses are usually well developed, though in some specimens the posterior sinus is indistinct, giving a relatively straight outer margin; the surface is ornamented with unevenly distributed small nodes, with a prominent node typically present on the outer anterior margin of the platform.

Remarks: *Palmatolepis spathula* differs from *Palmatolepis triangularis* Sannemann, 1955 by its a long rod-shaped lobe directed anteriorly or laterally.

Range: From the *Palmatolepis minuta minuta* Zone to the *Palmatolepis crepida* Zone (Spalletta et al., 2017)

Studied material: 13 elements from PZD section (samples PZD 9, PZD 12)

***Palmatolepis subperlobata* Branson & Mehl, 1934**

(Pl. 2, fig. 9-10)

1934 *Palmatolepis subperlobata* n. sp. Branson & Mehl, p. 235, pl. 18, figs. 11, 21

1993 *Palmatolepis subperlobata* Branson & Mehl – Ji & Ziegler, p. 72, pl. 20, figs. 3-9; pl. 21, figs. 11-12

1995 *Palmatolepis subperlobata* Branson & Mehl – Schülke, p. 52-53, pl. 12, figs. 1-4, 7

2003 *Palmatolepis subperlobata* Branson & Mehl – Corradini, p. 84, pl. 3, figs. 1-4

2004 *Palmatolepis subperlobata* Branson & Mehl – Klapper et al., p. 381-382, fig. 7.35-36

2014 *Palmatolepis subperlobata* Branson & Mehl – Mossoni, p. 108-109, pl. 1, fig. 17

2015 *Palmatolepis subperlobata* Branson & Mehl – Huang, p. 102-103, pl. 7, figs. 7-10; pl. 11, figs. 14-15

2019 *Palmatolepis subperlobata* Branson & Mehl – Zhang, pl. 22, figs. 1-16; pl. 18, figs. 1-4 [Only]

2023 *Palmatolepis subperlobata* Branson & Mehl – Farabegoli et al., pl. 7, fig. 7; pl. 8, figs. 5-7, 9-12, 15; pl. 11, fig. 13

2024 *Palmatolepis subperlobata* Branson & Mehl – Barrera Lahoz et al., p. 17, 19, fig. 5A

Description: Platform ornamentation smooth and shagreen-like, the most distinctive feature. Platform subtriangular, bearing a well-developed lobe with sinuses; lobe elongated, subtriangular to rounded, oriented laterally or anteriorly and positioned anterior; anterior carina arched to sigmoidal; posterior carina straight, composed of tiny nodules, terminating near the posterior end; posterior margin pointed to subtriangular and slightly upturned.

Remarks: Platform ornamentation distinguishes *Palmatolepis subperlobata* from *Palmatolepis ultima* Ziegler, 1958 and *Palmatolepis triangularis* Sannemann 1955. In *Pa. ultima* and *Pa. triangularis*, the platform surface bears nodes, whereas in *Pa. subperlobata* the platform is smooth and shagreen-like.

Range: From the *Palmatolepis subperlobata* Zone to the *Palmatolepis marginifera marginifera* Zone (Spalletta et al., 2017)

Studied material: 115 elements from PZD section (samples PZD 5-12)

***Palmatolepis tenuipunctata* Sannemann, 1955b**

(Pl. 2, fig. 11)

1955b *Palmatolepis tenuipunctata* n. sp. Sannemann, p. 136, pl. 6, fig. 22
1993 *Palmatolepis tenuipunctata* Sannemann – Ji & Ziegler, p. 72, pl. 19, figs. 1-6
2003 *Palmatolepis tenuipunctata* Sannemann – Corradini, p. 84, pl. 3, figs. 11-14
2014 *Palmatolepis tenuipunctata* Sannemann – Mossoni, p. 109, pl. 1, fig. 13
2015 *Palmatolepis tenuipunctata* Sannemann – Huang, p. 104, pl. 10, figs. 1-2
2019 *Palmatolepis tenuipunctata* Sannemann – Zhang, p. 246, pl. 23, figs. 9-12
2023 *Palmatolepis tenuipunctata* Sannemann – Farabegoli et al., pl. 11, figs. 11-12, 14-15
2024 *Palmatolepis tenuipunctata* Sannemann – Barrera Lahoz et al., p. 19-20, fig. 4C-D

Description: Elongated platform with small lobe, the most distinctive feature. Small lobe with a rounded outline, oriented laterally or posteriorly and positioned anterior to the azygous node; platform outline sigmoidal; platform surface smooth; anterior carina moderately curved;

posterior carina straight to slightly curved and nearly reaching the posterior end; outer margin meets the carina posteriorly to the inner margin, convex and elevated in the anterior half.

Remarks: *Palmatolepis tenuipunctata* differs from *Palmatolepis subperlobata* Branson & Mehl, 1934 primarily in having a relatively narrow, elongate platform with a small inner lobe positioned anterior to the azygous node.

Range: From the *Palmatolepis minuta minuta* Zone to the *Palmatolepis glabra pectinata* Zone (Spalletta et al., 2017)

Studied material: 12 elements from PZD section (samples PZD 10-12)

***Palmatolepis triangularis* Sannemann, 1955a**

(Pl. 2, fig. 13-14)

1955a *Palmatolepis triangularis* n. sp. Sannemann, p. 327-328, pl. 24, fig. 3

1990 *Palmatolepis triangularis* Sannemann – Ziegler & Sandberg, p. 64-65, pl. 14, figs. 1-5; pl. 16, figs. 8-10

1993 *Palmatolepis triangularis* Sannemann – Ji & Ziegler, p. 73, pl. 24, figs. 1-12

1995 *Palmatolepis triangularis* Sannemann – Schülke, p. 55-56, pl. 11, figs. 1-3, 5-6, 9-10, 14-15

2006 *Palmatolepis triangularis* Sannemann – Bardashev et al., pl. 2, fig. 18

2007b *Palmatolepis triangularis* Sannemann – Klapper, p. 72, 74, pl. 2, figs. 13-19

2015 *Palmatolepis triangularis* Sannemann – Huang, p. 104-105, pl. 7, fig. 6; pl. 8, figs. 1-7

2017 *Palmatolepis triangularis* Sannemann – Ovnatanova et al., p. 1111, pl. 44, figs. 1-4; pl. 45, figs. 1-2, 4, 6-9

2019 *Palmatolepis triangularis* Sannemann – Zhang, p. 222, pl. 14, figs. 9-12, 16

2004 *Palmatolepis triangularis* Sannemann – Klapper et al., p. 382, fig. 6.12-13

2023 *Palmatolepis triangularis* Sannemann – Farabegoli et al., pl. 7, figs. 1-5; pl. 8, figs 1-4, 8

Description: Coarse nodes throughout the platform constitute the most distinctive character; platform outline roughly triangular; outer lobe relatively narrow, its midline slightly anterior to

the central node and directed slightly anteriorly, laterally, or slightly posteriorly; moderate sinuses anterior and posterior of the lobe; blade carina sigmoidal; blade anterior of the platform relatively short.

Remarks: *Palmatolepis triangularis* and *Palmatolepis ultima* Ziegler, 1958 have very similar platform outlines and are difficult to distinguish; they are often separated by surface ornamentation. The platform of *Pa. triangularis* is more extensive along the anterior-posterior axis, the upper surface is covered with coarser nodes, and the central node is somewhat larger. The platform of *Pa. ultima* bears uniform small nodes**,** and the lobe is wide**.**

Range: From the *Palmatolepis triangularis* Zone to the *Palmatolepis crepida* Zone (Spalletta et al., 2017)

Studied material: 47 elements from PZD section (samples PZD 5A-12)

***Palmatolepis ultima* Ziegler, 1958**

(Pl. 2, fig. 15)

1958 *Palmatolepis ultima* n. sp. Ziegler, p. 67, pl. 9, figs. 2, 6, 10 (holotype: pl. 9, fig. 2)
2004 *Palmatolepis ultima* Ziegler – Klapper et al., p. 382-383
2007a *Palmatolepis ultima* Ziegler – Klapper, fig. 1.18-21
2007b *Palmatolepis ultima* Ziegler – Klapper, p. 74, pl. 2, figs. 2-8, 10-11
2015 *Palmatolepis ultima* Ziegler – Huang, p. 105-106, pl. 7, fig. 1-5; pl. 11, figs. 16-17
2019 *Palmatolepis ultima* Ziegler – Zhang, p. 222-223, pl. 10, fig. 4; pl. 15, figs. 1-4, 9-12
2023 *Palmatolepis ultima* Ziegler – Farabegoli et al., pl. 7, figs 6, 8-11; pl. 8, figs. 13-14, 16

Description: Relatively uniform small nodes throughout the platform constitute the most distinctive character. Outline approximately triangular; outer lobe broad, its midline slightly anterior to the central node; moderate sinuses anterior and posterior of lobe; blade–carina sigmoidal; platform bearing uniformly small nodes except for relatively larger on the anterior inner platform; anterior blade is relatively short.

Remarks: *Palmatolepis ultima* and *Palmatolepis subperlobata* Branson & Mehl, 1934 are difficult to distinguish because of their similar platform outlines. However, *Pa. subperlobata* has a smooth platform resembling the shagreen upper surface of many Famennian species. According to Klapper et al. (2004), nodes may occur only on and near the anterior inner margin. In contrast, *Pa. ultima* shows relatively uniform small nodes distributed across the entire platform.

Range: From FZ 13c to the *Palmatolepis delicatula platys Zone* (Klapper, 2007b; Spalletta et al., 2017)

Studied material: 10 elements from PZD section (samples PZD 4-5, PZD 5B-6)

***Palmatolepis werneri* Ji & Ziegler, 1993**

(Pl. 2, fig. 16)

1993 *Palmatolepis werneri* n. sp. Ji & Ziegler, p.73, pl. 22, figs. 8-11 (holotype: pl. 22, fig. 8)
2019 *Palmatolepis werneri* Ji & Ziegler – Zhang, pl. 23, figs. 1-4 [Only]

Description: A nodose oral surface as a prominent feature; a medium-sized platform; a short and weakly developed inner lobe; the blade-carina is moderately sigmoidal and increases evenly in height anteriorward; the posterior carina is generally low and narrow and may extend to the posterior tip of the platform; the central node is commonly large and situated slightly posterior to the midlength of the platform; the posterior end of the platform is generally upward flexed or nearly flat.

Remarks: *Palmatolepis werneri* differs from *Palmatolepis crepida* Sannemann, 1955 chiefly in platform outline, the curvature of the blade–carina, and the presence of an inner lobe.

Range: From the *Palmatolepis minuta minuta* Zone to the *Palmatolepis termini* Zone (Spalletta et al., 2017)

Studied material: 2 elements from PZD section (samples PZD 12)

***Palmatolepis winchelli* (Stauffer, 1938)**

(Pl. 2, fig. 17)

1938 *Bryantodus winchelli* n. sp. Stauffer, p. 423, pl. 48, fig. 33

1993 *Palmatolepis winchelli* (Stauffer, 1938) – Klapper & Foster, p. 24, 26, 31, figs. 13.1-2, 18.1-8, 18.10-11, 19.6-12, 20.12-24

2007a *Palmatolepis winchelli* (Stauffer, 1938) – Klapper, p. 529, 531, fig. 1.9-11

2007b *Palmatolepis winchelli* (Stauffer, 1938) – Klapper, p. 72, pl. 1, figs. 14-16

2015 *Palmatolepis subrecta* Miller & Youngquist – Huang, p. 103, pl. 3, figs. 1-3; pl. 4, figs. 1-4

2023 *Palmatolepis winchelli* (Stauffer, 1938) – Farabegoli et al., pl. 4, figs. 1-3, 7; pl. 6, figs. 14-16

Description: Parapet well developed in the anterior half of the platform as the most distinctive feature; platform elongated triangular with a relatively wide posterior part and a pointed posterior end; lobe small, directed laterally at the level of the azygous node and bordered by distinct anterior and posterior sinuses; median ridge slightly sigmoidal and terminating short of the posterior end of the platform; azygous node well developed; posterior ridge made up of two to five nodes that diminish in size toward the rear; the free blade measures roughly one-quarter to one-sixth of the platform length; the platform bears dense small nodes, some coalescing into short, discontinuous marginal ridges.

Remarks: We follow Klapper and Foster (1993) in applying the name *Palmatolepis winchelli* (Stauffer, 1938) to the species originally described as *Palmatolepis subrecta* Miller & Youngquist, 1947. Their revision showed that the Pb element included in the multielement apparatus of *Pa. subrecta* is identical with *Bryantodus winchelli* Stauffer, 1938, thereby demonstrating that the two nominal species are conspecific. The current usage of *Pa. winchelli* is thus based primarily on the Pa element morphology originally assigned to *Pa. subrecta*.

Range: From FZ 12-13c (Klapper, 2007a)

Studied material: 12 elements from PZD section (samples PZD 1, PZD 3-4)

Family POLYGNATHIDAE Bassler, 1925

Genus *Ancyrodella* Ulrich & Bassler, 1926

Type species: *Ancyrodella nodosa* Ulrich & Bassler,1926

***Ancyrodella curvata* (Branson & Mehl, 1934)**

(Pl. 1, fig. 1)

1934 *Ancyrognathus curvata* n. sp. Branson & Mehl, p. 241, pl. 19, figs. 6, 11

1993 *Ancyrodella curvata* (Branson & Mehl) – Ji & Ziegler, p. 51-52, pl. 2, figs. 4-5

2013 *Ancyrodella curvata* (Branson & Mehl) – Mossoni, p.19, fig. 5.3

2013 *Ancyrodella curvata* (Branson & Mehl) – Tagarieva, fig. 7M, 7N

2014 *Ancyrodella curvata* (Branson & Mehl) – Mossoni, p. 109-110, pl. 1, fig. 3

2023 *Ancyrodella curvata* (Branson & Mehl) – Farabegoli et al., pl. 1, figs. 3-7

Description: This species is commonly divided into two morphotypes: the nominal *Ancyrodella curvata* s.s. and an "early form." The s.s. morphotype bears a well-defined outer posterior lobe that is clearly bounded by sinuses both anteriorly and posteriorly, and this lobe carries a robust accessory carina. By contrast, the early form lacks a sharply demarcated outer posterior lobe, although it likewise exhibits a strong accessory carina in the same outer-posterior position; the platform outline is approximately trapezoidal.

Range: From FZ 7 - FZ 13c (Ji & Ziegler, 1993)

Studied material: 7 elements from PZD section (samples PZD 1, PZD 3-4)

***Ancyrodella hamata* Ulrich & Bassler, 1926**

(Pl. 1, fig. 2)

1926 *Ancyrodella hamata* n. sp. Ulrich & Bassler, p. 48, pl. 7, fig.7 (holotype)

2021 *Ancyrodella hamata* Ulrich & Bassler – Klapper, p. 309-310, figs. 2H, 3C-D

2023 *Ancyrodella hamata* Ulrich & Bassler – Farabegoli et al., pl. 1, figs. 1, 8-11

Description: With extremely rare exceptions, *Ancyrodella hamata* lacks posterior rows of nodes parallel to the carina. The secondary keels extend anteriorly.

Remarks: Klapper (2021) noted that *Ancyrodella hamata*, proposed in 1926, was largely unused except for Müller & Müller (1957), who applied it to a species closely related to *Ancyrodella nodosa* Ulrich & Bassler 1926, until its revival by Klapper & Kirchgasser (2016). Earlier, Huddle (1968) and Klapper & Lane (1985) had treated *An. hamata* as a junior synonym of *An. nodosa*, although both names originated in the same paper. Despite some intergradation, the two are distinguishable, particularly in platform outline (see Klapper & Kirchgasser 2016, fig. 9).

Range: From FZ 6 - FZ 13c (Klapper & Kirchgasser 2016)

Studied material: 3 elements from PZD section (samples PZD 1)

Genus *Ancyrognathus* Branson & Mehl, 1934

Type species: *Ancyrognathus symmetricus* Branson and Mehl, 1934

***Ancyrognathus cf. asymmetricus* (Ulrich & Bassler, 1926)**

(Pl. 5, fig. 1)

1926 *Palmatolepis asymmetrica* n. sp. (Ulrich & Bassler), p. 50, pl. 7, fig.18.

1990 *Ancyrognathus asymmetricus* (Ulrich & Bassler) – Klapper, p. 1003, pl. 14, figs. 4.1-4.16, 5.9-5.16

1995 *Palmatolepis asymmetrica* (Ulrich & Bassler) – Schülke, p. 63

Description: Fixed blade of Pa element typically on right side of platform; anterior carina interrupted or represented by extremely small denticles and commonly offset from fixed blade. The fixed blade is high and terminates abruptly distally, conspicuously offset from the centrally positioned carina; a wide, deep trough on its left side extends to mid-platform and contains very small, sometimes interrupted denticles of the anterior carina; the angle between the posterior and secondary carinae is acute, the secondary carina meets the anterior carina at an obtuse angle, and the free blade is generally undeveloped.

Range: From FZ 12 – FZ 13 (Schülke, 1995)

Studied material: 1 elements from PZD section (samples PZD 3)

***Ancyrognathus cryptus* Ziegler, 1962**

(Pl. 1, fig. 3)

1962 *Ancyrognathus crypta* n. sp. Ziegler, pp. 49-50, pl. 9, figs. 2-6 (holotype: pl. 9, figs. 2-4)

1995 *Ancyrognathus cryptus* Ziegler – Schülke, pl. 14, figs. 3-4

1996 *Ancyrognathus cryptus* Ziegler – Schülke, p. 39-40, pl. 1, figs. 4-14

Description: a slender platform that is strongly curved inward, with a sharply downward-bent posterior end. The free blade is very short, and the anterior three denticles are the highest. The platform's outer lobe, which is typical for the genus, is only weakly developed in this species.

Range: From the *Palmatolepis triangularis* Zone to the *Palmatolepis glabra pectinata* Zone (Spalletta et al., 2017)

Studied material: 1 elements from PZD section (samples PZD 8)

Genus *Branmehla* Hass, 1959

Type species: *Spathodus inornatus* Branson &Mehl, 1934

***Branmehla inornata* (Branson & Mehl, 1934)**

(Pl. 4, fig. 1)

1934 *Spathodus inornatus* n. sp. Branson & Mehl, p. 185, pl. 17, fig. 23

1959 *Branmehla inornata* (Branson & Mehl) – Hass, p. 381, pl. 50, fig. 3

2000 *Branmehla inornata* (Branson & Mehl) – Çapkinoğlu, p. 101-102, pl. 4, figs. 22-24

2003 *Branmehla inornata* (Branson & Mehl) – Corradini, p. 86, pl. 2, figs. 7-8

2013 *Branmehla inornata* (Branson & Mehl) – Kononova & Weyer, p. 27, pl. 1, figs. 1-4; pl. 2, figs. 3-5

Description: The blade is straight or gently arched, tapering gradually toward both the anterior and posterior extremities, and bears 16–18 denticles. The denticles are nearly uniform in size, laterally compressed, and basally fused. The basal cavity is slightly asymmetrical, relatively large, and positioned within the middle third of the blade.

Remarks: This genus differs from *Mehlina* YOUNGQUIST, 1945, in the relatively large basal cavity located in the posterior half of the blade and highest denticles located in the middle of the blade.

Range: From the *Palmatolepis marginifera utahensis* Zone to Tournaisian (Spalletta et al., 2017)

Studied material: 14 elements from QLX B section (samples QLXB C1-C3, QLXB C5)

Genus *Mehlina* Youngquist, 1945

Type species: *Mehlina gradata= Mehlina irregularis* Youngquist, 1945

***Mehlina gradata* (Branson & Mehl, 1934)**

(Pl. 1, fig. 7; Pl. 4, fig. 2)

1945 *Mehlina gradata* (Branson & Mehl, 1934) – Youngquist, 1945, p. 363, pl. 56, fig. 3

1957 *Mehlina gradata* (Branson & Mehl, 1934) – Müller & Müller, p. 1083, pl. 135, figs. 10

1985 Mehlina gradata (Branson & Mehl, 1934) – Klapper & Lane, p. 921, fig. 12.1

Description: A species of *Mehlina* characterized by a carminate, platform-less P1 element with a straight to gently arched blade; denticles subequal in height, laterally compressed and basally fused; cusp not markedly enlarged; basal cavity relatively large, slightly asymmetric, and situated near the middle third of the blade.

Remarks: This genus differs from *Branmehla* HASS, 1959, in the long and narrow basal cavity.

Range: From FZ 3 to the *Palmatolepis marginifera marginifera* Zone (Ziegler & Sandberg 1990; Spalletta et al., 2017)

Studied material: 2 elements from QLX A section (samples QLXA C1, QLXA C5-C14A); 70 elements from PZD section (samples PZD 5, PZD 10);

***Mehlina strigosa* (Branson & Mehl, 1934)**

(Pl. 4, fig. 3)

1934 *Spathodus strigosus* n. sp. Branson & Mehl, p. 187, pl. 17, fig. 17

1991 *Mehlina strigosa* (Branson & Mehl) – Perri & Spalletta, p. 60, 62, pl. 3, fig.6

1997 *Mehlina strigosa* (Branson & Mehl) – Çapkinoğlu, p. 182-183, pl. 4, figs. 3-7

2000 *Mehlina strigosa* (Branson & Mehl) – Çapkinoğlu, p. 99, pl. 4, figs. 19-21

2013 *Mehlina strigosa* (Branson & Mehl) – Kononova & Weyer, p. 28, pl. 1, figs. 8-10

2024 *Mehlina strigosa* (Branson & Mehl) – Barrera Lahoz et al., p. 30, fig. 8L

Description: Blade with long and slightly arched basement. Blade maximally high and four largest denticles usually located near anterior end. Lowest part of blade with 5–6 small denticles located behind largest denticles. Denticles vary from 12 to 14 in number, slightly enlarge towards the posterior end of blade, fused at the base, and have pointed tips. Basal cavity long, located behind middle of the basement, with narrow and symmetrical flank narrowing towards the ends of basal cavity.

Remarks: This species differs from *Mehlina irregularis* YOUNGQUIST, 1947, in the four large denticles located in the anterior part of the blade.

Range: From the *Palmatolepis termini* Zone to Tournaisian (Spalletta et al., 2017)

Studied material: 25 elements from QLX sections (samples QLXA C15, QLXA C17-C19, QLXB C1-C3, QLXB C5-C6);

Genus *Polygnathus* Youngquist, 1945

Type species: *Polygnathus dubius* Hinde, 1879

***Polygnathus aequalis* Klapper & Lane, 1985**

(Pl. 3, fig. 13)

1985 *Polygnathus aequalis* n. sp. Klapper & Lane, p. 930-931, pl. 16, figs. 7-14 (holotype: pl. 16, figs. 11-13)

1993 *Polygnathus aequalis* Klapper & Lane – Ji & Ziegler, p. 74, pl. 40, figs. 1-8

2008 *Polygnathus aequalis* Klapper & Lane – Ovnatanova & Kononova, p. 1109, 1111, pl. 23, fig. 12

2017 *Polygnathus aequalis* Klapper & Lane – Ovnatanova et al., p. 1115, pl. 34, fig. 4

2023 *Polygnathus aequalis* Klapper & Lane – Farabegoli et al., pl. 14, figs. 1-2; pl. 16, figs. 2-3

Description: Platform elongate-lanceolate with lateral margins equally elevated; free blade high, denticulate, about half the platform length with tallest denticles anteriorly; basal cavity small with narrow flanks, positioned in the anterior third; ornamentation ranges from nearly smooth to short transverse ridges best developed along the margins, which posteriorly may split into nodes; posterior end slightly pointed; anterior end of platform straight or angular.

Remarks: *Polygnathus aequalis* can be separated from *Polygnathus webbi* Stauffer, 1938 and *Polygnathus alatus* Huddle, 1934 by uniformly elevated along whole length of lateral margins, a comparatively longer free blade, and short transverse ridges lining the platform margins.

Range: About previously published ranges: Ovnatanova et al. (2017) reported FZ 3-12, while Klapper & Kirchgasser (2016) gave FZ 5–12. In our study, however, we also recognize this species in FZ 13b-13c, consistent with nearby sections (Farabegoli et al., 2023).

Studied material: 12 elements from PZD section (samples PZD 1, PZD 3, PZD 4)

***Polygnathus alatus* Huddle, 1934**

(Pl. 4, fig. 5)

1934 *Polygnathus alata* n. sp. Huddle, p. 100, pl. 8, figs. 19-20 (holotype)

1985 *Polygnathus alata* Huddle – Klapper & Lane, p. 932, fig. 16.15-16.17

1993 *Polygnathus alata* Huddle – Ji & Ziegler, p. 74, pl. 39, figs. 1-3

2001 *Polygnathus alata* Huddle – Ovnatanova & Kononova, p. 40, pl. 1, figs. 3-4; pl. 3, fig. 13; pl. 9, figs. 6-8

2008 *Polygnathus alata* Huddle – Ovnatanova & Kononova, p. 1111, 1113, pl. 18, figs. 9-12

2017 *Polygnathus alata* Huddle – Ovnatanova et al., p. 1115-1116, pl. 3, figs. 7, 9; pl. 5, figs. 4-5, 7; pl. 6, figs. 1-2; pl. 8, fig. 5

Description: Asymmetrical platform (Class IIIb symmetry; Lane, 1968), right margin higher than left); posterior end slightly rounded to pointed; free blade high and about half the platform length; median ridge low, nodular, and reaching or nearly reaching the posterior end; troughs deep and narrow; platform otherwise smooth, with only weak nodes or short ridges on the posterior parts of the lateral margins; basal cavity small, lens shaped, with narrow flanks and situated in the anterior third of the platform.

Remarks: *Polygnathus alatus* differs from *Polygnathus decorosus* Stauffer, 1938 in its platform outline and the nearly smooth platform surface.

Range: From FZ 1 - FZ 5 (Ovnatanova et al., 2017)

Studied material: 9 elements from QLX A section (samples QLXA C2-C5, QLXA C6A)

***Polygnathus brevilaminus* Branson & Mehl, 1934**

(Pl. 3, figs. 5-6 ; Pl. 4, fig. 6)

1934 *Polygnathus brevilaminus* n. sp. Branson & Mehl, p. 146, pl. 21, figs. 3-6

1985 *Polygnathus brevilaminus* Branson & Mehl – Klapper & Lane, p. 934

1995 *Polygnathus brevilaminus* Branson & Mehl – Schülke, p. 58, pl. 17, fig. 13-14

2013 *Polygnathus brevilaminus* Branson & Mehl – Tagarieva, fig. 7U, 7V

2015 *Polygnathus brevilaminus* Branson & Mehl – Huang, p. 109, pl. 12, fig. 10, 14; pl. 13, figs. 14-16

2019 *Polygnathus brevilaminus* Branson & Mehl – Zhang, pl. 41, figs. 8-14 [Only]

2023 *Polygnathus brevilaminus* Branson & Mehl – Farabegoli et al., pl. 13, figs. 1-4

2024 *Polygnathus brevilaminus* Branson & Mehl – Barrera Lahoz et al., p. 20-21, fig. 5J

Description: The carina extends behind the posterior margin of the platform as the most distinctive feature. Platform short and narrow-elongate, with parallel lateral margins, approximately square outline; free blade long and high, with denticles of unequal height; platform surface generally smooth, with lateral margins bearing poorly developed transverse ridges or fine nodose ornamentation. This taxon is characterized by a short, narrow platform that fails to reach the posterior end of the element and by its distinctive ornamentation; the generic placement of *P. brevilaminus* has been questioned, and some authors have proposed erecting a new genus (Ji & Ziegler, 1993; Corradini, 2003).

Remarks: *Polygnathus brevilaminus* differs from *Polygnathus angustidiscus* Youngquist, 1945 by its smoother platform, a more nearly square outline, and a carina almost as high as the platform.

Range: From FZ 13b/13c to the the *Pseudopolygnathus granulosus* Zone (Schülke 1995; Spalletta et al., 2017).

Studied material: 9 elements from PZD section (samples PZD 5A-6, PZD 7-8, PZD 12); 1 elements from QLX A section (sample QLXA C14).

***Polygnathus brevis* Miller & Youngquist, 1947**

(Pl. 3, fig. 4)

1947 *Polygnathus brevis* n. sp. Miller & Youngquist, p. 514, pl. 74, fig. 9 (holotype)

1993 *Polygnathus brevis* Miller & Youngquist – Ji & Ziegler, p. 75, pl. 37, fig. 22

1995 *Polygnathus brevis* Miller & Youngquist – Schülke, p. 58, pl. 13, fig. 24

2008 *Polygnathus brevis* Miller & Youngquist – Ovnatanova & Kononova, p. 1117, 1119, pl. 23, figs. 8-11
2015 *Polygnathus brevis* Miller & Youngquist – Huang, p. 109-110, pl. 12, fig. 9
2017 *Polygnathus brevis* Miller & Youngquist – Ovnatanova et al., p. 1116, 1119, pl. 42, fig. 9
2023 *Polygnathus brevis* Miller & Youngquist – Farabegoli et al., pl. 16, figs. 7-8

Description: Linguiform platform, wide, slightly asymmetric, and slightly convex; anterior lateral margins elevated and posterior margins flattened; posterior extremity discrete, turned inward and downward; ornamentation of coarse transverse ridges on the anterior platform grading posteriorly into thin transverse ridges, with the posterior tip bearing fine nodes in transverse rows that commonly coalesce into discontinuous transverse ridges; median ridge high, slightly arched, denticulate, and usually terminating near mid-platform; free blade with 4–5 denticles; troughs relatively deep and wide anteriorly, typically ending near the platform middle; basal cavity small, lens-shaped, with narrow flanks, situated in the anterior third of the platform.

Remarks: In juveniles, the lateral margins are upraised and the troughs stay deep all the way to the posterior tip; the median ridge likewise attains the posterior end.

Range: Ovnatanova et al. (2017) did not estabalish a full range, only confirmed in the Late *rhenana* Zone (FZ 12-13a Zone); Klapper & Kirchgasser (2016) documented a range of FZ 11–MN 13b, and Farabegoli et al. (2023) also reported sections in the Carnic Alps. Based on our material, the range may extend into FZ 13c.

Studied material: 1 elements from PZD section (samples PZD 4)

***Polygnathus decorosus* Stauffer, 1938**

(Pl. 3, fig. 12; Pl. 4, figs. 7-8)

1938 *Polygnathus decorosus* n. sp. Stauffer, p. 438, pl. 53, figs. 5-6, 10, 15-16
1985 *Polygnathus decorosus* Stauffer – Klapper & Lane, p. 935, fig. 18.7
1993 *Polygnathus decorosus* Stauffer – Ji & Ziegler, p. 77, pl. 40, figs. 16-18
2008 *Polygnathus decorosus* Stauffer – Ovnatanova & Kononova, p. 1121, pl. 17, figs. 8-11

2015 *Polygnathus decorosus* Stauffer – Huang, p. 110-111, pl. 12, figs. 15-17

2017 *Polygnathus decorosus* Stauffer – Ovnatanova et al., p. 1120, pl. 26, figs. 7-8; pl. 41, figs. 10-11

2023 *Polygnathus decorosus* Stauffer – Farabegoli et al., pl. 13, figs. 6, 8-10

Description: The most distinctive feature is the ornamentation by short transverse ridges or small nodes. Platform narrow, elongate, and arrow shaped; anterior end slightly pointed, somewhat detached, and ventrally arched; posterior end pointed and ventrally arched; lateral margins equally elevated and slightly compressed anteriorly; median ridge high, nearly straight and gently arched, nodose with basally fused nodes, reaching the posterior end; free blade long with denticles, nearly as long as the platform; troughs symmetrically narrow, deep anteriorly, flattening posteriorly, and continuing to the posterior end as narrow grooves flanking the median ridge; basal cavity small, rounded, with wide flanks.

Remarks: *Polygnathus decorosus* differs from *Polygnathus xylus* Stauffer, 1940 by its arrow-shaped platform and marginal ornamentation of nodes or short transverse ridges.

Range: According to Ovnatanova et al. (2017), ranges from FZ 5/6 - FZ 11/12, whereas Klapper & Kirchgasser (2016) record its highest occurrence in FZ 13c.

Studied material: 26 elements from PZD section (samples PZD 1, PZD 3-4); 2 elements from QLX A section (samples QLXA C6, QLXA C12A);

***Polygnathus elegantulus* Klapper & Lane, 1985,**

(Pl. 3, fig. 8)

1985 *Polygnathus elegantulus* n. sp. Klapper & Lane, p. 935, pl. 18, figs. 8-14, pl. 21, fig. 8

1993 *Polygnathus elegantulus* Klapper & Lane – Ji & Ziegler, p. 78, pl. 37, figs. 4-7

2019 *Polygnathus elegantulus* Klapper & Lane – Zhang, p. 264- 265, pl. 41, figs. 15-18

Description: The platform is elliptical, with the posterior end slightly incurved and pointed; ornamented by marginal transverse ridges or nodes, separated from the carina by deep adcarinal troughs; median ridge is curved, denticulate, and extends to the anterior end of the platform; basal cavity is relatively large but remains elongate in outline.

Remarks: *Polygnathus elegantulus* differs from *Polygnathus decorosus* Stauffer, 1938 by its wider platform and characteristic platform outline.

Range: From FZ 3 to the *Palmatolepis delicatula platys* Zone (Ji & Ziegler, 1993)

Studied material: 2 elements from PZD section (samples PZD 1)

***Polygnathus eoglaber* Ji & Ziegler, 1993**

(Pl. 3, fig. 9)

1993 *Polygnathus eoglaber* n. sp. Ji & Ziegler, p. 78, pl. 36, figs. 10-16; text-fig. 21.10 (holotype: pl. 36, figs. 14-15)
2015 *Polygnathus eoglaber* Ji & Ziegler – Huang, p. 111, pl. 13, figs. 8-9
2023 *Polygnathus eoglaber* Ji & Ziegler – Farabegoli et al., pl. 13, figs. 17-18

Description: Characterized by a small, heart-shaped platform with a convex latero-outer margin and a convex to weakly sinuous latero-inner margin; anterior free blade commonly longer than the platform and increasing in height anteriorward;adcarinal troughs are generally shallow and wide; median ridge is high and extends to the posterior end of the platform, in some cases even continuing beyond it to form a very short posterior free blade; basal cavity located at or near the anterior end of the platform.

Remarks: The combination of an anterior free blade and a distinctive small, heart-shaped platform makes it readily distinguishable.

Range: From the *Palmatolepis minuta minuta Zone* to the *Palmatolepis gracilis gracilis Zone* (Spalletta et al., 2017)

Studied material: 9 elements from PZD section (samples PZD 9-10, PZD 12)

***Polygnathus experplexus* Sandberg & Ziegler, 1979**

(Pl. 4, figs. 12-13)

1979 *Polygnathus experplexus* n. sp. Sandberg & Ziegler, p. 185-186, pl. 4, figs. 2-6 (holotype: pl. 4, fig. 2)

1991 *Polygnathus experplexus* Sandberg & Ziegler – Perri & Spalletta, p. 70, pl. 5, fig. 3

1993 *Polygnathus experplexus* Sandberg & Ziegler – Ji & Ziegler, p. 79, text-fig. 20.7

2003 *Polygnathus experplexus* Sandberg & Ziegler – Corradini, p. 87, pl. 9, fig. 18

2021 *Polygnathus experplexus* Sandberg & Ziegler – Over et al., fig. 5.9

Description: This species is characterized by a broad posterior part of the platform with an obviously constricted "rostrum area" and a moderately cello-like platform outline. In the anterior platform, a strong inner rostral ridge diverges from the carina, whereas a second ridge, almost parallel to the carina, and rostral trough broadly expanded; moderately to strongly curved platform; the posterior part of the platform is covered by thin nodes, arranged in weak transverse rows.

Remarks: *Polygnathus experplexus* differs from *Polygnathus perplexus* Thomas, 1949 in the strongly divergent inner rostral ridge and nodes arranged to form weak transverse ridges.

Range: From the *Palmatolepis gracilis manca Zone* to the *Bispathodus costatus Zone* (Spalletta et al., 2017)

Studied material: 6 elements from QLX B section (samples QLXB C2-C4)

***Polygnathus krestovnikovi* Ovnatanova, 1969**

(Pl. 4, fig. 11)

1969 *Polygnathus krestovnikovi* n. sp. Ovnatanova, p. 141, pl. 1, fig. 3 (holotype)

2001 *Polygnathus krestovnikovi* Ovnatanova – Ovnatanova & Kononova, p. 43, pl. 28, fig. 7; pl. 29, figs. 1-33; pl. 30, figs. 5, 8, 15-16
2008 *Polygnathus krestovnikovi* Ovnatanova – Ovnatanova & Kononova, p. 1131, 1133, pl. 23, figs. 13-14

Description: Platform asymmetrical pair (Class IIIb symmetry; Lane, 1968): in the left units the outer side is lobelike widened and the inner side is almost straight, whereas the right units show a convex inner side. The anterior end of the platform is stepped, and the posterior end is pointed and arched downwards; lateral margins are raised, producing a poorly pronounced short rostrum in the anterior third of the platform, with the outer-side margin behind the rostrum lobelike widened; the median ridge is arched, low, and nodular, well developed through the anterior two-thirds of the platform and terminating short of the posterior end; the free blade is high, denticulated, and half as long as the platform; weakly pronounced rostrum in the anterior third and platform become flattened toward the posterior end; ornamentation consists of denticulation of the anterior platform margins formed by the ends of coarse and long transverse ridges, while in the posterior part the ridges are thinner and usually divide into nodes; the basal cavity is small, lens-shaped, and located in the anterior third of the platform.

Remarks: Due to preservation, the ornamentation cannot be observed in sufficient detail in our element. *Polygnathus krestovnikovi* differs from *Polygnathus webbi* Stauffer, 1938 by short, weakly expressed rostrum, posteriorly flattened lateral platform margins, and troughs that become flattened toward the rear of the platform.

Range: From FZ 11/12 – FZ 13b/13c (Ovnatanova & Kononova, 2008)

Studied material: 1 elements from QLX A section (samples QLXA C13B)

***Polygnathus lodinensis* Pölster, 1969**

(Pl. 3, fig. 3)

1969 *Polygnathus lodinensis* n. sp. Pölster, p. 425-426, pl. 6, figs. 1-12 (holotype: pl. 6, figs. 1-3)

2008 *Polygnathus lodinensis* Pölster – Ovnatanova & Kononova, p. 1135, 1137, pl. 19, figs. 21-22

2015 *Polygnathus lodinensis* Pölster – Huang, p. 111-112, pl. 13, figs. 10-12

2017 *Polygnathus lodinensis* Pölster – Ovnatanova et al., p. 1128, pl. 35, figs. 7, 10-11; pl. 38, figs. 10-12; pl. 41, figs. 6-7; pl. 43, figs. 1-2

2019 *Polygnathus lodinensis* Pölster – Zhang, p. 267, pl. 48, figs. 14-18

2023 *Polygnathus lodinensis* Pölster – Farabegoli et al., pl. 13, figs. 7, 11-12

Description: Spear-shaped to lanceolate platform with strongly elevated margins and a broad anterior depression; anterior end semicircular or pointed, posterior end pointed and ventrally arched; free blade high, denticulate, approximately half the platform length; median ridge straight, high, denticulate, reaching the posterior extremity; ornamentation consisting of small nodes arranged along margins of smooth platform; basal cavity small, rounded, with narrow flanks, situated in the anterior third; troughs wide and deep in anterior half of platform, narrow posteriorly, and reaching posterior end of platform.

Remarks: This species mostly occurs in the deep water deposits of the basin. Compared with *Polygnathus aequalis* Klapper & Lane, 1985, *Polygnathus lodinensis* has troughs that are wide and deep in the anterior half of the platform.

Range: From FZ 7/8 – FZ 13b/13c (Ovnatanova et al., 2017)

Studied material: 98 elements from PZD section (samples PZD 1-4)

***Polygnathus macilentus* Kuzmin, 1993**

(Pl. 4, fig. 10)

1993 *Polygnathus macilentus* n. sp. Kuzmin – Obukhovskaya and Kuzmin, p. 47, pl. 2, fig. 9

2000 *Polygnathus macilentus* Kuzmin – Ziegler et al., pl. 9, fig. 13

2008 *Polygnathus macilentus* Kuzmin – Ovnatanova & Kononova, p. 1137, pl. 22, figs. 10-11

2013 *Polygnathus macilentus* Kuzmin – Tagarieva, fig. 7T

2015 *Polygnathus macilentus* Kuzmin – Huang, p. 112, pl. 13, figs. 17-19

Description: Platform outline short, spear-shaped, and elongate-triangular; the platform surface is smooth, with a semicircular anterior end and a pointed posterior end; free blade is nearly as long as the platform; median ridge is high, smooth, slightly arched, and reaches the posterior end of the platform or terminates near it; troughs are narrow and long, extending to the posterior end of the platform; basal cavity is small, with narrow flanks, and is situated near the anterior end of the platform.

Remarks: *Polygnathus macilentus* differs from *Polygnathus krestovnikovi* Ovnatanova, 1969 by platform spear-shaped elongated triangular and platform surface smooth.

Range: *Polygnathus macilentus* has been recorded from the Askyn Regional Stage of Russia (Ovnatanova & Kononova, 2008). The Askyn Stage corresponds to the interval from the base of the Upper *rhenana* Zone to the top of the *linguiformis* Zone (Ovnatanova et al., 2017, p. 983). Accordingly, the stratigraphic distribution of this species can be constrained to MN 12–MN 13c

Studied material: 4 elements from PZD section (sample PZD 4);1 elements from QLX A section (samples QLXA C13)

***Polygnathus margaritatus* Schäfer, 1976**

(Pl. 4, fig. 15)

1976 *Polygnathus margaritatus* n. sp. Schäfer, p. 144-145, pl. 1, figs. 1-6

1991 *Polygnathus margaritatus* Schäfer – Perri & Spalletta, p. 71

Description: The platform bears a well-developed long rostrum, nearly parallel to the median ridge, bearing denticles; nodes are arranged in longitudinal rows, almost connected with the rostrum; the platform surface is ornamented with small nodes; troughs are symmetrically narrow, deep anteriorly, and flattening posteriorly.

Remarks: *Polygnathus margaritatus* differs from *Polygnathus experplexus* Sandberg & Ziegler, 1979 by platform slightly curved and well-developed rostrum, with nodes arranged in longitudinal rows.

Range: From the *Pseudopolygnathus granulosus* Zone to the *Bispathodus costatus Zon*e (Spalletta et al., 2017)

Studied material: 1 elements from QLX B section (samples QLXB C6)

***Polygnathus mirificus* Ji & Ziegler, 1993**

(Pl. 3, fig. 1-2)

1993 *Polygnathus mirificus* n.sp. Ji & Ziegler, pl. 37, figs. 16-21 (holotype: pl. 37, fig. 21)

2014 *Polygnathus mirificus* Ji & Ziegler – Mossoni, p. 127

Description: The anterior outer platform margin with 3-5 denticles is the most distinctive feature.The platform outline is asymmetrical, lanceolate, and bears variably developed transverse ridges; anterior blade is moderately tall and occupies roughly one-third of the element's length; the inner margin is nearly straight to gently convex and only slightly upturned, whereas the outer margin is conspicuously convex, strongly upturned, and rises well above the inner margin; the median ridge is low, composed of discrete to coalescent denticles, and generally reaches the posterior tip of the platform; the basal cavity is relatively small and ovate, positioned in the anterior third of the platform; and the keel is sharply developed.

Remarks: *Polygnathus mirificus* differs from *Polygnathus webbi* Stauffer, 1938 by asymmetrical platform outline and denticulate outer platform margin, and from *Polygnathus decorosus* Stauffer, 1938 by its anterior outer platform margin with 3-5 denticles

Range: From FZ 11 – FZ 13 (Ji & Ziegler, 1993).

Studied material: 12 elements from PZD section (samples PZD 1, PZD 3-4)

***Polygnathus mosquensis* Litvinova, 1996**

1996 *Polygnathus mosquensis* n. sp. Litvinova – Ovnatanova & Kononova, p. 57-58, pl. 5, fig. 11 (holotype)

2001 *Polygnathus mosquensis* Litvinova – Ovnatanova & Kononova, p. 44, pl. 12, figs. 24-28

Description: A low, weakly nodose median ridge, not reaching the posterior end is the most distinctive feature. Pear-shaped platform; margins upturned along the whole platform length; posterior end rounded; troughs narrow and deep; platform smooth except for slight serration on the margins; basal cavity small, lenticular, in the anterior third.

Remarks: The material is represented only by fragmentary elements in our collections, for which no photographs are available. *Polygnathus mosquensis* differs from *Polygnathus znepolensis* Spassov, 1965 in median ridge, not reaching the posterior end is the most distinctive feature and posterior end well-rounded.

Range: Records of *Polygnathus mosquensis* are extremely scarce, with mention limited to Ovnatanova & Kononova (2001, p. 44), where its occurrence is reported from the Semiluki Horizon (a regional stage in Russia). The Semiluki Horizon corresponds to the interval from the base of the puncatata Zone to the top of the jamieae Zone (Ovnatanova et al., 2017, p. 983). Accordingly, the stratigraphic range of this fossil can be constrained to FZ 5 – FZ 11.

Studied material: 2 elements from QLX A section (samples QLXA C10-C11)

***Polygnathus nodocostatus nodocostatus* Branson & Mehl, 1934**

(Pl. 3, fig. 10)

1934 Polygnathus nodocostatus n. sp. Branson & Mehl, p. 246, pl. 20, figs. 9-13; pl. 2, fig.15

1985 *Polygnathus nodocostatus nodocostatus* Branson & Mehl – Klapper & Lane, p. 941, fig. 21.10

2003 *Polygnathus nodocostatus nodocostatus* Branson & Mehl – Corradini, p. 89, pl. 9, figs. 1-2

2014 *Polygnathus nodocostatus nodocostatus* Branson & Mehl – Mossoni, p. 128, pl. 2, figs. 3, 14

2023 *Polygnathus nodocostatus nodocostatus* Branson & Mehl – Farabegoli et al., pl. 16, fig. 13

2024 *Polygnathus nodocostatus nodocostatus* Branson & Mehl – Barrera Lahoz et al., p. 23, fig. 6I-6K

Description: Symmetrical platform with ovate to rhombic outlines; width variable but more commonly broad; short free blade bearing few, high denticles; median ridge straight to arched, not reaching the posterior end; inner margin straight to moderately convex, outer margin convex; ornamentation of node rows subparallel to the carina, in broad-platform forms aligned in a "V" to form ridges meeting the carina at an acute angle; adcarinal grooves deep but short, confined to the anterior platform; keel fine, with a reduced basal cavity in the anterior third, continuing posteriorly as thin keels.

Remarks: *Polygnathus nodocostatus nodocostatus* differs from *Polygnathus experplexus* Sandberg & Ziegler, 1979 by no low collar along the carina in the anterior part of the platform and platform outline.

Range: From the *Palmatolepis crepida* to the *Palmatolepis gracilis expansa* Zone (Spalletta et al., 2017)

Studied material: 1 elements from PZD section (samples PZD 10)

***Polygnathus perplexus* Thomas, 1949**

(Pl. 4, fig. 14)

1949 *Polygnathus perplexa*? n. sp. Thomas, p. 418-419, pl. 2, fig. 23
1989 *Polygnathus perplexus* Thomas – Metzger, p. 520-521, fig. 15.12-14, 15.25
1991 *Polygnathus perplexus* Thomas – Perri & Spalletta, p. 72
1993 *Polygnathus perplexus* Thomas – Ji & Ziegler, p. 83, text-fig. 20.2
2003 *Polygnathus perplexus* Thomas – Corradini, pl. 9, fig. 15
2014 *Polygnathus perplexus* Thomas – Mossoni, p. 131, pl. 2, fig. 5
2019 *Polygnathus perplexus* Thomas – Zhang, p. 279, pl. 44, figs. 6-8; pl. 47, fig. 17
2021 *Polygnathus perplexus* Thomas – Over et al., fig. 5.12

Description: The platform is slender and slightly asymmetry; the anterior platform carries two collar-like rostral ridge of unequal height that run parallel to the carina; ornamentation consists of nodes arranged in longitudinal rows.

Remarks: *Polygnathus perplexus* differs from *Polygnathus nodocostatus nodocostatus* Branson & Mehl, 1934 by collar-like rostral ridge.

Range: From the *Palmatolepis marginifera utahensis* Zone to the *Bispathodus ultimus* Zone (Spalletta et al., 2017)

Studied material: 1 elements from QLX B section (samples QLXB C3)

***Polygnathus praecursor* Matyja, 1993**

(Pl. 3, fig. 11)

1993 *Polygnathus praecursor* n. sp. Matyja, p. 40-41, pl. 24, figs. 12-13; pl. 25, fig. 4 (holotype: pl. 24, fig. 13)

2022 *Polygnathus praecursor* Matyja – Baranov et al., P. 60, fig. 4B-E

2023 *Polygnathus praecursor* Matyja – Farabegoli et al., pl. 14, figs. 6-10; pl. 15, figs. 10-11, 13; pl. 16, fig. 4

Description: The middle part of platform widest narrowing both anteriorly and posteriorly is the most distinctive feature. The platform long, curved; trough shallow; median ridge reaches the posterior end of the platform; platform anterior part smooth or ornamented weak ridge, middle part weak ridge or nodes, posterior part with nodes; posterior end rounded or pointed; develop small basal.

Remarks: *Polygnathus praecursor* differs from *Polygnathus procerus* Sannemann, 1955 by its middle part of platform widest.

Range: From the *Palmatolepis subperlobata* Zone to the *Palmatolepis crepida* Zone (Spalletta et al., 2017)

Studied material: 19 elements from PZD section (samples PZD 5B, PZD 6A, PZD 10, PZD 12)

Polygnathus praepolitus Kononova, Alekseev, Barskov & Reimers, 1996

(Pl. 4, fig. 9)

1996 *Polygnathus praepolitus* n. sp. Kononova, Alekseev, Barskov & Reimers, p. 96, pl. 12, figs. 1-5 (holotype: pl. 12, fig. 2)

2001 *Polygnathus praepolitus* Kononova, Alekseev, Barskov & Reimers – Ovnatanova & Kononova, p. 45-46, pl. 15, figs. 6-8, 23-24; pl. 25, figs. 6-13

2008 *Polygnathus praepolitus* Kononova, Alekseev, Barskov & Reimers – Ovnatanova & Kononova, p. 1147, pl. 21, figs. 8-9

2023 *Polygnathus praepolitus* Kononova, Alekseev, Barskov & Reimers – Farabegoli et al., pl. 13, figs. 13, 15-16

Description: The most distinctive feature is the posterior end of median ridge and the posterior end of the platform at the same point. Platform narrowed near anterior end and elongated lanceolate; lateral margins raised, usually at the same level from anterior to the posterior part; free blade denticulated, half the platform length; troughs narrow and deep; median ridge arched and denticulated; basal cavity small, lenticular, positioned within the anterior third of the platform.

Remarks: *Polygnathus praepolitus* differs from *Polygnathus xylus* Stauffer, 1940 in that *Po. xylus* possesses a longer free blade and more parallel lateral margins.

Range: From MN 1/2 – MN11/12 (Ovnatanova et al., 2017).

Studied material: 9 elements from QLX A section (samples QLXA C6D, QLXA C7A-C7D)

Polygnathus procerus Sannemann, 1955b

(Pl. 3, fig. 7)

1955b *Polygnathus procerus* n. sp. Sannemann, p. 150, pl. 1, fig. 11

1993 *Polygnathus procerus* Sannemann – Ji & Ziegler, p. 83-84, pl. 38, figs. 4-8

2003 *Polygnathus procerus* Sannemann – Corradini, p. 90, pl. 8, figs. 14

2015 *Polygnathus procerus* Sannemann – Huang, p. 112-113, pl. 13, figs. 1-2

2023 *Polygnathus procerus* Sannemann – Farabegoli et al., pl. 14, fig. 5; pl. 15, figs. 1-6, 7
2024 *Polygnathus procerus* Sannemann – Barrera Lahoz et al., p. 25-26, fig. 5I

Description: The anterior free blade with denticles arranged in a fan-shaped pattern is the most distinctive feature. The platform is small and slender, with a lanceolate outline and slight asymmetry; Trough deep and broad anteriorly, shallowing posteriorly to disappear; median ridge turned downward, denticles and reaching the posterior end of platform; platform surface irregularly pronounced transverse ridge; small basal cavity, thin keel.

Remarks: Compared to *Polygnathus procerus*, the platform of *Polygnathus decorosus* Stauffer, 1938 is more regular, its lateral margin almost parallel.

Range: From the *Palmatolepis minuta minuta* Zone to the *Palmatolepis glabra pectinata* Zone (Spalletta et al., 2017)

Studied material: 27 elements from PZD section (samples PZD 7-10, PZD 12)

***Polygnathus subirregularis* Sandberg & Ziegler, 1979**

(Pl. 4, fig. 17)

1974 *Polygnathus subirregularis* n. sp. Sandberg & Ziegler, p. 186, pl. 4, figs. 9-13
2021 *Polygnathus subirregularis* Sandberg & Ziegler – Over et al., fig. 5.5, 5.10

Description: The platform, with ovate to rhomboidal outline; carina from straight to sharply deflected outward at the middle of the platform. Ornamentation consists of ridges or nodal rows that lie subparallel to the carina. The platform bears two subparallel ridges (or nodal rows) separated from the carina by adcarinal grooves; inner adcarinal groove becomes shallower around midlength and persists to the posterior margin; outer adcarinal groove commonly extends to the posterior margin of the platform but is shallower than the inner.

Remarks: *Polygnathus subirregularis* differs from *Polygnathus perplexus* Thomas, 1949 by its inner adcarinal groove becoming shallow at the mid-platform and nodes being irregularly distributed.

Range: From the *Palmatolepis rugosa trachytera* Zone to the *Palmatolepis gracilis expansa* Zone (Spalletta et al., 2017)

Studied material: 5 elements from QLX A section (samples QLXA C18)

***Polygnathus webbi* Stauffer, 1938**

(Pl. 3, fig. 14)

1938 *Polygnathus webbi* n. sp. Stauffer, p. 439, pl. 53, figs. 25-26, 28-29

1985 *Polygnathus webbi* Stauffer – Klapper & Lane, p. 944-945, fig. 16.18

1947 *Polygnathus webbi* Stauffer – Miller & Youngquist, p. 515, pl. 74, figs. 1-2

1993 *Polygnathus webbi* Stauffer – Ji & Ziegler, p. 85-86, pl. 39, figs. 4-8

1995 *Polygnathus webbi* Stauffer – Schülke, p. 61, pl. 13, fig. 11-12

2015 *Polygnathus webbi* Stauffer – Huang, p. 113-114, pl. 12, figs. 12-13; pl. 13, figs. 6-7

2023 *Polygnathus webbi* Stauffer – Farabegoli et al., pl. 14, figs. 3-4; pl. 16, figs. 1, 11-12

Description: Asymmetrical platform (Class IIIb symmetry; Lane, 1968), with left- and right-curved specimens differing in platform outline. Anterior right margin distinctly higher than left margin in both left and right curved Pa elements; median ridge reaching posterior end of the platform, paralleled by adcarinal troughs and moderately arched; fine transverse ridges on the platform.

Remarks: In right curved specimens, the outer platform margin may be slightly to strongly constricted anteriorly and commonly posteriorly as well, although in some specimens the margin is a simple convex curve throughout. In left curved specimens, the outer platform margin appears to be constricted anteriorly. The originally named *Polygnathus webbi* Stauffer, 1938 represents the right-curved morph, whereas *Polygnathus normalis* Miller & Youngquist, 1947 represents the left-curved morph. This study concurs with Klapper (Klapper, 1971) two morphs are

synonymous, reflecting the development of Class IIIb symmetry (Lane, 1968); accordingly, the senior name, *Po. webbi* is retained.

Range: From FZ 2 – FZ 13c (Huang, 2014)

Studied material: 5 elements from PZD section (samples PZD 1-2, PZD 4)

***Polygnathus xylus* Stauffer, 1940**

1940 *Polygnathus xylus* n. sp. Stauffer, p. 430, pl. 60, figs. 54, 66, 72-74
2001 *Polygnathus xylus* Stauffer – Ovnatanova & Kononova, p. 48, pl. 1, figs. 5–7, 11
2008 *Polygnathus xylus* Stauffer – Ovnatanova & Kononova, p. 1158, pl. 17, figs. 1-7
2017 *Polygnathus xylus* Stauffer – Ovnatanova & Kononova, p. 1139-1140, pl. 2, figs. 3-4; pl. 7, fig. 1; pl. 8, figs. 1-6; pl. 10, figs. 1-2; pl. 19, figs. 3-4, 6-7; pl. 20, figs. 1, 7; pl. 21, fig. 1; pl. 25, fig. 5

Description: The free blade has peg-shaped denticles and reaches the platform length or a little more, which is the most distinctive feature. Platform almost symmetrical, elongated, arrow-shaped or lanceolate, and slightly curved, with lateral margins nearly parallel, elevated to the posterior end and higher than the median ridge; margins bear short, fine transverse ridges forming weak denticulation, the platform otherwise mostly smooth; posterior end pointed and lightly downturned; median ridge straight or slightly arched, vaguely denticulate, reaching the posterior end; troughs deep, symmetrical, and steeply inclined downward anteriorly; basal cavity rounded, near the anterior end of the platform or at the junction of the platform and free blade.

Remarks: *Polygnathus xylus* differs from *Polygnathus decorosus* Stauffer, 1938 by its smooth platform with slightly denticulated margins.

Range: From Givetian to FZ 5/6 (Ovnatanova et al., 2017)

Studied material: 4 elements from QLX A section (samples QLXA C2, QLXA C6-C6A)

Polygnathus zinaidae Kononova, Alekseev, Barskov & Reimers, 1996

(Pl. 4, fig. 16)

1996 *Polygnathus zinaidae* n. sp. Kononova, Alekseev, Barskov & Reimers, p. 98, pl. 12, figs. 6-8 (holotype: pl. 12, fig. 7)

2001 *Polygnathus zinaidae* Kononova, Alekseev, Barskov & Reimers – Ovnatanova & Kononova, p. 48-49, pl. 10, figs. 12–17; pl. 14, figs. 1–39; pl. 15, figs. 1–5, 9–14; pl. 23, figs. 30–41; pl. 24, figs. 12–32

2008 *Polygnathus zinaidae* Kononova, Alekseev, Barskov & Reimers – Ovnatanova & Kononova, p. 1158-1159, pl. 22, figs. 12-15

Description: The most distinctive feature is a wide, irregularly pear-shaped, asymmetrical platform (Class IIIb symmetry; Lane, 1968) whose lateral margins are raised along the entire length and narrow anteriorly to form a rostrum. Outer margin lobe-like widened; anterior end stepped and posterior end pointed; median ridge arched, weakly nodose, and reaching the posterior end of the platform; free blade high, slightly exceeding half the platform length, with denticles of uniform size; troughs narrow and deep; platform surface smooth, some with short, poorly pronounced transverse ridges; basal cavity small, lens-shaped with narrow flanks, situated in the anterior third.

Remarks: *Polygnathus zinaidae* differs from *Polygnathus alatus* Huddle, 1934 in the irregularly pearshaped platform and the slightly denticulated platform margins in its anterior part.

Range: From 7/8-11/12 (Ovnatanova & Kononova, 2008)

Studied material: 578 elements from QLX A section (samples QLXA C6, QLXA C6D-C19)

Polygnathus cf. *zinaidae* Kononova, Alekseev, Barskov & Reimers, 1996

(Pl. 4, figs. 20-21)

1996 *Polygnathus zinaidae* n. sp. Kononova, Alekseev, Barskov & Reimers, p. 98, pl. 12, figs. 6-8 (holotype: pl. 12, fig. 7)

Description: The most distinctive feature is a wide, irregularly pear-shaped, asymmetrical platform (Class IIIb symmetry; Lane, 1968) whose lateral margins are raised along the entire length and narrow anteriorly to form a rostrum. Outer margin lobe-like widened; anterior end stepped and posterior end pointed; median ridge arched, weakly nodose, and reaching the posterior end of the platform; free blade high, slightly exceeding half the platform length, with denticles of uniform size; troughs narrow and deep; inner margins surface pronounced transverse ridge.

Remarks: Notably, *Polygnathus zinaidae* and *Polygnathus cf. zinaidae* occur together well above the previously reported range of *P. zinaidae* (FZ 7/8–FZ 11/12; Ovnatanova & Kononova, 2008), marking a pronounced upward range extension into the uppermost Frasnian and across the Frasnian–Famennian (F–F) boundary. Their persistent co-occurrence and subtle morphological differences indicate that *Pa.* cf. *zinaidae* is more likely a morphologically transitional or environmentally adapted variant derived from *Pa. zinaidae* than an independent taxon. This association points to phylogenetic or ecological continuity within the *Pa. zinaidae* lineage, reflecting gradual evolutionary change or facies-controlled survival in the relatively stable shallow-marine setting of QLX.

Studied material: 36 elements from QLX A section (samples QLXA C13B-C19); 12 elements from QLX B section (samples QLXB C1, QLXB C4-C5)

***Polygnathus znepolensis* Spassov, 1965**

(Pl. 4, figs. 18-19)

1965 *Polygnathus znepolensis* n. sp. Spassov, p. 96, pl. 3, figs. 1-2

1991 *Polygnathus znepolensis* Spassov – Perri & Spalletta, p. 73, pl. 7, figs. 6-7

1993 *Polygnathus znepolensis* Spassov – Ji & Ziegler, p. 86, text-fig. 19.7

2000 *Polygnathus znepolensis* Spassov – Çapkinoğlu, p. 98, pl. 2, fig. 7

Description: The platform wide and irregularly pear-shaped; medin ridge reaching posterior end of platform or terminating near it; posterior end pointed or rounded; trough deep, latterly

margins raised up from anterior to posterior end of platform, inner margins surface pronounced strong transverse wide ridge.

Remarks: *Polygnathus znepolensis* differs from *Polygnathus* cf. *zinaidae* Kononova, Alekseev, Barskov & Reimers, 1996 by its inner atterly margins surface pronounced strong transverse ridge and wide. The co-occurrence of *Polygnathus cf. zinaidae* and *Polygnathus znepolensis* in this interval, coupled with the disappearance of *Polygnathus zinaidae*, suggests a phylogenetic transition within the *Po. zinaidae* lineage. The morphological convergence and subsequent replacement imply that *Polygnathus* cf. *zinaidae* may represent an intermediate or transitional form linking *Pa. zinaidae* to *Pa. znepolensis*, reflecting gradual evolutionary change rather than abrupt species turnover.

Range: From *Palmatolepis gracilis expansa* Zone to *Bispathodus ultimus* (Spalletta et al., 2017)

Studied material: 22 elements from QLX B section (samples QLXB C4-C5)

Reference

Aldridge, R. J., Smith, M. P., Norby, R. D., and Briggs, D. E. G., 1987, The architecture and function of Carboniferous polygnathacean conodont apparatuses, in Aldridge, R. J., ed., Palaeobiology of Conodonts: Chichester, Ellis Horwood for the British Micropalaeontological Society, p. 63-76.

Algeo, T. J., Berner, R. A., Maynard, J. B., and Scheckler, S. E., 1995, Late Devonian oceanic anoxic events and biotic crisis: "rooted" in the evolution of vascular land plants: GSA Today, v. 5, no. 3, p. 45-45.

Allan, J. R., and Matthews, R. K., 1982, Isotope signatures associated with early meteoric diagenesis: Sedimentology, v. 29, p. 797-817.

Anderson, W. I., 1966, Upper Devonian conodonts and the Devonian–Mississippian boundary of north-central Iowa: Journal of Paleontology, v. 40, no. 2, p. 395-415.

Averbuch, O., Tribovillard, N., Devleeschouwer, X., Riquier, L., Mistiaen, B., and Van Vliet-Lanoë, B., 2005, Mountain building–enhanced continental weathering and organic carbon burial as major causes for climatic cooling at the Frasnian–Famennian boundary (c. 376 Ma) ?: Terra Nova, v. 17, no. 1, p. 25-34.

Bahrami, A., Corradini, C., Over, D., and Yazdi, M., 2013, Conodont biostratigraphy of the upper Frasnian-lower Famennian transitional deposits in the Shotori Range, Tabas area, Central-East Iran Microplate: Bulletin of Geosciences, v. 88, no. 2, p. 369-388.

Bahrami, A., Corradini, C., and Yazdi, M., 2011, Upper Devonian conodont biostratigraphy of Shams Abad section, Kerman Province, Iran: Rivista Italiana di Paleontologia e Stratigrafia, v. 117, no. 2, p. 199-209.

Baliński, A., 2002, Frasnian-Famennian brachiopod extinction and recovery in southern Poland: Acta Palaeontologica Polonica, v. 47, no. 2, p. 289-305.

Baranov, V. V., Blodgett, R. B., and Kutygin, R. V., 2022, Platform conodonts from the Lower Famennian (Rhomboidea Zone) of the East Russian Arctic (Stolb Island): In Lucas, S. G., et al., eds., Fossil Record 8: New Mexico Museum of Natural History and Science, Bulletin 90, p. 57–63.

Barash, M. S., 2014, Evolution and development of marine biota in the Paleozoic under the influence of abiotic factors, in Galimov, E. M., ed., Problems of the Origination and Evolution of Biosphere: New York, Nova Science Publishers, p. 457-479.

Bardashev, I. A., Bardasheva, N. P., and Weddige, K., 2006, Stratigraphy of the Shiskat Paleozoic reference section (Southern Tien-Shan, Central Tajikistan): Senckenbergiana Lethaea, v. 86, no. 2, p. 289-316.

Barrera-Lahoz, H., Valenzuela-Ríos, J. I., and Liao, J.-C., 2024, Famennian conodont assemblage in the Compte section (Upper Devonian, Central Pyrenees) and its comparison with Eurasian sequences: Spanish Journal of Palaeontology, v. 39, no. 1.

Barskov, I. S., Alekseev, A. S., Kononova, L. I., and Migdissova, A. V., 1987, Opredelitel' Konodontov Verkhnego Devona i Karbona, Moscow, Izdatel'stvo Moskovskogo Universiteta, Geologicheskiy Fakul'tet, 1-144 p.

Bassler, R. S., 1925, Classification and stratigraphic use of conodonts: Geological Society of America Bulletin, v. 36, no. 1, p. 218-220.

Bateson, W., 1886, The ancestry of the Chordata: Quarterly Journal of Microscopical Science, v. 26, p. 535-571.

Bathurst, R. G. C., 1972, Carbonate Sediments and Their Diagenesis, Amsterdam, Elsevier.

Becker, R. T., 1993, Anoxia, eustatic changes, and Upper Devonian to lowermost Carboniferous global ammonoid diversity, in House, M. R., ed., The Ammonoidea: Environment, Ecology, and Evolutionary Change, Volume 47: Oxford, Clarendon Press, p. 115-163.

Becker, R. T., Königshof, P., and Brett, C. E., 2016, Devonian climate, sea level and evolutionary events: an introduction, in Becker, R. T., Königshof, P., and Brett, C. E., eds., Devonian Climate, Sea Level and Evolutionary Events, Volume 423: London, Geological Society of London, p. 1-10.

Becker, R. T., Marshall, J. E. A., Da Silva, A. C., Agterberg, F. P., Gradstein, F. M., and Ogg, J. G., 2020, The Devonian Period, Geologic Time Scale 2020, p. 733-810.

Berry, C. M., and Marshall, J. E., 2015, Lycopsid forests in the early Late Devonian paleoequatorial zone of Svalbard: Geology, v. 43, no. 12, p. 1043-1046.

Bischoff, G., 1956, Oberdevonische Conodonten (toIδ) aus dem Rheinischen Schiefergebirge: Notizblatt des Hessischen Landesamtes für Bodenforschung, v. 84, p. 115-137.

Blakey, R., 2016, Devonian-360 Ma, Global Paleogeography and Tectonics in Deep Time Series: Deep Time Maps™ Paleogeography.

Bond, D. P. G., and Wignall, P. B., 2008, The role of sea-level change and marine anoxia in the Frasnian–Famennian (Late Devonian) mass extinction: Palaeogeography, Palaeoclimatology, Palaeoecology, v. 263, no. 3-4, p. 107-118.

Bond, D. P. G., Zatoń, M., Wignall, P. B., and Marynowski, L., 2013, Evidence for shallow-water 'Upper Kellwasser' anoxia in the Frasnian–Famennian reefs of Alberta, Canada: Lethaia, v. 46, no. 3, p. 355-368.

Branson, E. B., and Mehl, M. G., 1934, Conodonts from the Grassy Creek shale of Missouri: Missouri University Studies, v. 8, p. 171-259.

Branson, E. B., and Mehl, M. G., 1938, The conodont genus Icriodus and its stratigraphic distribution: Journal of Paleontology, v. 12, no. 2, p. 156-166.

Brasier, M. D., Magaritz, M., and Corfield, R., 1990, The carbon- and oxygen-isotope record of the Precambrian–Cambrian boundary interval in China and Iran and their correlation: Geological Magazine, v. 127, no. 4, p. 319-332.

Briggs, D. E. G., Clarkson, E. N. K., and Aldridge, R. J., 1983, The conodont animal: Lethaia, v. 16, no. 1, p. 1-14.

Brime, C., Perri, M. C., Pondrelli, M., Spalletta, C., and Venturini, C., 2008, Polyphase metamorphism in the eastern Carnic Alps (N Italy–S Austria): clay minerals and conodont Colour Alteration Index evidence: International Journal of Earth Sciences, v. 97, p. 1213-1229.

Buggisch, W., and Joachimski, M. M., 2006, Carbon isotope stratigraphy of the Devonian of Central and Southern Europe: Palaeogeography, Palaeoclimatology, Palaeoecology, v. 240, no. 1, p. 68-88.

Bultynck, P., 2003, Devonian Icriodontidae: biostratigraphy, classification and remarks on paleoecology and dispersal: Revista Española de Micropaleontología, v. 35, no. 3, p. 295-314.

Bush, A. M., Csonka, J. D., DiRenzo, G. V., Over, D. J., and Beard, J. A., 2015, Revised correlation of the Frasnian–Famennian boundary and Kellwasser Events (Upper Devonian) in shallow marine paleoenvironments of New York State: Palaeogeography, Palaeoclimatology, Palaeoecology, v. 433, p. 233-246.

Cai, W., Hu, Z.-X., and Zheng, J.-F., 1996, Devonian conodonts from the Longmen Mountain area of Sichuan, China: Acta Micropalaeontologica Sinica, v. 13, no. 2, p. 195–204 (in Chinese).

Çapkınoğlu, Ş., 2000, Late Devonian (Famennian) conodonts from Denizliköyü, Gebze, Kocaeli, northwestern Turkey: Turkish Journal of Earth Sciences, v. 9, no. 2, p. 91-112.

Çapkınoğlu, Ş., 1997, Conodont fauna and biostratigraphy of the Famennian of Büyükada, İstanbul, Northwestern Turkey: Bollettino della Societa Paleontologica Italiana, v. 35, p. 165-185.

Carmichael, S. K., and Ferry, J. M., 2008, Formation of replacement dolomite in the Latemar carbonate buildup, Dolomites, northern Italy: Part 2. Origin of the dolomitizing fluid and the amount and duration of fluid flow: American Journal of Science, v. 308, no. 8, p. 885-904.

Carmichael, S. K., Waters, J. A., Königshof, P., Suttner, T. J., and Kido, E., 2019, Paleogeography and paleoenvironments of the Late Devonian Kellwasser event: A review of its sedimentological and geochemical expression: Global and Planetary Change, v. 183.

Carmichael, S. K., Waters, J. A., Suttner, T. J., Kido, E., and DeReuil, A. A., 2014, A new model for the Kellwasser Anoxia Events (Late Devonian): Shallow water anoxia in an open oceanic setting in the Central Asian Orogenic Belt: Palaeogeography, Palaeoclimatology, Palaeoecology, v. 399, p. 394-403.

Carozzi, A. V., 1989, Carbonate Rocks Depositional Models: A Microfacies Approach, Englewood Cliffs, NJ, Prentice Hall.

Chang, J., Bai, Z., Sun, Y., Peng, Y., Qin, S., and Shen, B., 2019, High resolution bio- and chemostratigraphic framework at the Frasnian-Famennian boundary: Implications for

regional stratigraphic correlation between different sedimentary facies in South China: Palaeogeography, Palaeoclimatology, Palaeoecology, v. 531.

Chen, D., Qing, H., and Li, R., 2005, The Late Devonian Frasnian–Famennian (F/F) biotic crisis: insights from δ13Ccarb, δ13Corg and 87Sr/86Sr isotopic systematics: Earth and Planetary Science Letters, v. 235, no. 1-2, p. 151-166.

Claeys, P., and Casier, J. G., 1994, Microtektite-like impact glass associated with the Frasnian–Famennian boundary mass extinction: Earth and Planetary Science Letters, v. 122, no. 3-4, p. 303-315.

Claeys, P., Casier, J. G., and Margolis, S. V., 1992, Microtektites and mass extinctions: Evidence for a Late Devonian asteroid impact: Science, v. 257, no. 5073, p. 1102-1104.

Clapham, M. E., and Renne, P. R., 2019, Flood basalts and mass extinctions: Annual Review of Earth and Planetary Sciences, v. 47, no. 1, p. 275-303.

Cooper, C. L., 1931, New conodonts from the Woodford Formation of Oklahoma: Journal of Paleontology, v. 5, no. 3, p. 230-243.

Copper, P., 1998, Evaluating the Frasnian–Famennian mass extinction: Comparing brachiopod faunas: Acta Palaeontologica Polonica, v. 43, no. 2, p. 137-154.

Copper, P., 2002, Reef development at the Frasnian/Famennian mass extinction boundary: Palaeogeography, Palaeoclimatology, Palaeoecology, v. 181, no. 1-3, p. 27-65.

Corradini, C., 1998, Famennian conodonts from two sections near Villasalto (SE Sardinia, Italy): Giornale di Geologia, v. 60, p. 122-135.

Corradini, C., 2003, Late Devonian (Famennian) conodonts from the Corona Mizziu Sections near Villasalto (Sardinia, Italy): Palaeontographia Italica, v. 89, p. 65-116.

Corradini, C., 2008, Revision of Famennian–Tournaisian (Late Devonian–Early Carboniferous) conodont biostratigraphy of Sardinia, Italy: Revue de Micropaléontologie, v. 51, p. 123-132.

Corradini, C., Corriga, M. G., Pondrelli, M., Spalletta, C., Zocchi, C., and Corradetti, A., 2025, Record of a sea level drop in the lower Mississippian limestones near Passo di Monte Croce Carnico (Carnic Alps, Italy): Geologica Acta, v. 23, p. 1-15.

Corradini, C., Corriga, M. G., Pondrelli, M., Spina, A., and Suttner, T. J., 2024a, The "Lochkovian-Pragian Event" re-assessed: New data from the low latitude shelf of peri-Gondwana: Palaeogeography, Palaeoclimatology, Palaeoecology, v. 656, p. 112580.

Corradini, C., Henderson, C., Barrick, J. E., and Ferretti, A., 2024b, Conodonts in Biostratigraphy. A 300-million-years long journey through geologic time: Newsletters on Stratigraphy, 40 pp.

Corradini, C., and Pondrelli, M., 2021, The Pre-Variscan Sequence of the Carnic Alps (Italy-Austria): Geological Field Trips & Maps, v. 13, no. 2.1, p. 1-72.

Corradini, C., Pondrelli, M., Simonetto, L., Corriga, M. G., Spalletta, C., Suttner, T. J., Kido, E., Mossoni, A., and Serventi, P., 2016, Stratigraphy of the La Valute area (Mt. Zermula massif, Carnic Alps, Italy): Bollettino della Società Paleontologica Italiana, v. 55, no. 1, p. 55-78.

Corradini, C., Spalletta, C., Mossoni, A., Matyja, H., and Over, D. J., 2016, Conodonts across the Devonian/Carboniferous boundary: a review and implications for the redefinition of the boundary and a proposal for an updated conodont zonation: Geological Magazine, p. 1-15.

Corradini, C., and Suttner, T.J., eds., 2015, The Pre-Variscan sequence of the Carnic Alps (Austria and Italy): Abhandlungen der Geologischen Bundesanstalt, v. 69, 158 p., Vienna, Austria.

Corradini, C., Suttner, T., Ferretti, A., Pohler, S., Pondrelli, M., Schönlaub, H. P., Spalletta, C., and Venturini, C., 2015, The Pre-Variscan sequence of the Carnic Alps-an introduction: Abhandlungen der Geologischen Bundesanstalt, v. 69, p. 7-15.

Courtillot, V., Kravchinsky, V. A., Quidelleur, X., Renne, P. R., and Gladkochub, D. P., 2010, Preliminary dating of the Viluy traps (Eastern Siberia): Eruption at the time of Late Devonian extinction events?: Earth and Planetary Science Letters, v. 300, p. 239-245.

Cui, Y., Shen, B., Sun, Y., Ma, H., Chang, J., Li, F., Lang, X., and Peng, Y., 2021, A pulse of seafloor oxygenation at the Late Devonian Frasnian-Famennian boundary in South China: Earth Science Reviews, v. 218.

De Vleeschouwer, D., Crucifix, M., Bounceur, N., and Claeys, P., 2014, The impact of astronomical forcing on the Late Devonian greenhouse climate: Global and Planetary Change, v. 120, p. 65-80.

De Vleeschouwer, D., Da Silva, A. C., Sinnesael, M., Chen, D. Z., Day, J. E., Whalen, M. T., Guo, Z. H., and Claeys, P., 2017, Timing and pacing of the Late Devonian mass extinction event regulated by eccentricity and obliquity: Nature Communications, v. 8, p. 2268.

De Vleeschouwer, D., Rakociński, M., Racki, G., Bond, D. P. G., Sobień, K., and Claeys, P., 2013, The astronomical rhythm of Late-Devonian climate change (Kowala section, Holy Cross Mountains, Poland): Earth and Planetary Science Letters, v. 365, p. 25-37.

Denison, R. E., Koepnick, R. B., Burke, W. H., Hetherington, E. A., and Fletcher, A., 1997, Construction of the Silurian and Devonian seawater 87Sr/86Sr curve: Chemical Geology, v. 140, no. 1-2, p. 109-121.

Donoghue, P. C. J., 2001, Conodonts Meet Cladistics: Recovering Relationships and Assessing the Completeness of the Conodont Fossil Record: Palaeontology, v. 44, no. 1, p. 65-93.

Dreesen, R., Sandberg, C. A., and Ziegler, W., 1986, Review of Late Devonian and Early Carboniferous conodont biostratigraphy and biofacies models as applied to the Ardenne shelf: Annales de la Société géologique de Belgique, v. 109, p. 27-42.

Dyer, B., Maloof, A. C., and Higgins, J. A., 2015, Glacioeustasy, meteoric diagenesis, and the carbon cycle during the Middle Carboniferous: Geochemistry, Geophysics, Geosystems, v. 16, no. 10, p. 3383-3399.

Dzik, J., 1976, Remarks on the evolution of Ordovician conodonts: Acta Palaeontologica Polonica, v. 21, no. 4, p. 395-453.

Dzik, J., 1991, Evolution of oral apparatuses in the conodont chordate: Acta Palaeontologica Polonica, v. 36, no. 3.

Dzik, J., 2002, Emergence and collapse of the Frasnian conodont and ammonoid communities in the Holy Cross Mountains, Poland: Acta Palaeontologica Polonica, v. 47, no. 4.

Dzik, J., 2006, The Famennian “Golden Age” of conodonts and ammonoids in the Polish part of the Variscan Sea. Warsaw: Institute of Paleobiology, Polish Academy of Sciences

(Palaeontologia Polonica, 63), 360 p.Eder, W., and Franke, W., 1982, Death of Devonian reefs: Neues Jahrbuch für Geologie und Paläontologie, Abhandlungen, v. 163, no. 2, p. 241-243.

Epstein, A. G., Epstein, J. B., and Harris, L. D., 1977, Conodont color alteration—an index to organic metamorphism: U.S. Geological Survey, Professional Paper 995.

Farabegoli, E., Perri, M. C., Spalletta, C., Joachimski, M. M., Andrew, A., and Pondrelli, M., 2023, Physical and biological events across the Frasnian-Famennian boundary (Late Devonian) in continuous oxic carbonate successions in the western Tethys (Carnic Alps of Italy and Austria): Bollettino della Società Paleontologica Italiana, v. 62, no. 2, p. 143-217.

Feist, R., 2002, Trilobites from the latest Frasnian Kellwasser crisis in North Africa (Mrirt, Central Moroccan Meseta): Acta Palaeontologica Polonica, v. 47, no. 2, p. 203-210.

Ferretti, A., Bancroft, A. M., and Repetski, J. E., 2020, GECkO: Global events impacting COnodont evolution: Palaeogeography, Palaeoclimatology, Palaeoecology, v. 549.

Flügel, E., 2010, Microfacies of Carbonate Rocks: Analysis, Interpretation and Application, Berlin Heidelberg, Springer-Verlag.

Forman, D. J., and Wales, D. W., 1981, Geological evolution of the Canning Basin, Western Australia: Bureau of Mineral Resources, Australia Bulletin, v. 210, p. 91.

Franke, W., Cocks, L. R. M., and Torsvik, T. H., 2017, The Palaeozoic Variscan oceans revisited: Gondwana Research, v. 48, p. 257-284.

Franseen, E. K., 2006, Mississippian (Osagean) shallow-water, mid-latitude siliceous sponge spicule and heterozoan carbonate facies: An example from Kansas with implications for regional controls and distribution of potential reservoir facies: Current Research in Earth Sciences, p. 1-23.

George, A. D., Chow, N., and Trinajstic, K. M., 2014, Oxic facies and the Late Devonian mass extinction, Canning Basin, Australia: Geology, v. 42, no. 4, p. 327-330.

Gharaie, M. H. M., Matsumoto, R., Racki, G., and Kakuwa, Y., 2007, Chemostratigraphy of Frasnian-Famennian transition: Possibility of methane hydrate dissociation leading to mass

extinction, Geological Society of America Special Papers, Volume 424, Geological Society of America, p. 109-125.

Gholamalian, H., 2007, Conodont biostratigraphy of the Frasnian-Famennian boundary in the Esfahan and Tabas areas, Central Iran: Geological Quarterly, v. 51, no. 4, p. 453-476.

Gholamalian, H., and Kebriaei, M. R., 2008, Late Devonian conodonts from the Hojedk section, Kerman Province, southeastern Iran: Rivista Italiana di Paleontologia e Stratigrafia, v. 114, no. 2, p. 171-181.

Girard, C., Charruault, A.-L., Gluck, T., Corradini, C., and Renaud, S., 2022, Deciphering the morphological variation and its ontogenetic dynamics in the Late Devonian conodont Icriodus alternatus: Fossil Record, v. 25, no. 1, p. 25-41.

Girard, C., and Feist, R., 1996, Eustatic trends in conodont diversity across the Frasnian–Famennian boundary in the stratotype area, Montagne Noire, Southern France: Lethaia, v. 29, no. 4, p. 329-337.

Girard, C., Klapper, G., and Feist, R., 2005, Chapter 7Subdivision of the terminal Frasnian linguiformis conodont Zone, revision of the correlative interval of Montagne Noire Zone 13, and discussion of stratigraphically significant associated trilobites, Developments in Palaeontology and Stratigraphy, Elsevier, p. 181-198.

Girard, C., and Renaud, S., 1996, Size variation in conodonts in response to the Upper Kellwasser crisis (Upper Devonian of the Montagne Noire France): CR Acad. Sci., v. 323, p. 435-442.

Glass, B. P., and Simonson, B. M., 2012, Distal impact ejecta layers: Spherules and more: Elements, v. 8, no. 1, p. 43-48.

Glenister, B. F., and Klapper, G., 1966, Upper Devonian conodonts from the Canning Basin, Western Australia: Journal of Paleontology, v. 40, no. 4, p. 777-842.

Han, Y., 1987, Study on Upper Devonian Frasnian/Famennian boundary in Ma-Anshan, Zhongping, Xiangzhou, Guangxi: Chinese Academy of Geological Sciences Bulletin, v. 17, p. 171-194 (in Chinese).

Hartenfels, S., 2024, Upper Devonian to Mississippian global environmental change and impact on conodonts: Palaeobiodiversity and Palaeoenvironments, v. 104, no. 3, p. 629-682.

Hass, W. H., 1959, Conodonts from the Chappel Limestone of Texas: U.S. Geological Survey.

Hayes, J. M., Strauss, H., and Kaufmann, A. J., 1999, The abundance of 13C in marine organic matter and isotopic fractionation in the global biogeochemical cycle of carbon during the past 800 Ma: Chemical Geology, v. 161, p. 103-125.

Helms, J., 1963, Zur "Phylogenese" und Taxionomie von Palmatolepis (Conodontida, Oberdevon): Geologie, v. 12, no. 4, p. 449-485.

Hillbun, K., Playton, T. E., Tohver, E., Ratcliffe, K., Trinajstic, K., Roelofs, B., Caulfield-Kerney, S., Wray, D., Haines, P., Hocking, R., Katz, D., Montgomery, P., and Ward, P., 2015, Upper Kellwasser carbon isotope excursion pre-dates the F-F boundary in the Upper Devonian Lennard Shelf carbonate system, Canning Basin, Western Australia: Palaeogeography, Palaeoclimatology, Palaeoecology, v. 438, p. 180-190.

Hinde, G. J., 1879, On Conodonts from the Chazy and Cincinnati Group of the Cambro-Silurian, and from the Hamilton and Genesee-Shale Divisions of the Devonian, in Canada and the United States: Quarterly Journal of the Geological Society, v. 35, p. 351-369.

Hinde, G. J., 1879, On conodonts from the Chazy and Cincinnati Group of the Cambro-Silurian, and from the Hamilton and Genesee-Shale Divisions of the Devonian, in Canada and the United States: Quarterly Journal of the Geological Society, v. 35, p. 351-369.

House, M. R., 1985, Correlation of mid-Palaeozoic ammonoid evolutionary events with global sedimentary perturbations: Nature, v. 313, no. 5997, p. 17-22.

House, M. R., 2002, Strength, timing, setting and cause of mid-Palaeozoic extinctions: Palaeogeography, Palaeoclimatology, Palaeoecology, v. 181, no. 1-3, p. 5-25.

Huang, C., 2015, The Peculiarities and Causes of the Devonian F–F Event: evidences from high-resolution conodont biostratigraphy and chemostratigraphy in South ChinaPh.D. thesis]: China University of Geosciences (Wuhan).

Huang, C., and Gong, Y., 2016, Timing and patterns of the Frasnian–Famennian event: Evidences from high-resolution conodont biostratigraphy and event stratigraphy at the Yangdi section, Guangxi, South China: Palaeogeography, Palaeoclimatology, Palaeoecology, v. 448, p. 317-338.

Huang, C., Joachimski, M. M., and Gong, Y., 2018a, Did climate changes trigger the Late Devonian Kellwasser Crisis? Evidence from a high-resolution conodont $\delta^{18}O_{PO4}$ record from South China: Earth and Planetary Science Letters, v. 495, p. 174–184.

Huang, C., Song, J., Shen, J., and Gong, Y., 2018b, The influence of the Late Devonian Kellwasser events on deep-water ecosystems: Evidence from palaeontological and geochemical records from South China: Palaeogeography, Palaeoclimatology, Palaeoecology, v. 504, p. 60-74.

Huang, S., Shi, H., Zhang, M., Wu, W., and Shen, L., 2002, Global correlation of the strontium isotope evolution curve and dating of marine strata in the Devonian of the Longmenshan Basin: Progress in Natural Science, v. 12, no. 9, p. 945-951.

Huddle, J. W., 1934, Conodonts from the New Albany Shale of Indiana: Bulletin of American Paleontology, v. 21, no. 72, p. 1-137.

Hudson, J. D., 1977, Stable isotopes and limestone lithification: Journal of the Geological Society, v. 133, no. 6, p. 637-660.

Huybers, P., and Langmuir, C., 2009, Feedback between deglaciation and volcanic emissions of CO_2: Earth and Planetary Science Letters, v. 268, p. 479-491.

International Commission on, S., 2024, International Chronostratigraphic Chart (v2024/12).

Jafarbeigloo, F., Majidifard, M. R., Hamdi, B., Asghari, A., and Arian, M., 2020, Depositional environment and sequence stratigraphy of the Khoshyeilagh Formation inBojnourd and Jajarm (NE Iran): Turkish Journal of Earth Sciences, v. 29, no. 6, p. 853-877.

Jain, S., 2020, Fundamentals of Invertebrate Palaeontology: Microfossils: Springer, 323 p.

Ji, Q., 1989, On the Frasnian–Famennian mass extinction event in South China: Courier Forschungsinstitut Senckenberg, v. 117, p. 275-301.

Ji, Q., and Ziegler, W., 1993, The Lali Section: an excellent Reference Section for Upper Devonian in South China: Courier Forschungsinstitut Senckenberg, v. 157, p. 1-183.

Joachimski, M., Pancost, R., Freeman, K., Ostertag-Henning, C., and Buggisch, W., 2002, Carbon isotope geochemistry of the Frasnian–Famennian transition: Palaeogeography, Palaeoclimatology, Palaeoecology, v. 181, no. 1-3, p. 91-109.

Joachimski, M. M., 1994, Subaerial exposure and deposition of shallowing upward sequences: evidence from stable isotopes of Purbeckian peritidal carbonates (basal Cretaceous), Swiss and French Jura Mountains: Sedimentology, v. 41, p. 805-824.

Joachimski, M. M., Breisig, S., Buggisch, W., Talent, J. A., Mawson, R., Gereke, M., Morrow, J. R., Day, J., and Weddige, K., 2009, Devonian climate and reef evolution: Insights from oxygen isotopes in apatite: Earth and Planetary Science Letters, v. 284, no. 3-4, p. 599-609.

Joachimski, M. M., and Buggisch, W., 1993, Anoxic events in the late Frasnian—Causes of the Frasnian-Famennian faunal crisis?: Geology, v. 21, no. 8, p. 675-678.

Joachimski, M. M., and Buggisch, W., 1993, Anoxic events in the late Frasnian—causes of the Frasnian-Famennian faunal crisis?: Geology, v. 21, no. 8, p. 675-678.

Joachimski, M. M., and Buggisch, W., 2002, Conodont apatite $\delta^{18}O$ signatures indicate climatic cooling as a trigger of the Late Devonian mass extinction: Geology, v. 30, no. 8, p. 711-714.

Johnson, J. G., Boucot, A. J., and Hallam, A., 1973, Devonian brachiopods, in Hallam, A., ed., Atlas of Palaeobiogeography: Amsterdam, Elsevier, p. 89-96.

Johnson, J. G., Klapper, G., and Sandberg, C. A., 1985, Devonian eustatic fluctuations in Euramerica: Geological Society of America Bulletin, v. 96, p. 567-587.

Kaiser, S. I., 2005, Mass extinctions, climatic and oceanographic changes at the Devonian–Carboniferous boundary: Ruhr-Universität Bochum.

Kaiser, S. I., Becker, R. T., Spalletta, C., and Steuber, T., 2009, High-resolution conodont stratigraphy, biofacies and extinctions around the Hangenberg Event in pelagic successions from Austria, Italy and France: Palaeontographica Americana, v. 63, p. 97-139.

Keppie, J. D., and Ramos, V. A., 1999, Odyssey of terranes in the Iapetus and Rheic oceans during the Paleozoic, in Ramos, V. A., and Keppie, J. D., eds., Laurentia-Gondwana Connections before Pangea: Boulder, Colorado, Geological Society of America, p. 267-276.

Kido, E., Pohler, S. M. L., Pondrelli, M., Schönlaub, H.-P., Simonetto, L., Spalletta, C., and Suttner, T. J., 2015, Kellergrat Formation, in Corradini, C., and Suttner, T. J., eds., The Pre-

Variscan sequence of the Carnic Alps (Austria and Italy), Volume 69: Vienna, Geologische Bundesanstalt, p. 101-104.

Klapper, G., 1971, Sequence within the conodont genus Polygnathus in the New York lower Middle Devonian: Geologica et Palaeontologica, v. 5, p. 59-79.

Klapper, G., 1989, The Montagne Noire Frasnian (Upper Devonian) conodont succession, in McMillan, N. J., Embry, A. F., and Glass, D. J., eds., Devonian of the World. Volume III: Paleontology, Paleoecology, Biostratigraphy, Volume 14: Calgary, Canadian Society of Petroleum Geologists, p. 449-468.

Klapper, G., 2007a, Conodont taxonomy and the recognition of the Frasnian/Famennian (Upper Devonian) stage boundary: Stratigraphy, v. 4, no. 1, p. 67-76.

Klapper, G., 2007b, Frasnian (Upper Devonian) conodont succession at Horse Spring and correlative sections, Canning Basin, Western Australia: Journal of Paleontology, v. 81, no. 3, p. 513–537.

Klapper, G., 2021, Revision of the Late Devonian conodont genus Ancyrodella: Bulletin of Geosciences, p. 295-325.

Klapper, G., and Becker, R. T., 1998, Comparison of Frasnian (Upper Devonian) conodont zonations: Bollettino della Società Paleontologica Italiana, v. 37, no. 2-3, p. 339-348.

Klapper, G., and Foster, C. T., 1993, Shape analysis of Frasnian species of the Late Devonian conodont genus Palmatolepis: Journal of Paleontology, v. 67, no. S32, p. 1-35.

Klapper, G., and Johnson, J. G., 1980, Endemism and dispersal of Devonian conodonts: Journal of Paleontology, v. 54, p. 400-455.

Klapper, G., and Kirchgasser, W. T., 2016, Frasnian Late Devonian conodont biostratigraphy in New York: graphic correlation and taxonomy: Journal of Paleontology, v. 90, no. 3, p. 525-554.

Klapper, G., Kuz'Min, A. V., and Ovnatanova, N. S., 1996, Upper Devonian conodonts from the Timan-Pechora region, Russia, and correlation with a Frasnian composite standard: Journal of Paleontology, v. 70, no. 1, p. 131-152.

Klapper, G., and Lane, H. R., 1985, Upper Devonian (Frasnian) Conodonts of the Polygnathus Biofacies, N.W.T., Canada: Journal of Paleontology, v. 59, no. 4, p. 904-951.

Klapper, G., Uyeno, T., Armstrong, D., and Telford, P., 2004, Conodonts of the Williams Island and Long Rapids formations (Upper Devonian, Frasnian-Famennian) of the Onakawana B Drillhole, Moose River Basin, northern Ontario, with a revision of Lower Famennian species: Journal of Paleontology, v. 78, no. 2, p. 371-387.

Knauth, L. P., and Kennedy, M. J., 2009, The late Precambrian greening of the Earth: Nature, v. 460, no. 7256, p. 728-732.

Kononova, L. I., Alekseev, A. S., Barskov, I. S., and Reimers, A. N., 1996, New species of polygnathid assemblages from the Frasnian Stage of the Moscow Syneclise: Paleontologicheskii Zhurnal, no. 3, p. 94-99.

Kononova, L. I., and Weyer, D., 2013, Upper Famennian conodonts from the Breternitz Member (Upper Clymeniid Beds) of the Saalfeld region, Thuringia (Germany): Freiberger Forschungshefte C, v. 545, p. 15-97.

Kravchinsky, V. A., 2012, Paleozoic large igneous provinces of northern Eurasia: Correlation with mass extinction events: Global and Planetary Change, v. 86, p. 31-36.

Krumhardt, A. P., Harris, A. G., and Watts, K. F., 1996, Lithostratigraphy, microlithofacies, and conodont biostratigraphy and biofacies of the Wahoo Limestone (Carboniferous), eastern Sadlerochit Mountains, Northeast Brooks Range, Alaska: U.S. Geological Survey Professional Paper 1568, 63 p.

Kump, L. R., 2013, The Geochemistry of Mass Extinction, Sediments, Diagenesis and Sedimentary Rocks, Volume 9, Elsevier Inc., p. 385-397.

Kump, L. R., and Arthur, M. A., 1999, Interpreting carbon isotope excursions, carbonates and organic matter: Chemical Geology, v. 161, p. 181-198.

Kürschner, W., Becker, R. T., Buhl, D., and Veizer, J., 1993, Strontium isotopes in conodonts: Devonian–Carboniferous transition, the Northern Rhenish Slate Mountains, Germany: Annales de la Société géologique de Belgique, v. 115, no. 2, p. 595-621.

Kusznir, N. J., Kovkhuto, A., and Stephenson, R. A., 1996, Syn-rift evolution of the Pripyat trough: Constraints from structural and stratigraphic modelling: Tectonophysics, v. 268, no. 1, p. 221-236.

Lakin, J. A., Marshall, J. E. A., Troth, I., and Harding, I. C., 2016, Greenhouse to icehouse: a biostratigraphic review of latest Devonian–Mississippian glaciations and their global effects: Geological Society, London, Special Publications, v. 423, p. 439-464.

Lane, H. R., 1968, Symmetry in conodont element-pairs: Journal of Paleontology, v. 42, no. 6, p. 1258-1263.

Lazreq, N., 1992, The Upper Devonian of M'Irirt (Morocco): Courier Forschungsinstitut Senckenberg, v. 154, p. 107-123.

Lohmann, K. C., 1988, Geochemical patterns of meteoric diagenetic systems and their application to studies to palaeokarst, in James, N. P., and Choquette, P. W., eds., Palaeokarst: Berlin, Springer-Verlag, p. 55-80.

Lüddecke, F., Hartenfels, S., and Becker, R. T., 2017, Conodont biofacies of a monotonous middle Famennian pelagic carbonate succession (Upper Ballberg Quarry, northern Rhenish Massif): Palaeobiodiversity and Palaeoenvironments, v. 97, no. 3, p. 591-613.

Ma, X., and Bai, S., 2002, Biological, depositional, microspherule, and geochemical records of the Frasnian/Famennian boundary beds, South China: Palaeogeography, Palaeoclimatology, Palaeoecology, v. 181, no. 1-3, p. 325-346.

Ma, X., Gong, Y., Chen, D., Racki, G., Chen, X., and Liao, W., 2016, The Late Devonian Frasnian–Famennian Event in South China—patterns and causes of extinctions, sea level changes, and isotope variations: Palaeogeography, Palaeoclimatology, Palaeoecology, v. 448, p. 224-244.

Ma, X. P., and Bai, S. L., 2002, Biological, depositional, microspherule, and geochemical records of the Frasnian/Famennian boundary beds, South China: Palaeogeography, Palaeoclimatology, Palaeoecology, v. 181, no. 1, p. 325-346.

Marshall, J. D., 1992, Climatic and oceanographic isotopic signals from the carbonate rock record and their preservation: Geological Magazine, v. 129, p. 143-160.

Matyja, H., 1993, Upper devonian of western Pomerania: Acta Geologica Polonica, v. 43, no. 1-2, p. 27-94.

McArthur, J. M., Howarth, R. J., and Shields, G. A., 2012, Strontium isotope stratigraphy, in Gradstein, F. M., Ogg, J. G., Schmitz, M. D., and Ogg, G. M., eds., The Geologic Time Scale 2012: Amsterdam, Elsevier, p. 127-144.

McGhee, G. R., 1996, The Late Devonian Mass Extinction: The Frasnian/Famennian Crisis, New York, Columbia University Press.

McGhee Jr, G. R., Clapham, M. E., Sheehan, P. M., Bottjer, D. J., and Droser, M. L., 2013, A new ecological-severity ranking of major Phanerozoic biodiversity crises: Palaeogeography, Palaeoclimatology, Palaeoecology, v. 370, p. 260-270.

McLaren, D. J., 1970, Time, life, and boundaries: Journal of Paleontology, v. 48, p. 801-815.

McLean, R. A., and Klapper, G., 1998, Biostratigraphy of Frasnian (Upper Devonian) strata in western Canada, based on conodonts and rugose corals: Bulletin of Canadian Petroleum Geology, v. 46, no. 4, p. 515-563.

Metcalfe, I., 2013, Gondwana dispersion and Asian accretion: tectonic and palaeogeographic evolution of eastern Tethys: Gondwana Research, v. 23, p. 186-203.

Metzger, R. A., 1989, Upper Devonian (Frasnian: Famennian) Conodont Biostratigraphy in the Subsurface of North-Central Iowa and Southeastern Nebraska: Journal of Paleontology, v. 63, no. 4, p. 503-524.

Metzger, R. A., 1994, Multielement reconstructions of Palmatolepis and Polygnathus (Upper Devonian, Famennian) from the Canning Basin, Australia, and Bactrian Mountain, Nevada: Journal of Paleontology, v. 68, no. 3, p. 617-647.

Miller, A. K., and Youngquist, W. L., 1947, Conodonts from the type section of the Sweetland Creek Shale in Iowa: Journal of Paleontology, v. 21, p. 501-517.

Morrow, J. R., Sandberg, C. A., Malkowski, K., and Joachimski, M. M., 2009, Carbon isotope chemostratigraphy and precise dating of middle Frasnian (lower Upper Devonian) Alamo Breccia, Nevada, USA: Palaeogeography, Palaeoclimatology, Palaeoecology, v. 282, no. 1-4, p. 105-118.

Mossoni, A., 2014, Selected Famennian (Late Devonian) events (Condroz, Annulata, Hangenberg) in Sardinia and in the Carnic Alps: conodont biostratigraphy, magnetic susceptibility and geochemistryPh.D. thesis]: Università degli Studi di Cagliari.

Müller, K. J., 1956, Zur Kenntnis der Conodonten-Fauna des europäischen Devons, 1; Die Gattung Palmatolepis, Frankfurt am Main, Senckenbergische Naturforschende Gesellschaft, Abhandlungen der Senckenbergischen Naturforschenden Gesellschaft, 1-70 p.

Müller, K. J., and Müller, E. M., 1957, Early Upper Devonian (Independence) conodonts from Iowa, part I: Journal of Paleontology, v. 31, p. 1069-1108.

Nance, R. D., Murphy, J. B., and Santosh, M., 2014, The supercontinent cycle: A retrospective essay: Gondwana Research, v. 25, p. 522-547.

Nicoll, R. S., and Playford, P. E., 1993, Upper Devonian iridium anomalies, conodont zonation and the Frasnian–Famennian boundary in the Canning Basin, Western Australia: Palaeogeography, Palaeoclimatology, Palaeoecology, v. 104, no. 1-4, p. 105-113.

Norris, A. W., Uyeno, T. T., and McCabe, H. R., 1982, Devonian rocks of the Lake Winnipegosis–Lake Manitoba outcrop belt, Manitoba: Geological Survey of Canada Memoir 392, 280 p.

Obukhovskaya, T. G., and Kuzmin, A. V., 1993, Spores and conodonts from the boundary Upper Frasnian–Lower Famennian deposits of the Ukhta–Tebuk region

Споры и конодонты из пограничных верхнефранских–нижнефаменских отложений Ухтинско–Тебукского района, Paleontological Method in Geology: Moscow, IGIRGI, p. 35-51.

O'Neil, J. R., Clayton, R. N., and Mayeda, T. K., 1969, Oxygen isotope fractionation in divalent metal carbonates: Journal of Chemical Physics, v. 51, no. 12, p. 5547-5558.

Over, D. J., 1992, Conodonts and the Devonian–Carboniferous boundary in the Upper Woodford Shale, Arbuckle Mountains, South-Central Oklahoma: Journal of Paleontology, v. 66, p. 293-311.

Over, D. J., 1997, Conodont biostratigraphy of the Java Formation (Upper Devonian) and the Frasnian–Famennian boundary in western New York State, in Klapper, G., Murphy, M. A., and Talent, J. A., eds., Paleozoic Sequence Stratigraphy, Biostratigraphy, and

Biogeography: Studies in Honor of J. Granville ("Jess") Johnson, Volume 321: Boulder, Colorado, Geological Society of America, p. 161-177.

Over, D. J., 2007, Conodont biostratigraphy of the Chattanooga Shale, Middle and Upper Devonian, Southern Appalachian Basin, Eastern United States: Journal of Paleontology, v. 81, no. 6, p. 1194-1217.

Over, D. J., Wistort, Z., Soar, L. K., Bullecks, C. J., and Hagadorn, J. W., 2021, Conodonts and the Devonian–Carboniferous transition in the Dyer Formation, Colorado: Rocky Mountain Geology, v. 56, no. 2, p. 51-67.

Ovnatanova, N. S., 1969, New Upper Devonian conodonts of the central regions of the Russian Platform and Timan: Trudy VNIGNI (Proceedings of the All-Russia Research Institute of Geology and Petroleum), issue 93, p. 139–141 (in Russian).

Ovnatanova, N. S.,1976, Novye pozdnedevonskie konodonty Russkoy Platformy: Paleontologicheskiy Zhurnal, no. 2, p. 106-115.

Ovnatanova, N. S., and Kononova, L. I., 1996, New Frasnian polygnathids from central areas of the Russian Platform: Paleontological Journal, v. 30, no. 1, p. 52–60 (in Russian).

Ovnatanova, N. S., and Kononova, L. I., 2001, Conodonts and Upper Devonian (Frasnian) biostratigraphy of central regions of Russian Platform: Courier Forschungsinstitut Senckenberg, v. 233, p. 1–115.

Ovnatanova, N. S., and Kononova, L. I., 2008, Frasnian conodonts from the eastern Russian Platform: Paleontological Journal, v. 42, no. 10, p. 997-1166.

Ovnatanova, N. S., Kononova, L. I., Kolesnik, L. S., and Gatovsky, Y. A., 2017, Upper Devonian conodonts of northeastern European Russia: Paleontological Journal, v. 51, no. 10, p. 973-1165.

Pander, C. H., 1856, Monographie der fossilen Fische des silurischen Systems des Russisch-baltischen Gouvernements, Sankt Petersburg, Buchdruckerei der Kaiserlichen Akademie der Wissenschaften.

Pander, C. H., 1856, Monographie der fossilen Fische des silurischen Systems des Russisch-baltischen Gouvernements: St. Petersburg, Buchdruckerei der Kaiserlichen Akademie der Wissenschaften, 91 p. (in German)

Pas, D., Da Silva, A.-C., Suttner, T. J., Kido, E., Bultynck, P., Pondrelli, M., Corradini, C., De Vleeschouwer, D., Dojen, C., and Boulvain, F., 2014, Insight into the development of a carbonate platform through a multi-disciplinary approach: a case study from the Upper Devonian slope deposits of Mount Freikofel (Carnic Alps, Austria/Italy): International Journal of Earth Sciences, v. 103, no. 2, p. 519-538.

Percival, L. M. E., Davies, J., Schaltegger, U., De Vleeschouwer, D., Da Silva, A. C., and Föllmi, K. B., 2018, Precisely dating the Frasnian–Famennian boundary: Implications for the cause of the Late Devonian mass extinction: Scientific Reports, v. 8, no. 1, p. 9578-9578.

Perri, M., and Spalletta, C., 1991, Famennian conodonts from Cava Cantoniera and Malpasso sections, Carnic Alps, Italy: Bollettino della Società Paleontologica Italiana, v. 30, no. 1, p. 47-78.

Perri, M. C., and Spalletta, C., 2000, Devonian–Early Carboniferous transgressions and regressions in the Carnic Alps (Italy): Records of the Western Australian Museum, Supplement, v. 58, p. 305-319.

Perri, M. C., and Spalletta, C., 2001, Hangenberg Event al limite Devoniano/Carbonifero al Monte Zermula, Alpi Carniche, Italia: Giornale di Geologia (Serie 3), Supplemento, v. 62, p. 31-40.

Pisarzowska, A., and Racki, G., 2020, Comparative carbon isotope chemostratigraphy of major Late Devonian biotic crises, Stratigraphy & Timescales, Elsevier, p. 387-466.

Plumb, K. A., 1979, The tectonic evolution of Australia: Earth-Science Reviews, v. 14, p. 205-249.

Pohler, S. M. L., Bandel, K., Kido, E., Pondrelli, M., Suttner, T. J., Schönlaub, H. P., and Mörtl, A., 2015, Polinik Formation, in Corradini, C., and Suttner, T. J., eds., The Pre-Variscan sequence of the Carnic Alps (Austria and Italy), Volume 69: Vienna, Geologische Bundesanstalt, p. 81-84.

Pölsler, P., 1969, Conodonten aus dem Devon der Karnischen Alpen (Findenigkofel, Österreich): Jahrbuch der Geologischen Bundesanstalt, v. 112, p. 399-440.

Polyansky, O. P., Prokopiev, A. V., Koroleva, O. V., Tomshin, M. D., Reverdatto, V. V., Babichev, A. V., Sverdlova, V. G., and Vasiliev, D. A., 2018, The nature of the heat source of mafic magmatism during the formation of the Vilyui rift based on the ages of dike swarms and results of numerical modeling: Russian Geology and Geophysics, v. 59, no. 10, p. 1217-1236.

Pondrelli, M., Corradini, C., Spalletta, C., Suttner, T. J., Simonetto, L., Perri, M. C., Corriga, M. G., Venturini, C., and Schönlaub, H.-P., 2020, Geological map and stratigraphic evolution of the central sector of the Carnic Alps (Austria–Italy): Italian Journal of Geosciences, v. 139, no. 3, p. 469-484.

Pondrelli, M., Pas, D., Spalletta, C., Schönlaub, H.-P., Farabegoli, E., Corradini, C., Suttner, T. J., Corriga, M. G., Perri, M. C., Da Silva, A.-C., Pohler, S. M. L., Simonetto, L., Dojen, C., Mossoni, A., Kido, E., and Hüneke, H., 2015, Freikofel Formation, in Corradini, C., and Suttner, T. J., eds., The Pre-Variscan sequence of the Carnic Alps (Austria and Italy), Volume 69: Vienna, Geologische Bundesanstalt, p. 121-124.

Pondrelli, M., Schönlaub, H.-P., Corradini, C., Spalletta, C., Suttner, T. J., Kido, E., Perri, M. C., Simonetto, L., Corriga, M. G., Mossoni, A., Pohler, S. M. L., and Hüneke, H., 2015, Hoher Trieb Formation, in Corradini, C., and Suttner, T. J., eds., The Pre-Variscan sequence of the Carnic Alps (Austria and Italy), Volume 69: Vienna, Geologische Bundesanstalt, p. 125-128.

Prestianni, C., and Gerrienne, P., 2010, Early seed plant radiation: an ecological hypothesis, in Vecoli, M., Clément, G., and Meyer-Berthaud, B., eds., The Terrestrialization Process: Modelling Complex Interactions at the Biosphere–Geosphere Interface, Volume 339: London, Geological Society of London, p. 71-80.

Purnell, M. A., 1995, Large eyes and vision in conodonts: Lethaia, v. 28, no. 2, p. 187-188.

Purnell, M. A., and Donoghue, P. C. J., 1997, Architecture and functional morphology of the skeletal apparatus of ozarkodinid conodonts: Philosophical Transactions of the Royal Society of London. Series B: Biological Sciences, v. 352, p. 1545-1564.

Purnell, M. A., and Donoghue, P. C. J., 2005, Between death and data: Biases in interpretation of the fossil record of conodonts, in Purnell, M. A., and Donoghue, P. C. J., eds., Conodont Biology and Phylogeny: Interpreting the Fossil Record, Volume 73: London, The Palaeontological Association, p. 7-25.

Qie, W., Qiao, L., Liang, K., Guo, W., Song, J., Liu, F., Xu, H., Huang, P., Mou, L., and Lu, J., 2020, *Devonian stratigraphy and index fossils of China*: Hangzhou, Zhejiang University Press, 540 p. (in Chinese).

Racki, G., 1998, Frasnian–Famennian biotic crisis: undervalued tectonic control?: Palaeogeography, Palaeoclimatology, Palaeoecology, v. 141, no. 3-4, p. 177-198.

Racki, G., 2005, Toward understanding Late Devonian global events: few answers, many questions, Developments in Palaeontology and Stratigraphy, Volume 20, Elsevier, p. 5-36.

Racki, G., 2005, Toward understanding Late Devonian global events: few answers, many questions, in Over, D. J., Morrow, J. R., and Wignall, P. B., eds., Understanding Late Devonian and Permian-Triassic Biotic and Climatic Events: Towards an Integrated Approach, Volume 20, p. 5-36.

Racki, G., 2005, Toward understanding Late Devonian global events: few answers, many questions, in Over, D. J., Morrow, J. R., and Wignall, P. B., eds., Understanding Late Devonian and Permian-Triassic Biotic and Climatic Events: Towards an Integrated Approach, Volume 20: Amsterdam, Elsevier, p. 5-36.

Racki, G., 2020, A volcanic scenario for the Frasnian–Famennian major biotic crisis and other Late Devonian global changes: More answers than questions?: Global and Planetary Change, v. 189, p. 103174.

Racki, G., Rakociński, M., Marynowski, L., and Wignall, P. B., 2018, Mercury enrichments and the Frasnian–Famennian biotic crisis: A volcanic trigger proved?: Geology, v. 46, p. 543-546.

Reimold, W. U., Kelley, S. P., Sherlock, S. C., Henkel, H., and Koeberl, C., 2005, Laser argon dating of melt breccias from the Siljan impact structure, Sweden: Implications for a possible relationship to Late Devonian extinction events: Meteoritics & Planetary Science, v. 40, no. 4, p. 591-607.

Rejebian, V. A., Harris, A. G., and Huebner, J. S., 1987, Conodont color and textural alteration: An index to regional metamorphism, contact metamorphism, and hydrothermal alteration: Geological Society of America Bulletin, v. 99, no. 4, p. 471-479.

Roemer, F. A., 1850, Beiträge zur geologischen Kenntnis des nordwestlichen Harzgebirges: Palaeontographica, v. 3, p. 1-67.

Sallan, L. C., and Coates, M. I., 2010, End-Devonian extinction and a bottleneck in the early evolution of modern jawed vertebrates: Proceedings of the National Academy of Sciences, v. 107, no. 22, p. 10131-10135.

Saltzman, M. R., and Thomas, E., 2012, Carbon isotope stratigraphy, in Gradstein, F. M., Ogg, J. G., Schmitz, M., and Ogg, G., eds., The Geologic Time Scale 2012: Amsterdam, Elsevier, p. 207-232.

Sandberg, C. A., 1976, Conodont biofacies of Late Devonian Polygnathus styriacus Zone in western United States, in Barnes, C. R., ed., Conodont paleoecology, Geological Association of Canada, p. 171-186.

Sandberg, C. A., and Dreesen, R., 1984, Late Devonian icriodontid biofacies models and alternate shallow-water conodont zonation, Geological Society of America Special Paper, Volume 196, p. 143-178.

Sandberg, C. A., Morrow, J. R., and Ziegler, W., 2002, Late Devonian sea-level changes, catastrophic events, and mass extinctions, in Koeberl, C., and MacLeod, K. G., eds., Catastrophic Events and Mass Extinctions: Impacts and Beyond, Volume 356: Boulder, Geological Society of America, p. 473-487.

Sandberg, C. A., and Ziegler, W., 1973, Refinement of standard Upper Devonian conodont zonation based on sections in Nevada and West Germany: Geologica et Palaeontologica, v. 7, p. 97-122.

Sandberg, C. A., and Ziegler, W., 1979, Taxonomy and biofacies of important conodonts of Late Devonian styriacus-Zone, United States and Germany: Geologica et Palaeontologica, v. 13, p. 173-212.

Sandberg, C. A., Ziegler, W., and Bultynck, P., 1989, New standard conodont zones and early Ancyrodella phylogeny across the Middle–Upper Devonian boundary: Courier Forschungsinstitut Senckenberg, v. 110, p. 195-230.

Sandberg, C. A., Ziegler, W., Dreesen, R., and Butler, J. L., 1988, Late Frasnian mass extinction: Conodont event stratigraphy, global changes, and possible causes, in Ziegler, W., ed., 1st International Senckenberg Conference and 5th European Conodont Symposium (ECOS V), Contribution 1, Volume 102, p. 267-307.

Sandberg, C. A., Ziegler, W., Leuteritz, K., and Brill, S. M., 1978, Phylogeny, speciation and zonation of Siphonodella (Conodonta, Upper Devonian and Lower Carboniferous): Newsletters on Stratigraphy, v. 7, no. 2, p. 102-120.

Sannemann, D., 1955a, Beitrag zur Untergliederung des Oberdevons nach Conodonten: Neues Jahrbuch für Geologie und Paläontologie, Abhandlungen, v. 100, p. 324-331.

Sannemann, D., 1955b, Oberdevonische Conodonten (Teil IIa): Senckenbergiana lethaea, v. 36, p. 123–156.

Sarmiento, J. L., and Gruber, N., 2006, Ocean Biogeochemical Dynamics, Princeton, NJ, Princeton University Press, 503 p.

Savage, N. M., 1992, Late Devonian (Frasnian and Famennian) conodonts from the Wadleigh Limestone, southeastern Alaska: Journal of Paleontology, v. 66, p. 277-292.

Savage, N. M., Sardsud, A., and Buggisch, W., 2006, Late Devonian conodonts and the global frasnian-famennian extinction event, thong pha phum, western Thailand: Palaeoworld, v. 15, no. 2, p. 171-184.

Savoy, L. E., and Harris, A. G., 1993, Conodont biofacies in a ramp to basin setting (latest Devonian and earliest Carboniferous) in the Rocky Mountains of southernmost Canada and northern Montana: U.S. Geological Survey Open-File Report 93–184, 38 p

Schäfer, W., 1976, Einige neue Conodonten aus dem höheren Oberdevon des Sauerlandes (Rheinisches Schiefergebirge): Geologica et Palaeontologica, v. 10, p. 141-152.

Schindler, E., 1990, The Late Frasnian (Upper Devonian) Kellwasser Crisis, in Kauffman, E. G., and Walliser, O. H., eds., Extinction Events in Earth History: Heidelberg, Springer, p. 151-159.

Schindler, E., Schülke, I., and Ziegler, W., 1998, The Frasnian/Famennian boundary at the Sessacker Trench section near Oberscheld (Dill Syncline, Rheinisches Schiefergebirge, Germany): Senckenbergiana Lethaea, v. 77, no. 1-2, p. 243-261.

Schobben, M., Heuer, F., Tietje, M., Ghaderi, A., Korn, D., Korte, C., and Wignall, P. B., 2019a, Chemostratigraphy across the Permian–Triassic boundary: the effect of sampling strategies on carbonate carbon isotope stratigraphic markers, Chemostratigraphy Across Major Chronological Boundaries, Volume 240, American Geophysical Union, p. 159-181.

Schobben, M., Schootbrugge, B. v. d., and Wignall, P. B., 2019b, Interpreting the carbon isotope record of mass extinctions: Elements, v. 15, p. 331-337.

Scholle, P. A., and Ulmer-Scholle, D. S., 2003, A Color Guide to the Petrography of Carbonate Rocks: Grains, Textures, Porosity, Diagenesis, Tulsa, American Association of Petroleum Geologists (AAPG).

Schönlaub, H. P., 1985, Das Paläozoikum der Karnischen Alpen: Arbeitstagung der Geologischen Bundesanstalt, v. 1985, p. 34-52.

Schönlaub, H. P., 1992, Stratigraphy, biogeography and paleoclimatology of the Alpine Paleozoic and its implications for plate movements: Jahrbuch der Geologischen Bundesanstalt, v. 135, no. 1, p. 381-418.

Schönlaub, H. P., 1998, The Carnic Alps: A key to the Variscan geodynamics of the southern margin of the European plate: Palaeogeography, Palaeoclimatology, Palaeoecology, v. 142, p. 141-158.

Schönlaub, H.-P., Attrep, M., Boeckelmann, K., Dreesen, R., Feist, R., Fenninger, A., Hahn, G., Klein, P., Korn, D., Kratz, R., Magaritz, M., Orth, C. J., and Schramm, J.-M., 1992, The Devonian/Carboniferous boundary in the Carnic Alps (Austria) – a multidisciplinary approach: Jahrbuch der Geologischen Bundesanstalt, v. 135, p. 57-98.

Schülke, I., 1995, Evolutive Prozesse bei Palmatolepis in der frühen Famenne-Stufe (Conodonta, Ober-Devon), Göttingen, Selbstverlag der Geologischen Institute der Georg-August-Universität Göttingen, Göttinger Arbeiten zur Geologie und Paläontologie, 1-108 p.

Schülke, I., 1996, Evolution of the early Famennian ancyrognathids (Conodonta, Late Devonian): Geologica et Palaeontologica, v. 30, p. 33-47.

Schülke, I., 1999, Conodont multielement reconstructions from the early Famennian (Late Devonian) of the Montagne Noire (southern France): Geologica et Palaeontologica, no. SB3, p. 1-124.

Schulte, P., Alegret, L., Arenillas, I., Arz, J. A., Barton, P. J., Bown, P. R., Bralower, T. J., Christeson, G. L., Claeys, P., Cockell, C. S., Collins, G. S., Deutsch, A., Goldin, T. J., Goto, K., Grajales-Nishimura, J. M., Grieve, R. A. F., Gulick, S. P. S., Johnson, K. R., and Kiessling, W., 2010, The Chicxulub asteroid impact and mass extinction at the Cretaceous–Paleogene boundary: Science, v. 327, no. 5970, p. 1214-1218.

Scotese, C. R., 2021, A PaleoAtlas for Paleogeography, Paleoclimate, and Plate Tectonics, Evanston, Illinois, USA, PALEOMAP Project.

Scott, A. C., and Glasspool, I. J., 2006, The diversification of Paleozoic fire systems and fluctuations in atmospheric oxygen concentration: Proceedings of the National Academy of Sciences, v. 103, no. 29, p. 10861-10865.

Seddon, G., and Sweet, W. C., 1971, An ecologic model for conodonts: Journal of Paleontology, v. 45, no. 5, p. 869-880.

Sobstel, M., Makowska-Haftka, M., and Racki, G., 2006, Conodont ecology in the Early–Middle Frasnian transition on the South Polish carbonate shelf: Acta Palaeontologica Polonica, v. 51, no. 4, p. 719-746.

Sorauf, J. E., and Pedder, A. E. H., 1986, Late Devonian rugose corals and the Frasnian–Famennian crisis: Canadian Journal of Earth Sciences, v. 23, no. 9, p. 1265-1287.

Spalletta, C., and Corradini, C., 2018, History of conodont researches in the Carnic Alps (Austria and Italy): an overview: *Gortania. Geologia, Paleontologia, Paletnologia*, v. 39 (2017), p. 5–26.

Spalletta, C., Corradini, C., Feist, R., Korn, D., Kumpan, T., Perri, M. C., Pondrelli, M., and Venturini, C., 2021, The Devonian–Carboniferous boundary in the Carnic Alps (Austria and Italy): Palaeobiodiversity and Palaeoenvironments, v. 101, no. 2, p. 487-505.

Spalletta, C., Ferretti, A., Kido, E., Perri, M. C., Pohler, S. M. L., Pondrelli, M., Schönlaub, H.-P., Suttner, T. J., and Vai, G. B., 2015a, Creta di Collina Formation, in Corradini, C., and Suttner, T. J., eds., The Pre-Variscan sequence of the Carnic Alps (Austria and Italy), Volume 69: Vienna, Geologische Bundesanstalt, p. 105-108.

Spalletta, C., Perri, M. C., Pondrelli, M., Corradini, C., Mossoni, A., and Schönlaub, H.-P., 2015b, Pal Grande Formation, in Corradini, C., and Suttner, T. J., eds., The Pre-Variscan sequence of the Carnic Alps (Austria and Italy), Volume 69: Vienna, Geologische Bundesanstalt, p. 137-140.

Spangenberg, J. E., and Herlec, U., 2006, Hydrocarbon biomarkers in the Topla–Mežica zinc–lead deposits, northern Karavanke/Drau range, Slovenia: paleoenvironment at the site of ore formation: Economic Geology, v. 101, no. 5, p. 997-1021.

Spassov, H., 1965, The carbonate Upper Devonian in the Kraishte and its conodont fauna: Trudove na Geologicheskiya institut, Seriya Paleontologiya (Proceedings of the Geological Institute, Series Paleontology), v. 7, p. 71–113 (in Bulgarian).

Stampfli, G. M., von Raumer, J. F., and Borel, G. D., 2002, Paleozoic evolution of pre-Variscan terranes: From Gondwana to the Variscan collision, in Martinez Catalan, J. R., Hatcher Jr, R. D., Arenas, R., and Diaz Garcia, F., eds., Variscan-Appalachian dynamics: The building of the late Paleozoic basement: Boulder, Colorado, Geological Society of America, p. 263-280.

Stauffer, C. R., 1938, Conodonts of the Olentangy Shale: Journal of Paleontology, v. 12, no. 5, p. 411-443.

Stauffer, C. R., 1940, Conodonts from the Devonian and Associated Clays of Minnesota: Journal of Paleontology, v. 14, no. 5, p. 417-435.

Stearn, C. W., 1987, Effect of the Frasnian–Famennian extinction event on the stromatoporoids: Geology, v. 15, no. 7, p. 677-679.

Stearn, C. W., 2015, Diversity trends of the Paleozoic Stromatoporoidea, in Selden, P. A., ed., Treatise on Invertebrate Paleontology, Part E (Revised), Porifera, Volumes 4–5: Lawrence, Kansas, University of Kansas, Paleontological Institute, p. 594-597.

Sundquist, E. T., and Visser, K., 2011, The geologic history of the carbon cycle, in Holland, H. D., and Turekian, K. K., eds., Geochemistry of Earth Surface Systems From the Treatise on Geochemistry: Amsterdam, Elsevier & Academic Press, p. 341-387.

Suttner, T. J., Kido, E., Corradini, C., Vodrážková, S., Pondrelli, M., and Simonetto, L., 2017, Conodont diversity across the late Eifelian Kačák Episode of the southern Alpine realm (central Carnic Alps, Austria/Italy): Palaeogeography, Palaeoclimatology, Palaeoecology, v. 479, p. 34-47.

Svensson, N. B., 1971, Probable meteorite impact crater in central Sweden: Nature Physical Science, v. 229, no. 3, p. 90.

Svensson, N. B., 1973, Shatter cones from the Siljan structure, central Sweden: Geologiska Föreningen i Stockholm Förhandlingar, v. 95, no. 1, p. 139-143.

Swart, P. K., 2008, Global synchronous changes in the carbon isotopic composition of carbonate sediments unrelated to changes in the global carbon cycle: Earth-Science Reviews, v. 85, no. 3–4, p. 45-60.

Sweet, W. C., 1988, The Conodonta: morphology, taxonomy, paleoecology, and evolutionary history of a long-extinct animal phylum, New York, Oxford University Press.

Sweet, W. C., and Donoghue, P. C. J., 2001, Conodonts: Past, present and future: Journal of Paleontology, v. 75, no. 6, p. 1174-1184.

Tagarieva, R. C., 2013, Conodont biodiversity of the Frasnian–Famennian boundary interval (Upper Devonian) in the Southern Urals: Bulletin of Geosciences, v. 88, no. 2, p. 297-314.

Thomas, L. A., 1949, Devonian-Mississippian formations of southeast Iowa: Geological Society of America Bulletin, v. 60, no. 3, p. 403-438.

Torsvik, T. H., Van Der Voo, R., Preeden, U., Mac Niocaill, C., Steinberger, B., Doubrovine, P. V., van Hinsbergen, D. J. J., Domeier, M., Gaina, C., Tohver, E., Meert, J. G., McCausland,

P. J. A., and Cocks, L. R. M., 2012, Phanerozoic polar wander, paleogeography and dynamics: Earth Science Reviews, v. 114, p. 325-368.

Trotter, J. A., Williams, I. S., Barnes, C. R., Lécuyer, C., and Nicoll, R. S., 2008, Did cooling oceans trigger Ordovician biodiversification? Evidence from conodont thermometry: Science, v. 321, no. 5888, p. 550-554.

Tucker, M. E., 1981, Sedimentary Petrology: An Introduction to the Origin of Sedimentary Rocks, Oxford, Blackwell Scientific Publications.

Ulrich, E. O., and Bassler, R. S., 1926, A classification of the toothlike fossils, conodonts, with descriptions of American Devonian and Mississippian species: Proceedings of the United States National Museum, v. 68, no. 2613, p. 1-63.

van den Boogaard, M., and Kuhry, B., 1979, Statistical reconstruction of the Palmatolepis apparatus (Late Devonian conodontophorids) at the generic, subgeneric, and specific level: Scripta Geologica, v. 49, p. 1-55.

Van Geldern, R., Joachimski, M. M., Jansen, U., Alvarez, F., Yolkin, E. A., and Ma, X.-P., 2006, Carbon, oxygen and strontium isotope records of Devonian brachiopod shell calcite: Palaeogeography, Palaeoclimatology, Palaeoecology, v. 240, p. 47-67.

Venturini, C., 1991, Introduction to the geology of the Pramollo Basin (Carnic Alps) and its surroundings: Giorn. Geol., v. 53, p. 13-47.

von Raumer, J. F., and Stampfli, G. M., 2008, The birth of the Rheic Ocean—Early Palaeozoic subsidence patterns and subsequent tectonic plate scenarios: Tectonophysics, v. 461, no. 1-4, p. 9-20.

Walliser, O. H., 1996, Global events in the Devonian and Carboniferous, in Walliser, O. H., ed., Global Events and Event Stratigraphy in the Phanerozoic: Berlin; Heidelberg, Springer-Verlag, p. 225-250.

Wang, C., and Ziegler, W., 2004, Conodont mass extinction and subsequent recovery across the Devonian Frasnian–Famennian transition in Guilin, South China, in Rong, J., and Fang, Z., eds., Mass Extinction and Recovery—Evidence from the Paleozoic and Triassic of South China: Hefei, University of Science and Technology of China Press, p. 281-316.

Wang, C. Y., and Ziegler, W., 2002, The Frasnian–Famennian conodont mass extinction and recovery in South China: Senckenbergiana Lethaea, v. 82, no. 2, p. 463-493.

Wang, K., and et al., 1991, Geochemical evidence for a catastrophic biotic event at the Frasnian/Famennian boundary in South China: Geology, v. 19, no. 8, p. 776-779.

Wang, X., Wang, X., Zhang, F., and Zhang, H., 2006, Carboniferous and Permian rugose corals in South China: diversity pattern and environmental change: Geological Journal, v. 41, p. 329-343.

Weary, D. J., and Harris, A. G., 1994, Early Frasnian (Late Devonian) conodonts from the Harrell Shale, western foreland fold-and-thrust belt, West Virginia, Maryland, and Pennsylvania, U.S.A: Courier Forschungsinstitut Senckenberg, v. 168, p. 195-225.

Weissert, H., Joachimski, M. M., and Sarnthein, M., 2008, Chemostratigraphy: Newsletters on Stratigraphy, v. 42, no. 3, p. 145-179.

Whalen, M. T., and Day, J. E., 2008, Magnetic Susceptibility, Biostratigraphy, and Sequence Stratigraphy: Insights into Devonian Carbonate Platform Development and Basin Infilling, Western Alberta, in Lukasik, J., and Simo, J. A., eds., Controls on Carbonate Platform and Reef Development, Volume 89: Tulsa, OK, SEPM (Society for Sedimentary Geology), p. 291-314.

Whalen, M. T., and Day, J. E., 2010, Cross-Basin Variations in Magnetic Susceptibility Influenced by Changing Sea Level, Paleogeography, and Paleoclimate: Upper Devonian, Western Canada Sedimentary Basin: Journal of Sedimentary Research, v. 80, no. 12, p. 1109-1127.

Wolska, Z., 1967, Upper Devonian conodonts from the south-west region of the Holy Cross Mountains, Poland: Acta Palaeontologica Polonica, v. 12, no. 4, p. 363-465.

Wu, F. Y., Arzamastsev, A. A., Mitchell, R. H., Li, Q. L., Sun, J., Yang, Y. H., and Wang, R. C., 2013, Emplacement age and Sr–Nd isotopic compositions of the Afrikanda alkaline ultramafic complex, Kola Peninsula, Russia: Chemical Geology, v. 353, p. 210-229.

Wu, Y., Gong, Y. M., and Du, Y., 1997, *Devonian sequence stratigraphy and sea-level change of South China*: Wuhan, China University of Geosciences Press, 110 p. (in Chinese).

Xiong, J., Qian, Y., and Tian, C., 1988, Conodonts, Devonian Stratigraphy, Palaeontology and Sedimentary Facies of the Longmen Mountain Area, Sichuan, China: Beijing, Geological Publishing House, p. 314-339. (in Chinese)

Yan, D.-P., Zhou, Y., Qiu, L., Wells, M. L., Mu, H., and Xu, C.-G., 2018, The Longmenshan Tectonic Complex and adjacent tectonic units in the eastern margin of the Tibetan Plateau: A review: Journal of Asian Earth Sciences, v. 164, p. 33-57.

Yan, Z., Hou, H.-F., and Ye, L.-F., 1993, Carbon and oxygen isotope event markers near the Frasnian–Famennian boundary, Luoxiu section, South China: Palaeogeography, Palaeoclimatology, Palaeoecology, v. 104, p. 97–104.

Yazdi, M., 1999, Late Devonian-Carboniferous conodonts from eastern Iran: Rivista Italiana di Paleontologia e Stratigrafia, v. 105, p. 167-200.

Youngquist, W., 1945, Upper Devonian conodonts from the Independence Shale(?) of Iowa: Journal of Paleontology, v. 19, p. 355-367.

Youngquist, W. L., and Peterson, R. F., 1947, Conodonts from the Sheffield Formation of north-central Iowa: Journal of Paleontology, v. 21, no. 3, p. 242-253.

Zhang, L., Zhao, H., Lü, Z., and Wang, X., 2025, Progress in Study of Conodont Bioapatite Geochemistry: Earth Science, v. 50, no. 3, p. 1122-1141.

Zhang, X., 2019, Late Devonian conodont biostratigraphy, event stratigraphy and chemostratigraphy in South China and Western Junggar, NW ChinaPh.D. thesis]: China University of Geosciences (Wuhan), (in Chinese).

Zhang, X., Joachimski, M. M., Over, D. J., Ma, K., Huang, C., and Gong, Y., 2019, Late Devonian carbon isotope chemostratigraphy: A new record from the offshore facies of South China: Global and Planetary Change, v. 182, p. 103024.

Zheng, R., and Liu, W., 1997, Carbon and strontium isotope effects of the Devonian sequence stratigraphy in the Longmenshan area: Geological Review, v. 43, no. 3, p. 264-272.

Zheng, R., Wen, H., Wang, C., Chang, H., Hu, Z., and Zhou, G., 2016, Field Practice Guide to Longmenshan Devonian System, Beijing, Geological Publishing House, 262 p.

Ziegler, W., 1958, Conodonten-feinstratigraphische Untersuchungen an der Grenze Mitteldevon/Oberdevon und in der Adorfstufe: Notizblatt des Hessischen Landesamtes für Bodenforschung, v. 87, p. 7–77 (in German).

Ziegler, W., 1962, Taxonomie und Phylogenie oberdevonischer Conodonten und ihre stratigraphische Bedeutung: Abhandlungen des Hessischen Landesamtes für Bodenforschung, Heft 38, 166 p. (in German).

Ziegler, W., 1971, Conodont stratigraphy of the European Devonian, in Sweet, W. C., and Bergström, S. M., eds., Symposium on Conodont Biostratigraphy: Boulder, CO, Geological Society of America, p. 227-284.

Ziegler, W., Ovnatanova, N. S., and Kononova, L. I., 2000, Devonian polygnathids from the Frasnian of the Rheinisches Schiefergebirge, Germany, and the Russian Platform: Senckenbergiana Lethaea, v. 80, no. 2, p. 593-645.

Ziegler, W., and Sandberg, C. A., 1984, Palmatolepis-based revision of upper part of standard Late Devonian conodont zonation, in Clark, D. L., ed., Conodont Biofacies and Provincialism, Volume 196: Boulder, CO, Geological Society of America, p. 179-194.

Ziegler, W., and Sandberg, C. A., 1990, The Late Devonian standard conodont zonation, Frankfurt am Main, Senckenberg Forschungsinstitut, Courier Forschungsinstitut Senckenberg, 1-115 p.

Plates

Plate 1

Late Devonian conodonts from the Plan di Zermula D (PZD) section, Carnic Alps

Fig. 1 - *Ancyrodella curvata* (Branson & Mehl, 1934); upper view of P1 element DMGTS 125; sample PZD 1, Frasnian Zone 13b.

Fig. 2 - *Ancyrodella hamata* Ulrich & Bassler, 1926; upper view of P1 element DMGTS 126; sample PZD 1, Frasnian Zone 13b.

Fig. 3 - *Ancyrognathus cryptus* Ziegler, 1962; upper view of P1 element DMGTS 146; sample PZD 8, *Pa. crepida* Zone.

Fig. 4 - *Icriodus alternatus* Branson & Mehl, 1934; upper view of P1 element DMGTS 128; sample PZD 12, *Pa. crepida* Zone.

Fig. 5 - *Icriodus cornutus* Sannemann, 1955b; upper view of P1 element DMGTS 147; sample PZD 12, *Pa. crepida* Zone.

Fig. 6 - *Icriodus iowaensis iowaensis* Youngquist & Peterson, 1947; upper view of P1 element 148; sample PZD 12, *Pa. crepida* Zone.

Fig. 7 - *Melina gradata* Youngquist, 1945; lateral view of P1 element DMGTS 149; sample PZD 10, *Pa. crepida* Zone.

Fig. 8 - *Palmatolepis beckeri* Klapper, 2007a; lateral view of P1 element DMGTS 171; sample PZD 4, Frasnian Zone 13c.

Fig. 9 - *Palmatolepis bogartensis* (Stauffer, 1938); upper view of P1 element DMGTS 130; sample PZD 1, Frasnian Zone 13b.

Fig. 10 - *Palmatolepis bogartensis* (Stauffer, 1938); upper view of P1 element DMGTS 172; s ample PZD 4, Frasnian Zone 13c.

Fig. 11 - *Palmatolepis boogaardi* Klapper & Foster, 1993; upper view of P1 element DMGTS 173; sample PZD 1, Frasnian Zone 13b.

Fig. 12 - *Palmatolepis boogaardi* Klapper & Foster, 1993; upper view of P1 element DMGTS 131; sample PZD 4, Frasnian Zone 13c.

Fig. 13 - *Palmatolepis clarki* Ziegler, 1962; upper view of P1 element DMGTS 150; sample PZD 9, *Pa. crepida* Zone.

Fig. 14 - *Palmatolepis clarki* Ziegler, 1962; upper view of P1 element DMGTS 174; sample PZD 10, *Pa. crepida* Zone.

Fig. 15 - *Palmatolepis crepida* Sannemann, 1955b; upper view of P1 element DMGTS 151; sample PZD 8, *Pa. crepida* Zone.

Fig. 16 - *Palmatolepis delicatula delicatula* Branson & Mehl, 1934; upper view of P1 element DMGTS 152; sample PZD 7, *Pa. minuta minuta* Zone,

Fig. 17 - *Palmatolepis delicatula platys* Ziegler & Sandberg, 1990; upper view of P1 element DMGTS 153; sample PZD 10, *Pa. crepida* Zone.

Fig. 18 - *Palmatolepis juntianensis* Han, 1987; upper view of P1 element DMGTS 132, sample PZD 1, Frasnian Zone 13b.

Fig. 19 - *Palmatolepis juntianensis* Han, 1987; upper view of P1 element DMGTS 175, sample PZD 1, Frasnian Zone 13b.

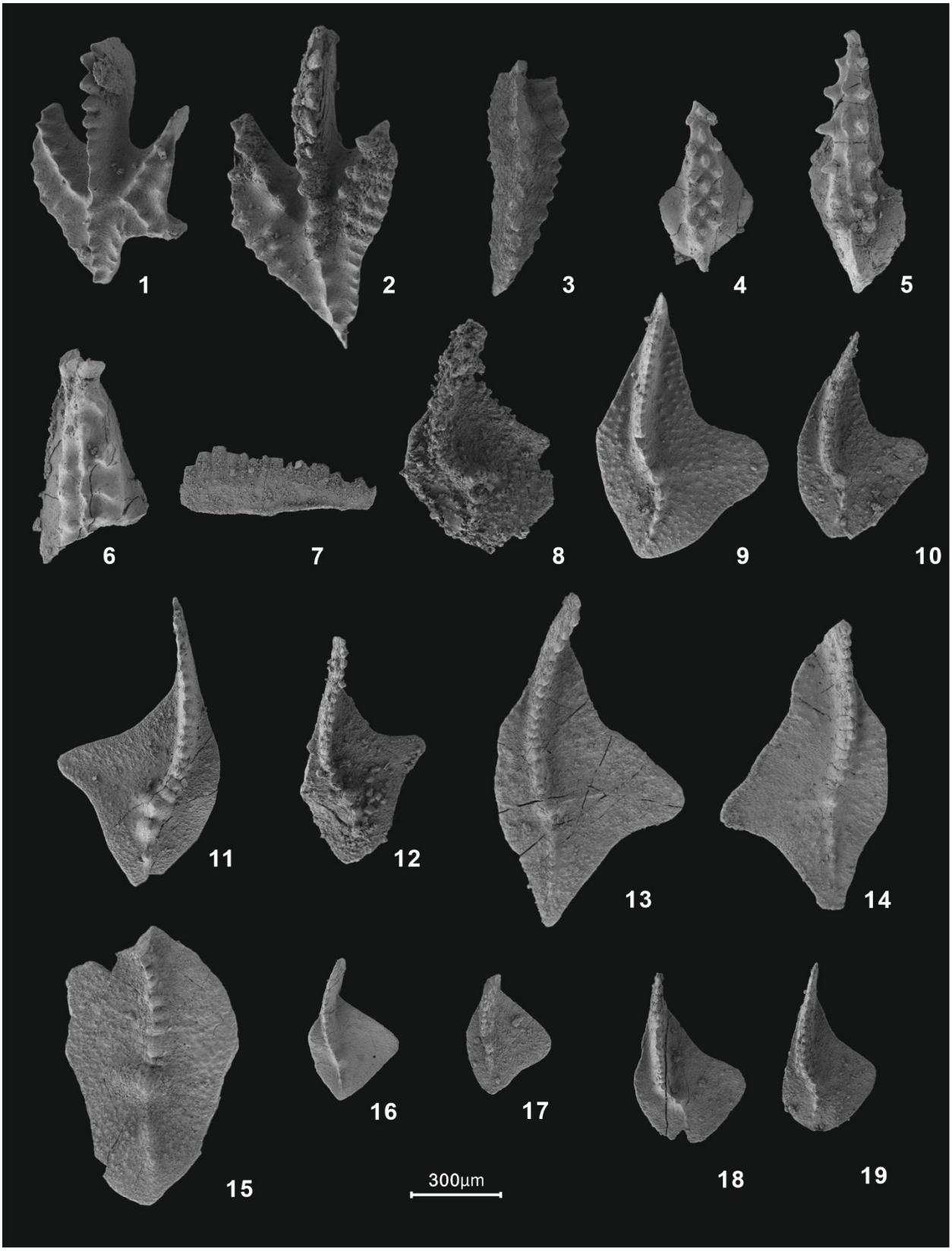
1
2
3
4
5
6
7
8
9
10
11
12
13
14
15
16
17
18
19
300µm

Plate 2

Late Devonian conodonts from the Plan di Zermula D (PZD) section, Carnic Alps

Fig. 1 - *Palmatolepis linguiformis* Müller, 1956; upper view of P1 element DMGTS 133; sample PZD 1, Frasnian Zone 13b.
Fig. 2 - *Palmatolepis minuta minuta* Branson & Mehl, 1934; upper view of P1 element DMGTS 155; sample PZD 9, *Pa. crepida* Zone.
Fig. 3 - *Palmatolepis regularis* Cooper, 1931; upper view of P1 element DMGTS 158; sample PZD 10, *Pa. crepida* Zone.
Fig. 4 - *Palmatolepis quadrantinodosalobata* Sannemann, 1955a; upper view of P1 element DMGTS 157; sample PZD 10, *Pa. crepida* Zone.
Fig. 5 - *Palmatolepis robusta* Schülke, 1995; upper view of P1 element DMGTS 159; sample PZD 10, *Pa. crepida* Zone.
Fig. 6 - *Palmatolepis protorhomboidea* Sandberg & Ziegler, 1973; upper view of P1 element DMGTS 156; sample PZD 9, *Pa. crepida* Zone.
Fig. 7 - *Palmatolepis rhenana* Bischoff, 1956; upper view of P1 element DMGTS; sample PZD 4; Frasnian Zone 13c.
Fig. 8 - *Palmatolepis lobicornis* Schülke, 1995; upper view of P1 element DMGTS 154; sample PZD 12, *Pa. crepida* Zone.
Fig. 9 - *Palmatolepis subperlobata* Branson & Mehl, 1934; upper view of P1 element DMGTS 161, sample PZD 10, *Pa. crepida* Zone.
Fig. 10 - *Palmatolepis subperlobata* Branson & Mehl, 1934; upper view of P1 element DMGTS 176, sample PZD 10, *Pa. crepida* Zone.
Fig. 11 - *Palmatolepis spathula* Schülke, 1995; upper view of P1 element DMGTS 160; sample PZD 12, *Pa. crepida* Zone.
Fig. 12 - *Palmatolepis tenuipunctata* Sannemann, 1955b; upper view of P1 element DMGTS 162; sample PZD 10, *Pa. crepida* Zone, DMGTS162.
Fig. 13 - *Palmatolepis triangularis* Sannemann, 1955a; upper view of P1 element DMGTS 177; sample PZD 6A, *Pa. minuta minuta* Zone.
Fig. 14 - *Palmatolepis triangularis* Sannemann, 1955a; upper view of P1 element DMGTS 163; sample PZD 10, *Pa. crepida* Zone.
Fig. 15 - *Palmatolepis ultima* Ziegler, 1958; upper view of P1 element DMGTS 135; sample PZD 4, Frasnian Zone 13c.
Fig. 16 - *Palmatolepis werneri* Ji & Ziegler, 1993; upper view of P1 element DMGTS 178; sample PZD 12, *Pa. crepida* Zone.
Fig. 17 - *Palmatolepis winchelli* (Stauffer, 1938); upper view of P1 element DMGTS 136; sample PZD 1, Frasnian Zone 13b.
Fig. 18 - *Pelekysgnathus planus* Sannemann, 1955b; lateral view of P1 element DMGTS 137; sample PZD 12, *Pa. crepida* Zone.

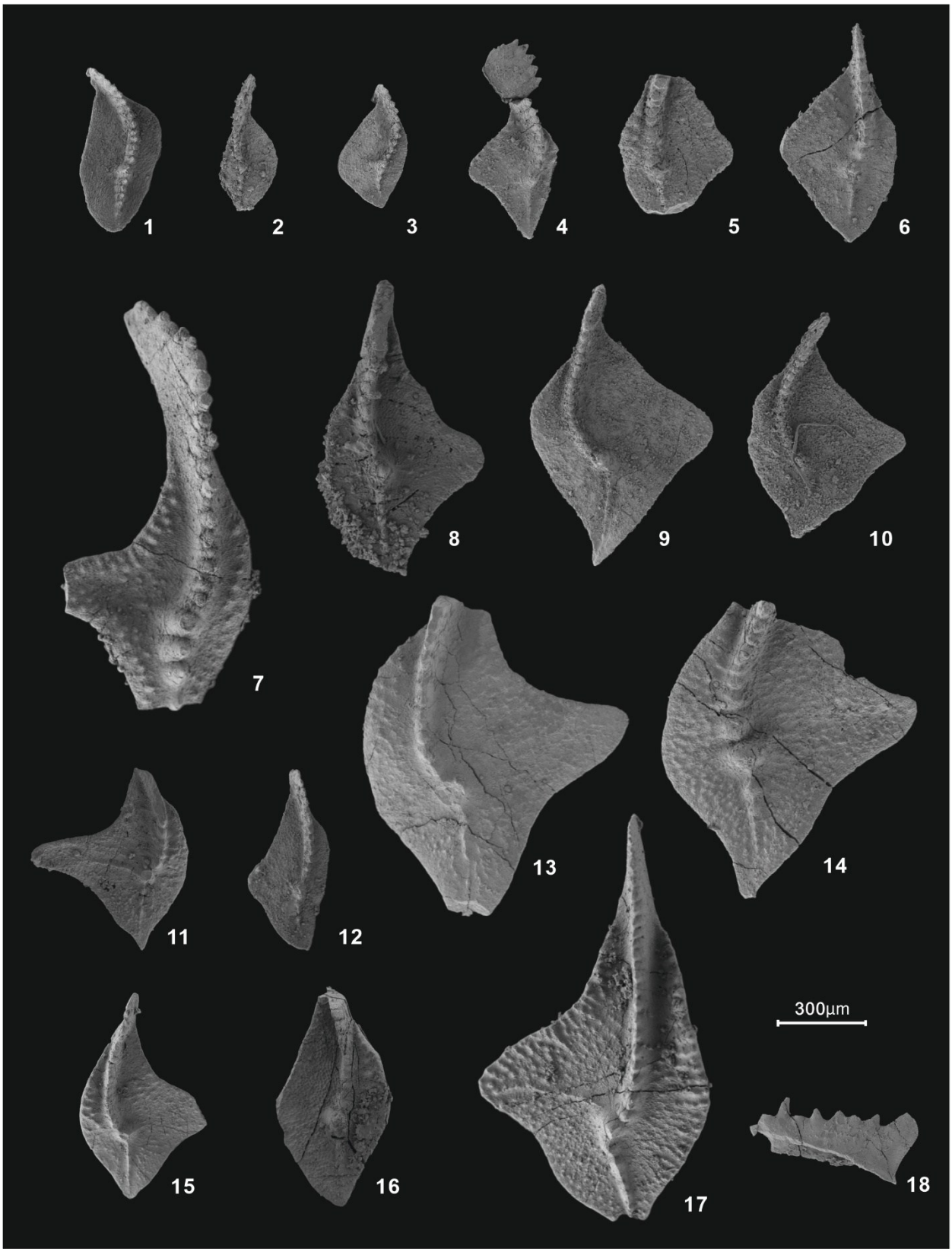
1
2
3
4
5
6
7
8
9
10
11
12
13
14
15
16
17
18
300µm

Plate 3

Late Devonian conodonts from the Plan di Zermula D (PZD) section, Carnic Alps

Fig. 1 - *Polygnathus mirificus* Ji & Ziegler, 1993; upper (1a) and lateral views (1b) of P1 element DMGTS 179; sample PZD 1, Frasnian Zone 13b.

Fig. 2 - *Polygnathus mirificus* Ji & Ziegler, 1993; upper (2a) and lateral views (2b) of P1 element DMGTS 144; sample PZD 1, Frasnian Zone 13b.

Fig. 3 - *Polygnathus lodinensis* Pölsler, 1969; upper (3a) and lateral views (3b) of P1 element DMGTS 142; sample PZD 3, Frasnian Zone 13b.

Fig. 4 - *Polygnathus brevis* Miller & Youngquist, 1947; upper view of P1 element DMGTS 139; sample PZD 4, Frasnian Zone 13c.

Fig. 5 - *Polygnathus brevilaminus* Branson & Mehl, 1934; lateral view of P1 element DMGTS 165; sample PZD 8, *Pa. crepida* Zone.

Fig. 6 - *Polygnathus brevilaminus* Branson & Mehl, 1934; upper view of P1 element DMGTS 166; sample PZD 12, *Pa. crepida* Zone.

Fig. 7 - *Polygnathus procerus* Sannemann, 1955b; upper (7a) and lateral views (7b) of P1 element DMGTS 180; sample PZD 9, *Pa. crepida* Zone.

Fig. 8 - *Polygnathus elegantulus* Klapper & Lane, 1985; upper-lateral view of P1 element DMGTS 141; sample PZD 1, Frasnian Zone 13b.

Fig. 9 - *Polygnathus eoglaber* Ji & Ziegler, 1993; upper view of P1 element DMGTS 167; sample PZD 12, *Pa. crepida* Zone.

Fig. 10 - *Polygnathus nodocostatus nodocostatus* Branson & Mehl, 1934; upper view of P1 element DMGTS 181; sample PZD 10, *Pa. crepida* Zone.

Fig. 11 - *Polygnathus praecursor* Matyja, 1993; upper view of P1 element DMGTS 169; sample PZD 10, *Pa. crepida* Zone.

Fig. 12 - *Polygnathus decorosus* Stauffer, 1938, upper view of P1 element DMGTS 140; sample PZD 1, Frasnian Zone 13b.

Fig. 13 - *Polygnathus aequalis* Klapper & Lane, 1985; lateral view of P1 element DMGTS 138; sample PZD 1, Frasnian Zone 13b.

Fig. 14 - *Polygnathus webbi* Stauffer, 1938; upper view of P1 element DMGTS 145, sample PZD1, Frasnian Zone 13b.

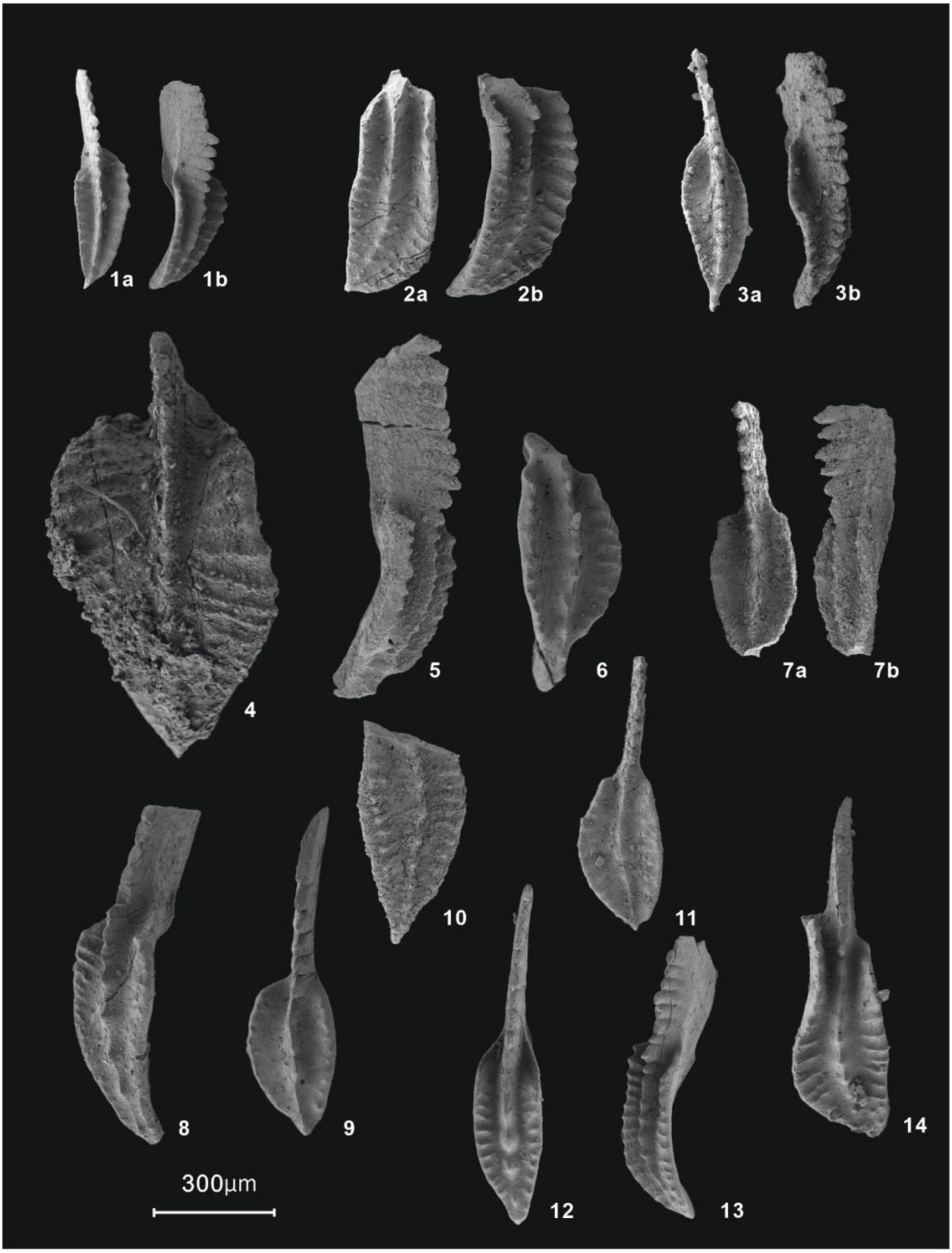
1a
1b
2a
2b
3a
3b
4
5
6
7a
7b
8
9
10
11
12
13
14
300µm

Plate 4

Late Devonian conodonts from the Qinglongxia (QLX) sections, Longmenshan

Fig. 1 - *Branmehla inornata* (Branson & Mehl, 1934); upper (1a) and lateral views (1b) of P1 element; sample QLXB C5, *Pa. gr. expansa- Bi. costatus* Zone

Fig. 2 - *Mehlina gradata* (Branson & Mehl, 1934); upper (2a) and lateral views (2b) of P1 element ; sample QLXA C7, FZ 6-FZ 11 Zone

Fig. 3 - *Mehlina strigosa* (Branson & Mehl, 1934); upper (3a) and lateral views (3b) of P1 element ; sample QLXA C18, *Pal. ru. trachytera-Pa. gr. expansa* Zone

Fig. 4 - *Polygnathus alatus* Huddle, 1934; upper view of P1 element; sample QLXA C2, FZ 3-FZ 4 Zone

Fig. 5 - *Polygnathus alatus* Huddle, 1934; upper view of P1 element; sample QLXA C5, FZ 3-FZ 4 Zone

Fig. 6 - *Polygnathus brevilaminus* Branson & Mehl, 1934; upper view of P1 element; sample QLXA C14, FZ 13b- Pa. *crepida* Zone

Fig. 7 - *Polygnathus decorosus* Stauffer, 1938, upper view of P1 element; sample QLXA C12A, FZ 6-FZ 11 Zone

Fig. 8 - *Polygnathus decorosus* Stauffer, 1938, upper view of P1 element; sample QLXA C6, FZ 5 Zone

Fig. 9 - *Polygnathus praepolitus* Kononova, Alekseev, Barskov & Reimers, 1996; upper view of P1 element; sample QLXA C7A, FZ 6-FZ 11 Zone

Fig. 10 - *Polygnathus macilentus* Kuzmin, 1993; upper view of P1 element; sample QLXA C13, FZ 12-FZ 13a Zone

Fig. 11 - *Polygnathus krestovnikovi* Ovnatanova, 1969; upper view of P1 element; sample QLXA C13B, FZ 12-FZ 13a Zone

Fig. 12 - *Polygnathus experplexus* Sandberg & Ziegler, 1979; upper view of P1 element; sample QLXB C2, *Pa. marg. utahensis-Pa. gr. manca* Zone

Fig. 13 - *Polygnathus experplexus* Sandberg & Ziegler, 1979; upper view of P1 element; sample QLXB C2, *Pa. marg. utahensis-Pa. gr. manca* Zone

Fig. 14 - *Polygnathus perplexus* Thomas, 1949; upper-lateral of P1 element; sample QLXB C3, *Pa. marg. utahensis-Pa. gr. manca* Zone

Fig. 15 - *Polygnathus margaritatus* Schäfer, 1976; upper-lateral view of P1 element; sample QLXB C6, *Pa. gr. expansa- Bi. costatus* Zone

Fig. 16 - *Polygnathus zinaidae* Kononova, Alekseev, Barskov & Reimers, 1996; upper view of P1 element; sample QLXA C7A, FZ 6-FZ 11 Zone

Fig. 17 - *Polygnathus subirregularis* Sandberg & Ziegler, 1979; upper view of P1 element; sample QLXA C18, *Pal. ru. trachytera-Pa. gr. expansa* Zone

Fig. 18 - *Polygnathus znepolensis* Spassov, 1965; upper view of P1 element; sample QLXB C5, *Pa. gr. expansa- Bi. costatus* Zone

Fig. 19 - *Polygnathus znepolensis* Spassov, 1965; upper view of P1 element; sample QLXB C5, *Pa. gr. expansa- Bi. costatus* Zone

Fig. 20 - *Polygnathus* cf. *zinaidae* Kononova, Alekseev, Barskov & Reimers, 1996; upper view of P1 element; sample QLXA C18, *Pa. r. trachytera-Pa. g. expansa* Zone

Fig. 21 - *Polygnathus* cf. *zinaidae* Kononova, Alekseev, Barskov & Reimers, 1996; upper view

of P1 element; sample QLXA C14A, *Pa. r. trachytera-Pa. g. expansa* Zone

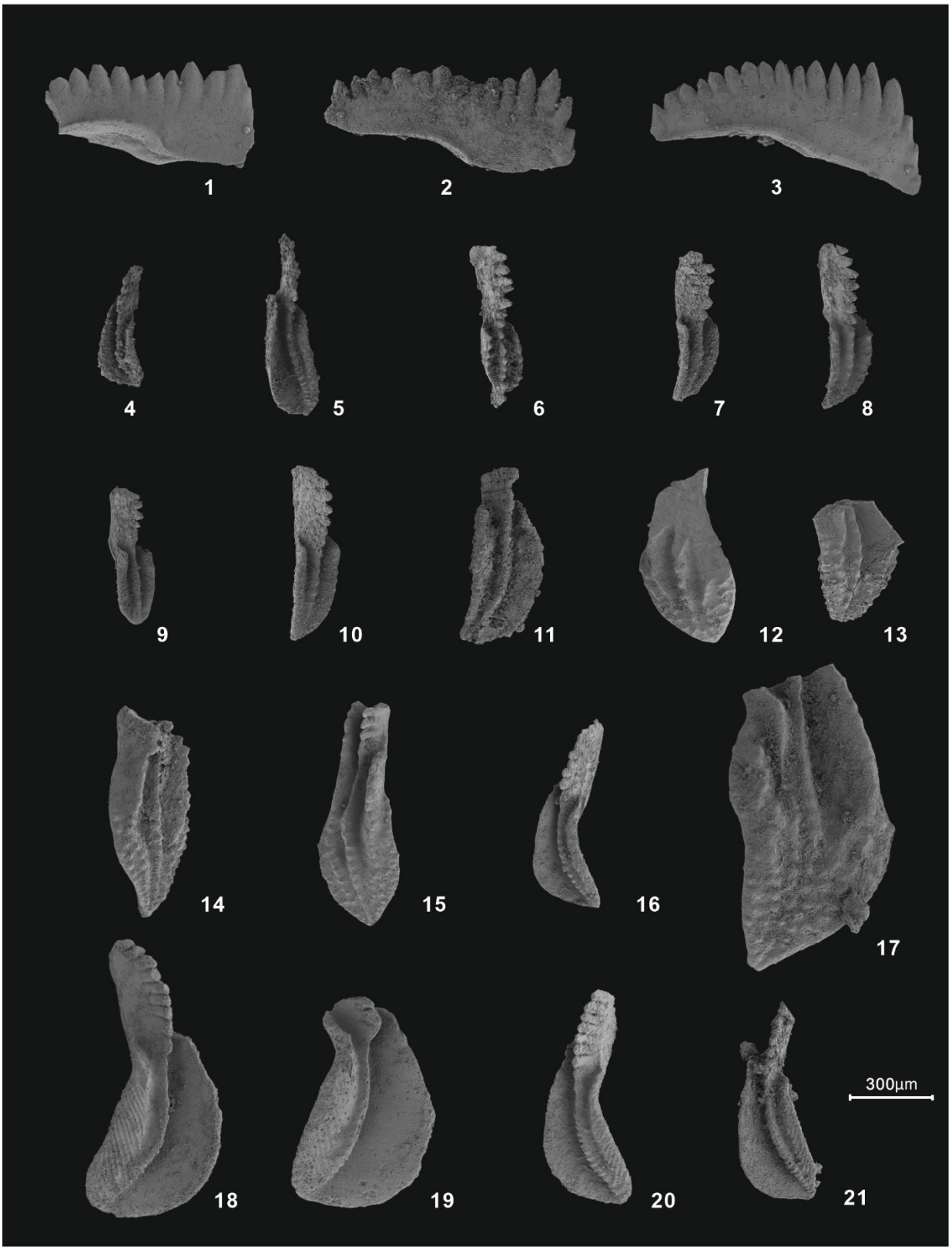

Plate 5

Late Devonian conodonts and associated vertebrate remains from the Qinglongxia (QLX) sections, Longmenshan, and the Plan di Zermula D (PZD) section, Carnic Alps

Fig. 1 - *Ancyrognathus* cf. *asymmetricus* (Ulrich & Bassler, 1926); upper view of P1 element; sample PZD 3, Frasnian Zone 13b.

Fig. 2 - *Polygnathus* sp. A; upper (2a) and lateral views (2b) of P1 element; sample PZD 10, *Pa. crepida* Zone.

Fig. 3 - *Polygnathus* sp. B; upper view of P1 element; sample PZD C10, *Pa. crepida* Zone.

Fig. 4 - *Polygnathus* sp. C; upper view of P1 element; sample PZD C10, *Pa. crepida* Zone.

Fig. 5 - *Polygnathus* sp. D; upper-lateral of P1 element; sample QLXA C18, *Pal. ru. trachytera-Pa. gr. expansa Zone*

Fig. 6 - *Phoebodus* sp. ; upper (6a) and lateral views (6b) of P1 element; sample QLXA C10, FZ 6-FZ 11 Zone.

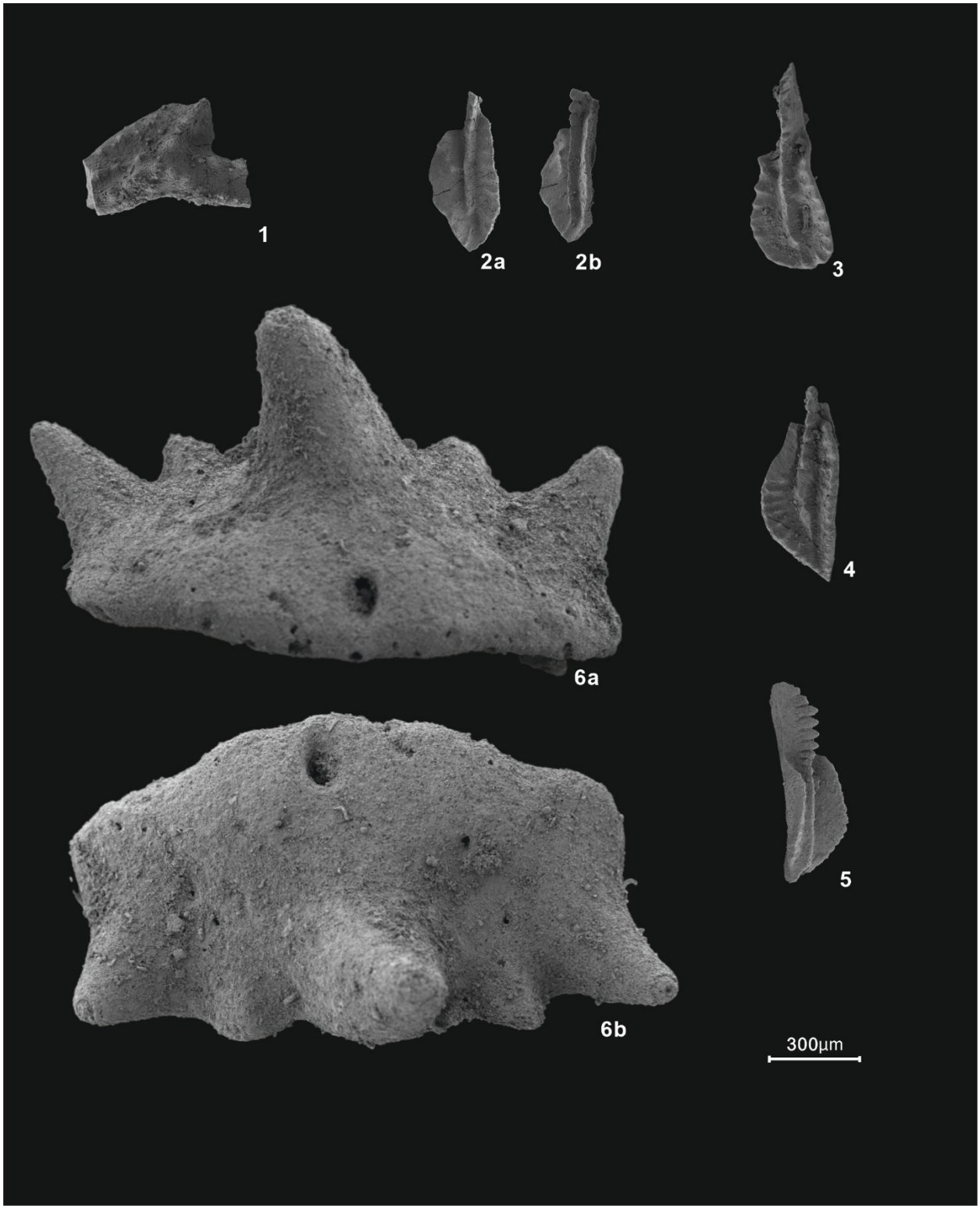
1
2a
2b
3
6a
4
5
6b
300µm